# The Effects of Autophagic Deficiencies on the Leukemia Mitochondrial Phenotype and Implications in Strategic Drug Targeting

by

Rowena Rodrigo

A Thesis

presented to the University of Waterloo

in fulfillment of the

thesis requirement for the degree of

Master of Science

in

Pharmacy

Waterloo, Ontario, Canada, 2016

# Author's Declaration

I hereby declare that I am the sole author of this thesis. This is a true copy of the thesis, including any required final revisions, as accepted by my examiners.

I understand that my thesis may be made electronically available to the public.

# Abstract

Acute myeloid leukemia (AML) is a cancer that develops when hematopoietic stem cells in the bone marrow transform into malignant cells and subsequently grow and replicate aberrantly. Autophagy, a pathway by which cellular components are sequestered and degraded in response to a variety of signals, is modified in AML. Here, we sought to understand the mitochondria-specific changes that occur in autophagy-deficient leukemia cells by silencing the genes ATG7, BNIP3L, or SQSTM1. We examined mitochondrial function using the probe rhodamine 123 (Rho 123), which accumulates according to the mitochondrial membrane potential (ΔΨM). We examined mitochondrial health using two probes: dihydroethidium (DHE): a probe for the main mitochondrial reactive oxygen species (ROS) superoxide, and 2', 7-dichlorodihydrofluorescein diacetate (H2DCFDA): a broad-range probe for other ROS. In all knockdowns, Rho 123 was increased indicating hyperpolarization of ΔΨM, and DHE was increased indicating accumulation of superoxide, however the fluorescent product of H2DCFDA was decreased indicating lower levels of other ROS. Taken together, these results indicated mitochondrial dysfunction in the gene-silenced lines. We measured mitochondrial content using the fluorescent probe nonyl acridine orange and quantitative polymerase chain reaction analysis of mitochondrial DNA (mtDNA) – both of which indicated no significant changes in mitochondrial content. We performed a serum starvation and dose-response analysis using an autophagy activator to demonstrate the effects of these knockdowns on autophagy dynamics - which indicated altered autophagy. Finally, we ran a dose response which demonstrated that AML cells with deficiencies in autophagy proteins are more sensitive to mitochondrial-targeting drugs but not DNA-targeting drugs, suggesting that the former classes may provide an excellent opportunistic therapy for AML patients with substantial autophagy deficits.

# Acknowledgements

First and foremost, I would like to thank my supervisor Dr. Paul Spagnuolo for his guidance, patience, and support throughout this project. Dr. Spagnuolo encouraged me to reach my full potential and provided me with an environment in which I could learn and grow with a fantastic team of lab mates. Thank you to my advisory committee, Dr. Shawn Wettig and Dr. Roderick Slavcev for lending your excellent advice and encouragement throughout this project. To our wonderful graduate coordinators at the school of Pharmacy: Gail, Penny, and Sarah Rae, thank you for supporting me throughout my project. To my lab mates: Alessia Roma, Matthew Tcheng, Nawaz Ahmed, and Sarah Rota, thank you for sharing your knowledge, friendship, and humour – my spirits were always highest when you were around. A special thank you goes out to Dr. Jonathan Blay and the Blay lab, who provided me with excellent mentorship and welcomed me to use their laboratory equipment. To my fellow graduate students at the school of pharmacy and my wonderful friends outside of school: thank you for providing friendship, support, and distractions as they were needed throughout my M.Sc. Thank you Spencer Berg for your companionship – I am so fortunate to have had you to hold me up through all of the challenges. Last but certainly not least, thank you to my parents for their continual love and support. I could not have done this without you. My successes are yours.

# Table of Contents

List of Figures

# List of Tables

# List of Abbreviations

| Acronym | Full Form |
|---|---|
| AML | Acute myeloid leukemia |
| ATG | Autophagy-related |
| BSA | Bovine serum albumin |
| CMA | Chaperone-mediated autophagy |
| DCF | 2',7'-Dichlorofluorescein |
| DMEM | Dulbecco's modified eagle medium |
| DHE | Dihydroethidium (Hydroethidine) |
| DNA | Deoxyribonucleic acid |
| FBS | Fetal bovine serum |
| H2DCFDA | 2',7'-Dichlorodihydrofluorescein diacetate |
| HBSS | Hank's buffered saline solution |
| KD | Knockdown (gene product) |
| LIR | LC3-interacting region |
| MDS | Myelodysplastic syndromes |
| mtDNA | Mitochondrial DNA |
| NAO | Nonyl-acridine orange/ 10-N-nonyl acridine orange |
| Rho 123 | Rhodamine 123 |
| RIPA | Radioimmunoprecipitation assay |
| RNA | Ribonuceic acid |
| TRC | Transduced control |
| $\Delta\Psi M$ | Mitochondrial membrane potential |

# List of Proteins

| Protein[1] | Gene[1] | Autophagy-Related Function[1] |
|---|---|---|
| AMBRA1 | *AMBRA1* | AUTOPHAGY AND BECLIN1 REGULATOR 1: Autophagy receptor with a LIR |
| AMPK | *PRKAA1, PRKAA2* | AMP-ACTIVATED PROTEIN KINASE: Key energy sensor |
| ATG10 | | AUTOPHAGY RELATED 10: Catalyzes the conjugation of ATG12 to ATG5 forming the ubiquitin-like conjugation system |
| ATG101 | *ATG101* | AUTOPHAGY RELATED 101: Phosphorylates ATG13 and FIP200, complexes with ATG13 |
| ATG12 | *ATG12* | AUTOPHAGY RELATED 12: Part of one of the ubiquitin-like conjugation systems in autophagy |
| ATG13 | *ATG13* | AUTOPHAGY RELATED 13: Part of the autophagy initiation complex |
| ATG14 | *ATG14* | AUTOPHAGY-RELATED 14: Determines the localization of the PI3K complex. Plays a role in LC3-I conjugation to phosphatidylethanolamine. Regulates Beclin 1 by phosphorylation |
| ATG16L1 | *ATG16L1* | AUTOPHAGY RELATED 16 LIKE 1: Complexes with the ATG12-ATG5 ubiquitin-like conjugation system |
| ATG3 | *ATG3* | AUTOPHAGY RELATED 3: Interacts with ATG12-ATG5 to form the ubiquitin-like conjugation system. Mediates the conjugation of phosphatidylethanolamine to LC3-I to form LC3-II. |
| ATG4B | *ATG4B* | AUTOPHAGY RELATED 4B CYSTEINE PEPTIDASE: Protease that cleaves  to form LC3-I |
| ATG5 | *ATG5* | AUTOPHAGY RELATED 5: Part of one of the ubiquitin-like conjugation systems in autophagy |
| ATG7 | *ATG7* | AUTOPHAGY RELATED 7: Activates ATG12 in the ubiquitin-like conjugation system. With the help of ATG3, conjugates LC3-I to phosphatidylethanolamine to form LC3-II |
| Beclin 1 | *BECN1* | BECLIN 1: Acts as a core subunit of the PI3K complex which initiates autophagosome formation |
| BNIP3 | *BNIP3* | BCL2/ADENOVIRUS E1B 19kDa INTERACTING PROTEIN 3: Autophagy receptor on mitochondria with a LIR |
| FIP200 | *RB1CC1* | RB1 INDUCIBLE COILED-COIL 1: Part of the autophagy initiation complex |

| | | |
|---|---|---|
| FUNDC1 | *FUNDC1* | FUN14 DOMAIN CONTAINING 1:<br>Autophagy receptor on mitochondria with a LIR |
| (ATG8) | *MAP1A, MAP1B* | MICROTUBULE ASSOCIATED PROTEIN 1 LIGHT CHAIN 3 ALPHA AND BETA:<br>Involved in the formation of autophagosome vacuoles. Involved in conjugating cargo to the autophagosome. |
| MIRO | *RHOT1, RHOT2* | RAS HOMOLOG FAMILY MEMBER T1:<br>Parkin substrate |
| Mitofunsin 2 | *MFN2* | MITOFUSIN 2:<br>Parkin substrate |
| Mitofusin 1 | *MFN1* | MITOFUSIN 1:<br>Parkin substrate |
| mTOR | *mTOR* | MAMMALIAN/MECHANISTIC TARGET OF RAPAMYCIN:<br>Major control center mediating cellular responses to stress |
| NBR1 | *NBR1* | NEIGHBOUR OF BRCA1 GENE 1:<br>Autophagy receptor with a LIR |
| NDP52 | *CALCOCO2* | CALCIUM BINDING AND COILED COIL DOMAIN 2:<br>Autophagy receptor with a LIR |
| NIX | *BNIP3L* | BCL2/ADENOVIRUS E1B 19kDa INTERACTING PROTEIN 3-LIKE:<br>Depolarizes the mitochondrial membrane. Autophagy receptor on mitochondria with a LIR. |
| OPTN | *OPTN* | OPTINEURIN:<br>Autophagy receptor with a LIR |
| P62 | *SQSTM1* | SEQUESTOME 1:<br>Autophagy receptor with a LIR |
| PARKIN | *PARK2* | PARKIN RBR E3 UBIQUITIN LIGASE:<br>Activated by PINK1. Ubiquitinates proteins on the outer mitochondrial membrane to be substrates for PINK1 to amplify the mitophagy signal |
| PINK1 | *PINK1* | PTEN INDUCED PUTATIVE KINASE 1:<br>Phosphorylates mitochondrial proteins to tag them for mitophagy. Mediates activation and translocation of PARK2. |
| TAX1BP1 | *TAX1BP1* | TAX1 BINDING PROTEIN 1:<br>Autophagy receptor with a LIR |
| TBK1 | *TBK1* | TANK BINDING KINASE 1:<br>Signal amplification factor for autophagosome recruitment |
| ULK1 | *ULK1/ ATG1* | UNC-51 LIKE AUTOPHAGY ACTIVATING KINASE 1:<br>Part of regulatory feedback loop of autophagy |
| VDAC1 | *VDAC1* | VOLTAGE-DEPENDENT ANION CHANNEL PROTEIN:<br>Forms a channel in the outer mitochondrial membrane; involved in cell volume regulation. Parkin substrate. |

# Chapter 1: Introduction

## 1.1 Cancer Genetics

Cancer is a term for a group of heterogeneous diseases characterized by aberrant cell growth and uncontrolled proliferation. Various cell types can transform into cancer cells when mutations arise in key regions of the genetic material, deoxyribonucleic acid (DNA). Cancer-causing mutations may arise as chance mistakes in DNA replication, as a result of an infection or disease, or due to DNA damage caused by physical or chemical agents (i.e., mutagens)[2]. These mutations can be the result of insertions, deletions, or translocations of genetic material, leading to changes in function or expression of transcribed proteins. Many of the known cancer-related genes affect cell survival, DNA damage repair, angiogenesis, metastasis, or regulation of cell cycle progression– providing a means to achieve aberrant proliferation[2].

### *1.1.1 Acute Myeloid Leukemia*

Leukemia is a cancer which arises when blood cells in the bone marrow are transformed by mutations, and produce undifferentiated, aberrantly growing blast cells[3]. Clinically and pathologically, leukemia can be classified as being acute or chronic - based on the speed of progression, and myelogenous or lymphocytic - based on the lineage from which the leukemic cells diverge[4]. Acute myeloid leukemia (AML) is thus a rapidly progressing leukemia that diverges from the myeloid lineage. Formation of blasts in AML occurs at the expense of producing healthy myeloid-derived blood cells, resulting in a deficit of functional red blood cells, white blood cells, dendritic cells, and platelets, which can lead to death. Figure 1.1 provides an overview of hematopoiesis and leukemic cell development.

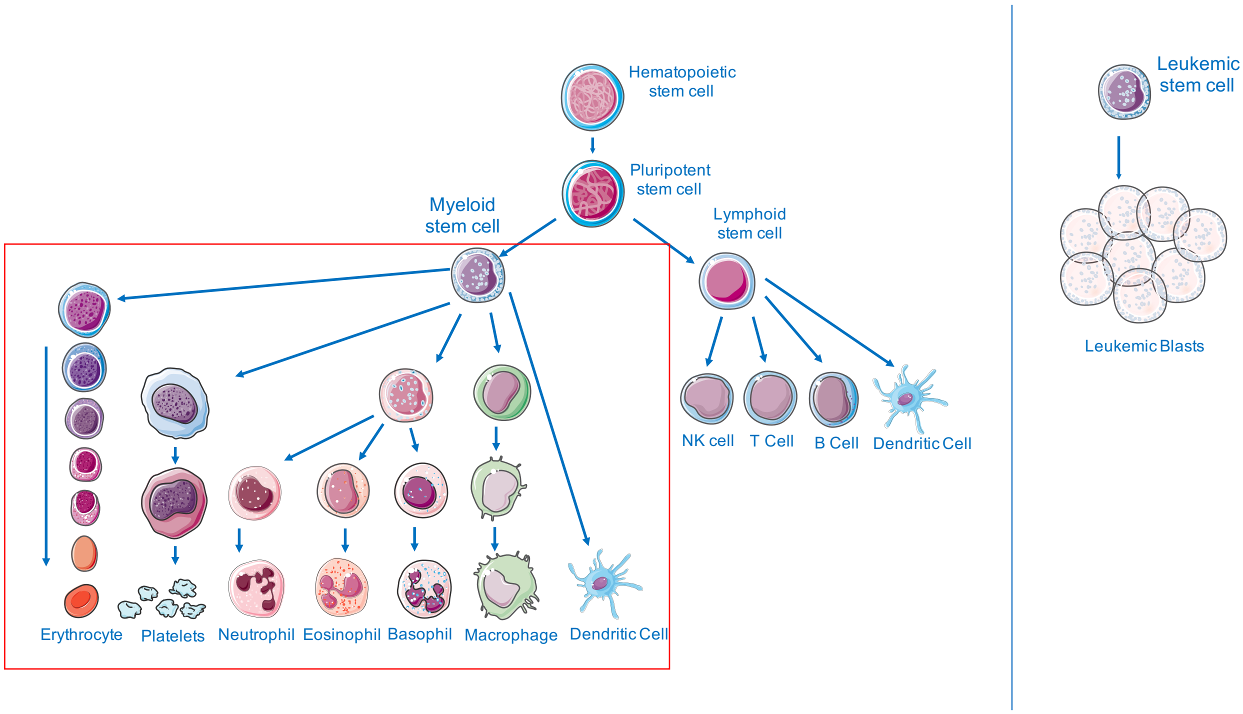


**Figure 1.1 Hematopoiesis and AML Development**
(A) Normal hematopoiesis: a common progenitor cell diverges to produce the myeloid and lymphoid lineages. (B) A leukemic stem cell derived from the myeloid lineage produces immature, intermediately differentiated blasts at the expense of producing healthy blood cells of the myeloid lineage. *Images adapted from Servier Medical Art by Servier, licensed under CC BY 3.0.*

Variable genetic alterations can result in the transformation to AML, creating heterogeneous leukemic cell populations between patients and within an individual[4,5]. With evidence that patient outcomes are inextricably linked to leukemia genetics, the search for genes which can serve as prognostic markers for AML has become increasingly important[6]. Currently prognostics are stratified based on a particular set of genes which include tyrosine kinases and transcription factors involved in proliferation, differentiation, and survival[6]. Cytogenics and molecular genetic tests provide a means to assess these molecular alterations[6].

*1.1.2 Epidemiology*

The genetic defects from which AML arises can be hereditary, resultant from a blood disorder, or caused by exposure to a mutagenic agent (e.g. radiation, benzene, formaldehyde, or past chemotherapy)[7,8,9]. Adult AML is considered separately from childhood AML, for which the latter's prognoses are typically more favourable[10]. In 2010, there were 1215 new cases and 971 deaths from adult AML in Canada, with the median age of diagnosis being 66[11,12]. With a five year survival rate of less than 30% in Canada, there is a pressing need to uncover targeted therapies with better efficacy and fewer side effects than the current gold standard treatment[10,13].

*1.1.3 Treatment of AML*

Since the early 1970's the gold standard chemotherapy for AML has consisted of cytarabine combined with an anthracycline[14]. Cytarabine, an antimetabolite drug, exerts its effects by combining a cytosine base with arabinose instead of deoxyribose, thus disrupting DNA replication[15]. Anthracyclines such as daunorubicin, doxorubicin, and idarubicin, intercalate with DNA and inhibit the action of topoisomerase II, the enzyme responsible for creating transient breaks in the phosphodiester backbone to facilitate the un-winding of tangled DNA during replication[13,16,17].

As cancer is often attributed to uncontrollable cell replication, inhibiting essential processes in the replication cycle is a commonly harnessed therapeutic option[18]. In many cancers, increased proliferation contributes to replication-associated DNA damage which renders cancer cells more sensitive to drugs targeting DNA repair pathways[18]. Unfortunately, the effectiveness of these therapy options is limited by the susceptibility of healthy replicating cells to succumb to the same fate[19]. Furthermore, DNA damage in healthy cells can result in the development of secondary malignancies and dose-limiting toxicities [20]. Small advances in the study of cancer cell dysfunction continues to yield promise for the discovery of more selective therapies.

## 1.2 Autophagy

Cellular homeostasis is dependent on a balance of synthesis and destruction of cellular components. Though other mechanisms provide a means to achieve protein catabolism (e.g., the ubiquitin proteasome system), autophagy is unique in its ability to attend to the bulk of cellular components[21]. At basal level, autophagy acts as a mechanism of quality control; however, it can be initiated in response to cellular stress as an adaptive survival mechanism to increase the turnover of cellular components to release their basic units for the cell's immediate needs[22]. Research in this field continues to uncover new proteins and functions, allowing for a better understanding of cellular homeostasis.

### *1.2.1 Discovery [Types, Terminology]*

Analyses of the starvation response in yeast in the early 1990s paved the way for our current understanding of the molecular basis of autophagy, and allowed for the identification of 40 autophagy-related (ATG) proteins, most of which have now been described in mammals[23,24]. These proteins, along with a variety of other signaling and modulating molecules, mediate the complex sequence of membrane remodeling and trafficking pathways that are necessary for targeted destruction of intracellular components.

The most common classification system of autophagy is based on differences in the substrate to be degraded and the mode of delivery to the lysosome, which contains digestive hydrolases. Macroautophagy (the focus of this research, and hereby referred to as just "autophagy") refers to autophagy involving a double-membraned vacuole known as the autophagosome, which sequesters cytoplasmic components in either a bulk or cargo-specific manner before fusing with a lysosomal vacuole[25]. In contrast, microautophagy implies the direct uptake of cytoplasmic components by the lysosomal vacuole, which again can function in a bulk or cargo-specific manner[25,26,27]. Finally, chaperone-mediated autophagy (CMA) denotes a form of autophagy in which proteins are recognized at specific motifs and delivered to a lysosome by a chaperone protein[28]. Figure 1.2 depicts the three kinds of autophagy.

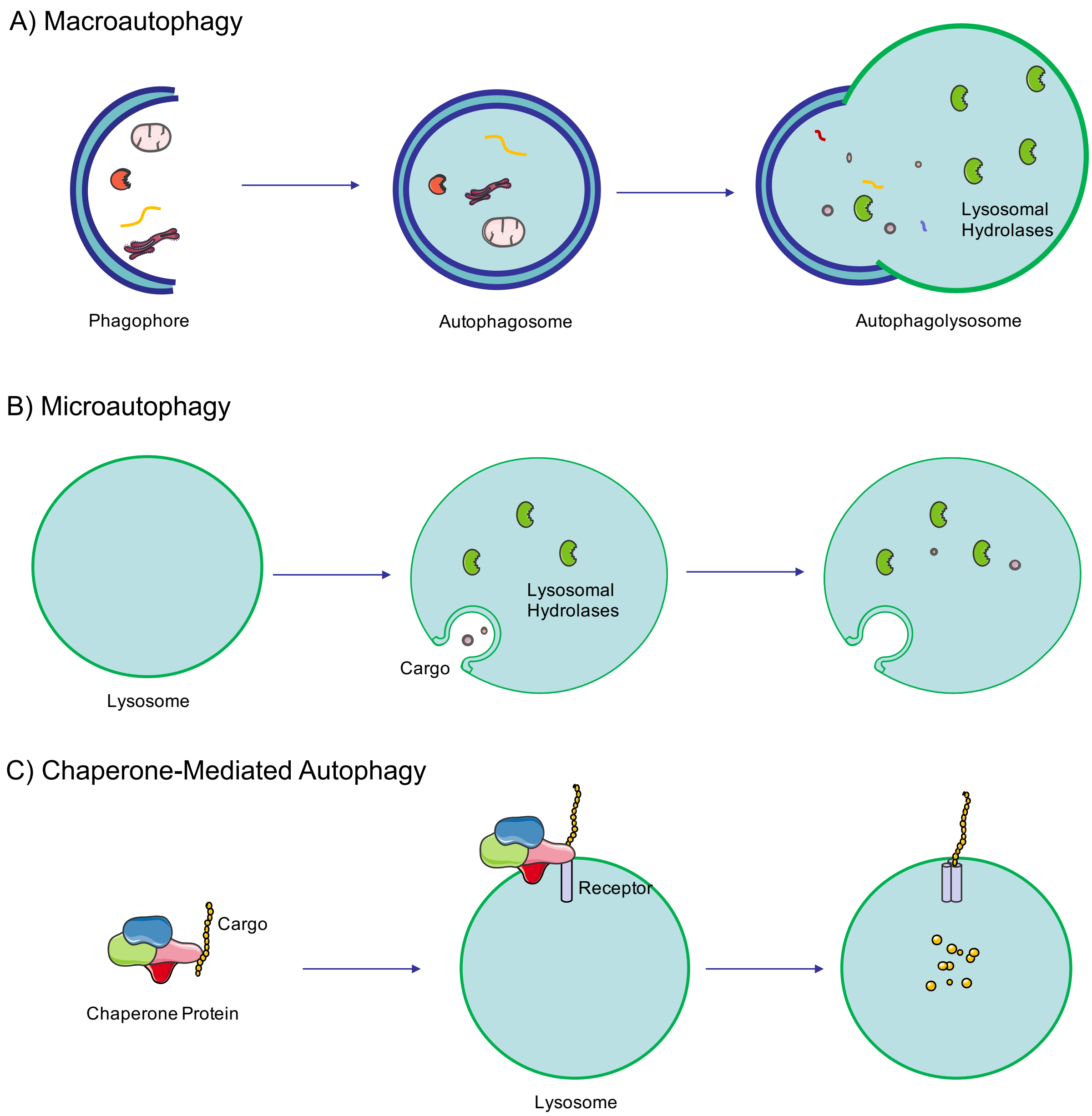


**Figure 1.2 Types of Autophagy**
A) Macroautophagy refers to autophagy involving a double-membraned vesicle called an autophagosome, which sequesters cellular components before fusing with a lysosome containing hydrolases[25]. B) Microautophagy is the direct uptake of cellular components, which are digested by lysosomal hydrolases[25]. C) Chaperone-mediated autophagy involves a chaperone (ex. HSC70 and co-chaperones) which binds KFERQ-motif containing substrates and brings them to a lysosomal receptor (ex. LAMP2A) where it will be degraded[200]. *Images adapted from Servier Medical Art by Servier, licensed under CC BY.*

While autophagy was initially regarded as a simple bulk process in which a portion of cytoplasm was engulfed in response to cell stress, we now know that cargo-selective autophagy mechanisms also exist and are both common and necessary for a variety of homeostatic and cell-specific tasks[29]. Autophagy can target mitochondria (mitophagy), peroxisomes (pexophagy), ribosomes (ribophagy), lipid stores (lipophagy), the endoplasmic reticulum (ERphagy), etc. with specificity attributed to cargo recruitment receptors[30]. Figure 1.3 depicts bulk autophagy, specific autophagy, and chaperone-mediated autophagy.

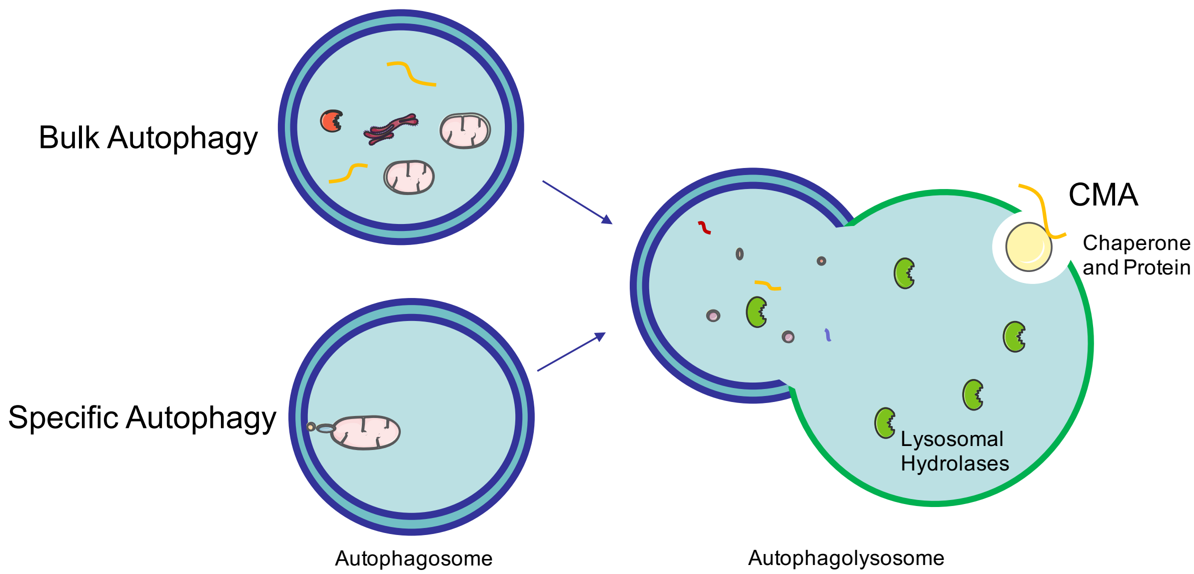


**Figure 1.3 Specificity in Autophagy**
Autophagy can be bulk, specific, or mediated by chaperone proteins[201]. *Images adapted from Servier Medical Art by Servier, licensed under CC BY.*

*1.2.2 Initiation and General Pathway*

Autophagy begins with nucleation of an isolation membrane (or "phagophore") which can be derived from various sources, such as the plasma membrane, endoplasmic reticulum, Golgi complex, or mitochondrial membrane[31]. The isolation membrane will enclose the target particle(s) to create an autophagosome, and subsequently bind to a lysosome, forming an autolysosome or autophagolysosome, in which the cargo will be degraded[32]. Autophagy is closely linked to endocytosis, a means by which cells absorb extracellular material, and as such, an autophagosome may fuse with an endosome to produce an amphisome, which will then fuse with a lysosome for degradation[32]. Several signaling cascades have been reported to regulate autophagy. The major control complexes for autophagy are the mammalian target of rapamycin (mTOR) and an upstream regulator of mTOR, 5' adenosine monophosphate-activated protein (AMPK), both of which phosphorylate unc-51 like activating kinase I (ULK1) on different residues to initiate or repress autophagy respectively[33]. Ultimately, inputs regarding stress, nutrient deprivation, and energy levels converge on the mTOR/AMPK pathways to regulate autophagy [33]. In the context of these inputs, autophagy is initiated when ULK1 (ATG1) is activated, resulting in it phosphorylating ATG13 and FIP200 to create the initiation complex, and Beclin 1, which enhances the activity of ATG14L-containing VPS34 complexes, causing nucleation[34]. The newly discovered protein ATG101 has also been shown to phosphorylate ATG13 and FIP200 and complex with ATG13[35]. Two ubiquitin-like conjugation systems are also involved in initiation: the first is the ATG12-ATG5 system (which is formed when ATG12 is activated by ATG7, and transferred to ATG10 before being covalently linked to ATG5, and subsequently forming a complex with ATG16)[36,37]. The second is the  system, in which  (ATG8) is cleaved by the protease ATG4B to form LC3-I (which resides in the cytosol), then conjugated to phosphatidylethanolamine (PE) by ATG7 and ATG3 to generate LC3-II[34,36,38]. LC3-II is involved in joining cargo to the autophagosome and additionally in the closure of the phagophore[39]. Figure 1.4 depicts mTOR-dependent autophagy.

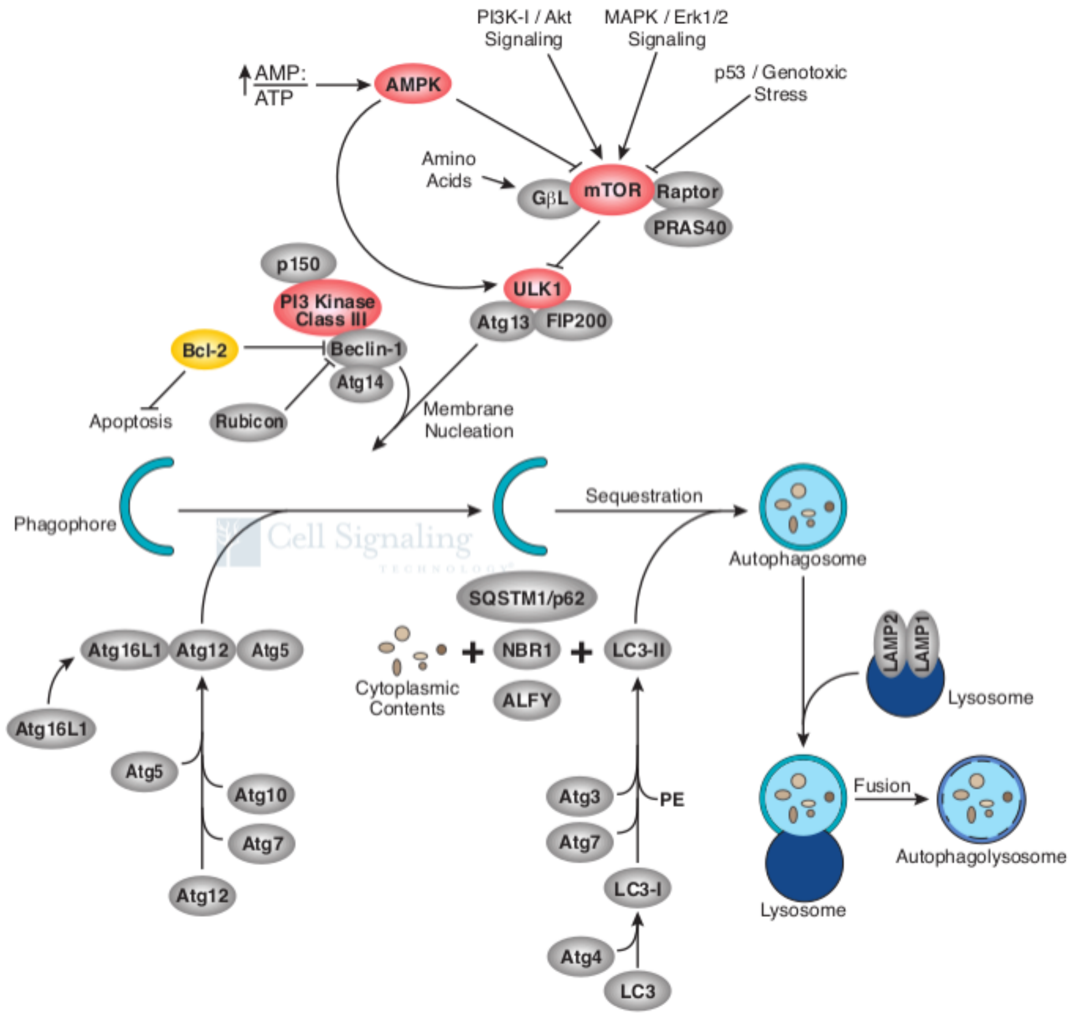


**Figure 1.4 Macroautophagy**
mTOR-dependent autophagy is initiated by inhibition of mTOR, which leads to a complex cascade of signaling events which mediate membrane nucleation, elongation, and sequestration of cargo[33]. *Illustration reproduced courtesy of Cell Signaling Technology, Inc. (www.cellsignal.com)*

*1.2.3 Regulation of Autophagy*

As previously mentioned, inputs regarding starvation, energy availability, and cellular stress converge at the AMPK and mTOR pathways, which will in turn activate or repress autophagy directly to maintain cellular homeostasis[33]. Recent studies have also demonstrated the existence of mTOR-independent pathways: where 1) ERK-mediated induction of cyclin E increases cAMP signaling, resulting in enhanced recruitment of Beclin 1 and the formation of autophagosomes, and 2) cAMP/EPAC appears to inhibit autophagy by activation of complex signaling involving the cAMP-Epac-Rap2B-PLC-ε-IP3 and $Ca2^{+}$-calpain-Gsα pathways[40,41,42,43]. When initiated by distress, autophagy is believed to be unspecific in the nature of the cargo targeted, often called "bulk autophagy" or "cargo independent" autophagy[34]. Autophagy which is tightly regulated to maintain a functional pool of organelles, or remove a specific set of organelles during development, is called "selective autophagy" or "cargo-dependent/cargo-specific autophagy"[34]. Selective autophagy requires the efficient coordination of autophagosome formation and cargo recruitment to effectively clear out organelles – however the sequence in which these two events occur has yet to be determined[44,29]. It is possible that pre-existing isolation membranes may be recruited to tagged cargo, or alternatively, the cargo itself may signal and induce the formation of an isolation membrane to form around it. Regardless of the order, selectivity for substrates is mediated by autophagy receptors which accumulate on the surface of the target organelle and directly or indirectly link to the autophagosome[30].

### *1.2.4 Mitophagy*

As the powerhouse of the cell, mitochondria produce ATP by utilizing the proton motive force (Δp) generated by sequential reduction of electrons though the complexes of the electron transport chain (ETC)[45]. The electron transport chain is a main site of production of reactive oxygen species (ROS): highly reactive molecules capable of propagating oxidative chain reactions and causing cellular damage[46]. As a result, a healthy pool of mitochondria must be maintained by tight quality control[47]. In some cell types, mitochondria are removed completely during development, and mitophagy serves as the mechanism to achieve this[48,49].

Programmed mitochondria clearance is well described in the eye lens and in red blood cell/reticulocyte maturation[48,49]. In both cases, the selective clearance of mitochondria appears to be stimulated by upregulation of the gene BNIP3L, producing a protein called NIX, which has the ability to cause mitochondrial membrane depolarization[48,49]. Following loss of mitochondrial membrane potential, PTEN-induced putative kinase 1 (PINK1) localizes to the outer mitochondrial membrane, where it resides in its full-length, active form[50]. PINK1 phosphorylates ubiquitinated proteins on the outer mitochondrial membrane and additionally phosphorylates and activates the E3 ubiquitin ligase, Parkin, which then ubiquitinates proteins on the outer mitochondrial membrane to become substrates for PINK1, resulting in an amplification of the mitophagy signal[51,52,53,54,55,56]. Finally, the phosphorylated ubiquitin chains will recruit signal amplification factors such as tank-binding kinase 1 ( TBK1), and autophagy receptors such as neighbor of BRCA1 gene 1 (NBR1), optineurin (OPTN), nuclear dot protein 52 (NDP52), tax1-binding protein 1 (TAX1BP1), autophagy and Beclin 1 regulator 1 (AMBRA1) and sequestome-1 (p62) which associate with various autophagosome-associated factors via their -interacting regions (LIR) to deliver the autophagy machinery[57,58,59,60].

The above scenario provides an example of ubiquitin-mediated autophagy, a process by which poly-ubiquitinated mitochondria are recognized and recruited to the autophagosome via autophagy receptors. In addition to induction during specific stages of cell development, ubiquitin-mediated autophagy is common to mitochondria which have altered mitochondrial membrane potential due to damage. In other cases, autophagy may be receptor-mediated, with a specific receptor found on the surface of the mitochondria forming the link to an autophagosomal factor via its -interacting region (LIR)[59]. Some known mitochondrial membrane receptors are BCL2/Adenovirus E1B 19kDa Interacting Protein 3 (BNIP3), BCL2/Adenovirus E1B 19kDa

Interacting Protein 3-Like (NIX), fun14 domain-containing 1 (FUNDC1) and the phospholipid cardiolipin (CL)[59]. Research in this area continues to explore the specific contexts in which each protein recruits the autophagosome, however; evidence suggests the existence of redundancy in the system[55]. Furthermore, many of the factors involved in autophagic recruitment possess numerous roles in diverse cellular processes, leading to complexity in the study and targeting of autophagy in disease.

*1.2.5 Autophagy Defects in AML*

Although a relatively recent discovery, several studies have shown that the loss of autophagy genes and reduction in gene products is a characteristic of leukemia. Activation of the Akt/mTOR pathway (and thus repression of autophagy) has been shown to be essential for leukemia cell propagation[61]. Mice lacking ATG7 in the hematopoietic system displayed increased myeloproliferation which resembled human myelodysplastic syndromes and developed into AML[62]. Similarly, mice lacking FIP200 in the hematopoietic system displayed increased myeloproliferation combined with a significant decrease in healthy blood cell maturation[63]. The parallel effects of these studies support the hypothesis that autophagic dysfunction produced these phenotypes [64,65,66]. AML cells with a mutation in splicing factor U2AF35 (common in both AML and MDS patients) have been shown to inefficiently produce the essential autophagy factor ATG7 leading to defective autophagy[67]. The dysfunctional ATG7 pre-mRNA produced by these cells was found in primary patient samples with this mutation[67]. The mitochondrial depolarizing factor and autophagy receptor NIX has been shown to be downregulated in high-risk MDS and further decreased after disease progression to AML[68]. A recent in silico analysis of AML showed that several autophagy genes are found within chromosomal regions commonly heterozygously deleted in AML, and these deletions were accompanied by decreased expression of mRNA for many of these genes[69]. The same study examined primary patient samples and found decreased expression of autophagy genes in the dominant blast cell population compared to the blast marker negative population[69]. With evidence of various autophagy defects in cancer, and a link between the genes that regulate autophagy, carcinogenesis, and cell death, it is clear that autophagy plays a complex role in cancer. As such, the effect of modulating autophagy now holds considerable promise for cancer therapy.

*1.2.6 Multiple Roles of Autophagy Proteins*

Adding complexity to an already intricate system, the majority of autophagy-related proteins play various autophagy-independent functions in cell signaling and homeostasis[70]. Of specific interest to this study, all three proteins of interest (i.e., ATG7, NIX, and p62) are involved in cell death/survival pathways. ATG7, which within the context of autophagy activates one of the ubiquitin-like conjugation systems and additionally is involved in conjugating PE to LC3-I to form LC3-II, has been shown to modulate p53/TP53 activity to regulate cell cycle and survival during metabolic stress[71]. NIX, which is able to depolarize the mitochondrial membrane and acts as a mitophagy receptor, is also known to be an apoptosis inducer and potentially also a tumor suppressor[72,73]. Finally, p62, a mitophagy receptor protein, has been shown regulate cell proliferation, tumorigenesis, and act as a signaling hub for apoptosis[74,75,76]. Indeed, autophagy is not the isolated mechanism it was once believed to be; it is inseparably connected to major signaling pathways in the cell where it is capable of modulating growth, development, survival and death.

### 1.3 Proteins of Interest

Since an all-encompassing study of autophagy proteins was not feasible, we focused our study instead on three autophagy proteins which would serve to exemplify autophagy deficiency at two key stages: autophagosome formation (ATG7), and cargo recruitment (p62 and NIX). Autophagy protein ATG7 was selected to provide key data on deficiency of all types of autophagy, as it is essential for activation of the two ubiquitin-like conjugation systems which guide autophagosome formation[36]. As dysregulated mitochondria are a common feature of AML – characterized by increased mitochondrial mass, low mitochondrial spare reserve capacity, and a dependence on mitochondrial fatty acid oxidation for cell proliferation – we additionally selected two factors involved in mitochondrial autophagy[77,78,79]. NIX and p62 both serve as mitochondrial receptors whereby they guide the recognition and sequestration of mitochondria to the autophagosome[80,81,82,83,84]. These two proteins differ in their mode of attachment and sequestration – NIX, found on the mitochondrial membrane, contains an LIR domain allowing for linkage to LC3-II found on the autophagosome, while p62 binds to ubiquitin on mitochondria (a modification which serves as a tag for degradation), and also links to LC3-II on the autophagosome via an LIR domain[30,59,85]. Figure 1.5 provides a visual depiction of the roles of these proteins.

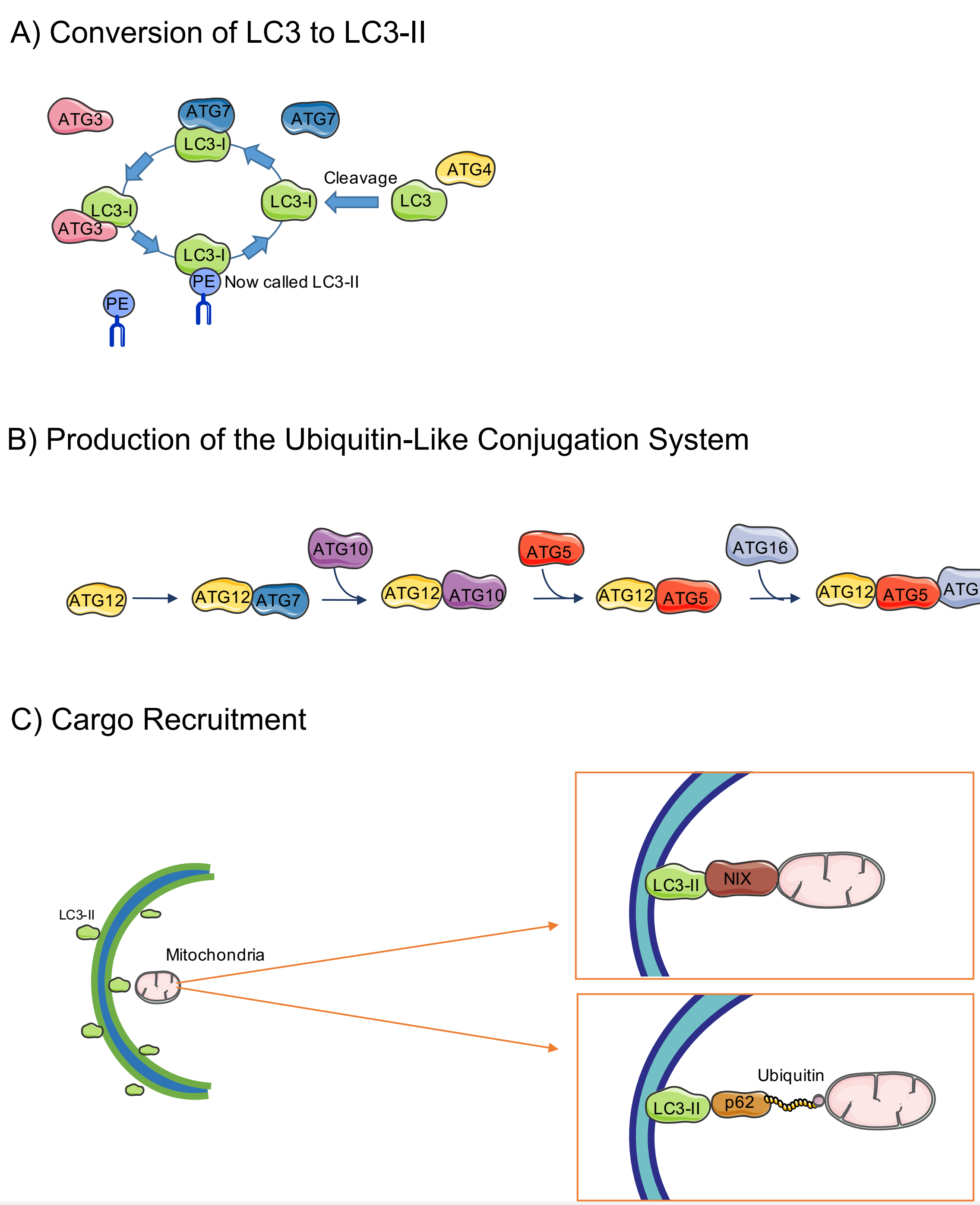


**Figure 1.5 Roles of Selected Autophagy Proteins in Autophagy**
A) ATG7 plays a role in the conjugation of LC3-I to phosphatidylethanolamine[36]. B) ATG7 is also involved in production of one of the ubiquitin-like conjugation systems which is essential for autophagy induction[36]. C) NIX (box above) is an autophagy receptor found in mitochondria which has an LIR domain for binding to LC3-II on the phagophore[81]. p62 (box below) is an autophagy receptor which binds ubiquitinated mitochondria and has an LIR domain for binding to LC3-II on the phagophore[60,202]. *Images adapted from Servier Medical Art by Servier, licensed under CC BY.*

# Chapter 2: Rationale, Objectives, and Hypothesis

## 2.1 Targeting Autophagy in Cancer

There is currently a pressing need to understand the settings in which autophagy should be targeted in order to optimize cancer therapeutics and overcome drug resistance. The paradox of autophagy provides two different modulating schemes whereby: 1) upregulation of autophagy confers advantage to cells with high metabolic needs or therapy-induced cellular stress by recycling unnecessary or dysfunctional cellular components; it would appear best to inhibit autophagic activation so that the cells will succumb to the therapy; and 2) activation of autophagy permits the clearance of fusion oncoproteins or a reduction in organelles necessary for the cell to survive, it would be best to initiate autophagy. Several agents for each class have been described and proposed as potential anticancer therapeutics to be used on their own, or in combinatorial treatments[86].

Recent studies have indicated that disruption of various homeostatic signaling pathways such as mTOR, AMPK, and Akt are potential targets for inducing pro-death autophagy in cancer cells[87,88,89,90,91,92,93]. The addition of the mTOR inhibitor ciclopirox, an antifungal agent, to the established preclinical anti-leukemia agent parthenolide, demonstrated greater toxicity against AML than either compound independently[94]. The induction of autophagy through drugs targeting AML fusion oncoproteins (e.g. AML1-eight-twenty-one (ETO) targeting drugs) had a pro-survival effect, however, combined treatment of the AML1-ETO–targeting drugs with the mTOR-inhibiting agent chloroquine increased cell death, indicating that autophagy activators and inhibitors could even be used as a combinatorial therapy[95]. Arsenic trioxide ($As_2O_3$) inhibits cell proliferation in a manner dependent on autophagic induction[96,97]. To prove the essential nature of autophagy in this mechanism, HL60 (human promyelocitic leukemia) cells were treated with the autophagy inhibitor 3-methyladenine (3-MA) after $As_2O_3$, which attenuated the cell death[97]. Interestingly, the addition of 3-MA prior to treatment with $As_2O_3$ potentiated cell death[97]. These conflicting results ultimately led to the conclusion that autophagy was inhibitory in the initiation stage of $As_2O_3$-induced apoptosis, however it amplified $As_2O_3$-induced apoptosis post-initiation, demonstrating the temporal complexity of autophagy-targeting[97].

Given that autophagy may confer survival advantage to cells via recycling of cellular components, autophagy inhibitors also show potential as anti-cancer therapeutics[86]. Indeed, Class-III-PI3K inhibitors such as 3-MA, mentioned above, inhibit the formation of autophagosomes and have been shown to enhance the effects of various chemotherapy and radiation-based treatments[98,99,100]. The inhibitor of vacuolar ATPase, bafilomycin $A_1$, which prevents the fusion of autophagosomes and lysosomes, and autophagosome-degradation inhibitor chloroquine have both been shown to increase the cytotoxicity of other anticancer medications[101,102,103].

As some cancers have been found to display characteristics similar to dysfunctional autophagy systems, understanding the role and modulating potential of autophagy in cancer has become a subject of great interest. While the effects of targeting autophagy in cancer are complex, the modulating potential of this pathway provides novel ways to eliminate cancer cells and increase the efficacy of other treatments.

## 2.2 Rationale of Study

This project aimed to explore the relationship between autophagy and AML using genetic silencing of autophagy genes ATG7, SQSTM1 and BNIP3L. In particular, we were interested in the response of these cells to a panel of drugs with hopes of defining the value of using autophagy genes as a marker for tailored chemotherapy with mitochondrial-targeting agents.

## 2.3 Objectives

1. Produce knockdown AML cell lines of genes ATG7, BNIP3L, and SQSTM1, and describe changes in mitochondrial phenotype in these cell lines compared to the transduced control.
2. Characterize the effects of these autophagy deficiencies on chemotherapy efficacy using DNA-targeting and mitochondrial-targeting drugs.

## 2.4 Hypothesis

AML cell lines with knockdown in autophagy genes ATG7, BNIP3L, or SQSTM1 will accumulate mitochondrial dysfunctions resulting in increased sensitivity to mitochondrial-targeting drugs, but not DNA-targeting drugs compared to the transduced control AML cell line.

# Chapter 3: Materials and Methods

## 3.1 Cell Culture

### *3.1.1 Growth Media*

Acute myeloid leukemia (OCI-AML2) cell lines were cultured in Iscove's Modified Dulbecco's Medium (IMDM; Fischer Scientific, Grand Island, NY) supplemented with 10% fetal bovine serum (FBS; Sigma, St. Louis, MO) and 2% penicillin-streptomycin (Sigma, Product of USA). All cell lines were grown in T25 or T75 vented filter cap tissue culture flasks (Sarstedt, Product of Germany) and incubated in a humidified air atmosphere containing 5% $CO_2$ at 37°C.

### *3.1.2 Lentiviral Transduction to Produce Knockdown Cell lines*

OCI-AML2 cells were brought to a concentration of 5 x $10^6$ cells/mL, spun down, and re-suspended in 6.5 mL of media containing protamine sulphate (5 μg/mL), 1 mL of virus cocktail (containing virus carrying the short hairpin RNA (shRNA) sequence and a gene for puromycin resistance). Following incubation overnight at 37°C, the cells were centrifuged and then washed and re-suspended in fresh puromycin media (1 ug/mL). Subsequent culturing of these cells was done with 1 ug/mL puromycin to maintain knockdown. A shRNA scramble sequence was used to produce the transduced control (TRC) cell line. The shRNA coding sequences are shown in table 3.1.

**Table 3.1 shRNA Coding Sequences for Lentiviral Transfection**

| Gene | ID | Vector # (Sigma-Aldrich) | shRNA Coding Sequence (5'-3') |
|---|---|---|---|
| *ATG7* | #6 | TRCN0000007588 | CCGGCCAAGGTCAAAGGACGAAGATCTCGAGATCTTCGTCCTTTGACCTTGGTTTTT |
| *ATG7* | #9 | TRCN0000007586 | CCGGGCTTTGGGATTTGACACATTTCTCGAGAAATGTGTCAAATCCCAAAGCTTTTT |
| *BNIP3L (NIX)* | #1 | TRCN0000298517 | CCGGTATTGTCACAGTAGCTTATTTCTCGAGAAATAAGCTACTGTGACAATATTTTTG |
| *BNIP3L (NIX)* | #3 | TRCN0000007846 | CCGGGCTAGGCATCTATATTGGAAACTCGAGTTTCCAATATAGATGCCTAGCTTTTT |
| *BNIP3L (NIX)* | #5 | TRCN0000007847 | CCGGCAGTCAGAAGAAGAAGTTGTACTCGAGTACAACTTCTTCTTCTGACTGTTTTT |
| *SQSTM1 (p62)* | #11 | TRCN00000435931 | CCGGTGCCTAATGGCTTTCACTTTCCTCGAGGAAAGTGAAAGCCATTAGGCATTTTTTG |
| *SQSTM1 (p62)* | #12 | TRCN00000431509 | CCGGGAGGATCCGAGTGTGAATTTCCTCGAGGAAATTCACACTCGGATCCTCTTTTTTG |
| *Scramble Control* | TRC | TRCN0000007847 | CCGGCAGTCAGAAGAAGAAGTTGTACTCGAGTACAACTTCTTCTTCTGACTGTTTTT |

## 3.2 Growth and Size Analysis

### *3.2.1 Cell Counting*

Cells were counted approximately every other day (during scheduled cell replication analysis; every day) using a hemocytometer. To enumerate the cells, cells were diluted in 10x Trypan Blue stain (Gibco by Life Technologies, Grand Island, NY) at a 1:1 ratio, and 10 µL of this mixture was loaded onto the hemocytometer. The number of cells in adjacent sections was counted, added, and multiplied by $10^6$ to obtain the cells/mL concentration.

### *3.2.2 Cell Size Analysis*

Average cell size for each cell line was determined in triplicate on separate days using the Multisizer 4 Particle Analyzer (Beckman Coulter). Approximately 1 x $10^5$ – 1 x $10^6$ cells were diluted 1:20 in PBS (to a final volume of 10 mL) and then loaded into the machine for average cell size determination.

### *3.2.3 Colony Growth Formation Assay*

Colony growth formation assays determine the ability of a cell to proliferate indefinitely, thereby producing a large colony or clone. In this assay, $10^3$ cells were added to 3 ml of MethoCult GF H4434 medium (StemCell Technologies) containing 30% FCS, 1% BSA, 1% methylcellulose in IMDM, 10 ng/mL recombinant human IL-3, 3U/mL recombinant human erythropoietin, $10^{-4}$ M 2-mercaptoethanol (2ME), 2mM L-glutamine, 50 ng/mL recombinant human stem cell factor, 10 ng/mL recombinant human granulocyte macrophage-colony stimulating factor. Cells in this medium were plated at 1.1 mL per 35mm dish (in duplicate) using a blunt-tip syringe. Duplicate dishes were kept alongside a dish containing only distilled water (humidity control), within a single 100 mm Petri dish. The plates were then incubated at 37°C for one to two weeks, after which time the number of colonies was enumerated. A colony is defined as a cluster of 50 or more cells[104].

## 3.3 Quantitative PCR

### *3.3.1 Sample Preparation and Analysis*

Genomic DNA samples were isolated using the Purelink Genomic DNA Mini Kit (Invitrogen, Product of USA) according to the manufacturer protocol (eluted with 150 µL elution buffer). The concentration of gDNA was measured using a Nanodrop 200c at 260nm (Thermo Scientific). Quantitative PCR was performed in triplicate on a 96-well plate probing for the mitochondrial gene NADH dehydrogenase 1 (ND1) alongside the nuclear control gene beta globin (HBB). To each well, 10 µL Maxima SYBR Green/ROX qPCR Master Mix (Thermo Scientific), 6 µL Nuclease-free water (Thermo Scientific), 1 µL PrimePCR Assay HBB, Hsa (Bio-Ra; Product of USA), or 1 µL PrimePCR Assay MT-ND1, Hsa (Bio-Rad; Product of USA) and 3 µL of 25 ng/ µL template DNA was added. For negative controls, 3 µL of nuclease-free water was added instead of DNA template. For positive controls, 3 µL of PrimePCR Template

(Bio-Rad) was added instead of DNA template. The qPCR assay was run on the StepOnePlus Real-Time PCR System (Applied Bioscience). Initial gDNA content was determined using the ΔΔCT method[105].

## 3.4 Cell Stress Analysis

### *3.4.1 Serum Starvation*

Cells were grown up to approximately 1.5 x$10^6$ cells/mL in 50 mL of media over the course of 3 days. On the day of the assay, the cells were spun down at 1200 RPM for 5 minutes and re-suspended in Hank's buffered saline solution (HBSS; Fischer Scientific, Grand Island, NY) to starve the cells. Samples of 7 mL were removed and centrifuged (1200 RPM x 5 minutes) at set time intervals (0, 5, 10, 30, 60, 90, 120 minutes) following the switch into HBSS. The samples were then re-suspended in 500 mL PBS and transferred into a 1.5 mL Eppendorf tube before centrifuging again for 1 minute at 13.2 x $10^3$ RPM, after which the PBS was removed and the pellet frozen for future lysis. Proteins Beclin 1, ATG7, , NIX, and p62 were selected to provide key information on the process of autophagy at various atages (initiation, elongation, and recruitment, respectively). Information pertaining to Western blotting (protein size, antibody concentrations, etc.) is found in section 3.5, table 3.2.

## 3.5 Western Blotting

### *3.5.1 Protein Collection*

Cells were collected as a pellet following centrifugation at 1200 RPM, washed with cold PBS, and then lysed with a 2:1 ratio of cold Radioimmunoprecipitation assay (RIPA) buffer

(Sigma-Aldrich; St. Louis, MO) for 20 minutes on ice. The cells were then centrifuged at 1.32 x $10^4$ RPM for 20 minutes at 4°C and the supernatant was collected.

*3.5.2 BSA/BCA Assay*

The total protein content of the supernatant was quantified using the BCA protein assay, in which a set of standards of BSA (Sigma-Aldrich, Product of USA) diluted in distilled water at 0, 20, 40, 60, 80, and 100 mg/ mL were compared against the acquired protein samples (diluted tenfold). The standards and samples were plated on a 96-well plate, and to each well, 200 µL of bicinchoinic acid (BCA) working reagent was added (containing 50 parts BCA to one-part copper II sulphate (Sigma Aldrich). The optical density was measured at 527 nm using the SpectraMax Pro M5 spectrophotometer and SoftMax V5 software. Samples were then prepared to contain 30 µg of total protein with 1/6 sample buffer volume (50% w/v sucrose, 7.5% w/v SDS, 62.5 mM Tris-HCl at pH 6.8, 2 mM EDTA at pH 7, 3.1% w/v DTT (DL-Dithiothreiol), 0.01% bromophenol blue) and topped to 30 µL with extra RIPA buffer. The prepared samples were stored in an -80°C freezer.

*3.5.3 SDS-PAGE and Immunoblotting*

Proteins were separated by size using sodium dodecyl sulphate polyacrylamide gel electrophoresis (SDS-PAGE). Samples were boiled at 95°C for five minutes to denature the protein, after which 20 µL of the samples were loaded into the wells of a 10-12% polyacrylamide gel and run at 150 V on a Mini Trans-Blot Cell (Bio-Rad) containing electrophoresis buffer (25 mM Tris base, 190 mM glycine, 3.5 mM sodium dodecyl sulphate) until the loading dye reached the bottom of the cell (45 minutes-1 hour). Proteins were transferred from the gel to a polyvinyl difluoride (PVDF) membrane (Bio-Rad) in transfer buffer (25 mM Tris base, 190 mM glycine, 20% v/v methanol) using a Trans-Blot semi-dry transfer cell set to 25V for 45 minutes. Membranes were blocked in 5% BSA (Sigma-Aldrich; St. Louis, MO) in Tris-buffered saline (TBS-T: 20 mM Tris base (TBS) plus 0.1% Tween) for 1 hour at room temperature on a rocker, followed by two rinse washes and a 5 minute rocker wash with TBS-T. Blocking was followed by incubation with the desired primary antibody in 5% BSA-TBST overnight on a rocker at 4°C. Membranes were then subjected to two rinse washes, a 15-minute rocker wash, and three 5-minute rocker washes with TBST. Afterwards, the membrane was incubated with the appropriate secondary antibody in 5% BSA-TBST for 1 hour at room temperature on a rocker. Following this, membranes were rinsed twice, then washed for 15 minutes and five 5-minute rocker washes with TBST. Membranes were incubated for five minutes in Clarity Western ECL Substrate (Bio-Rad, Product of USA), and promptly transferred (via a plastic sleeve) to the Kodak 4000MM Pro Imaging Station (using Kodak Molecular Imaging Software) for visualization of the proteins. Relative levels of luminescence were assessed by region of interest (ROI) markers and compared to a control protein. Proteins of interest are shown in Table 3.2 below.

**Table 3.2 Proteins of Interest for Western Blotting**

| Primary Antibody | Isotype | Molecular Weight (kDa) | Dilution | Catalog Code | Manufacturer |
|---|---|---|---|---|---|
| NIX | Rabbit | 38, 76 | 1:700 | D4R4B | Cell Signaling |
| P62 | Rabbit | 60 | 1:1000 | 5114 | Cell Signaling |
| Beclin 1 | Rabbit | 60 | 1:1000 | D40C5 | Cell Signaling |
| ATG7 | Rabbit | 78 | 1:1000 | D12B11 | Cell Signaling |
| | Rabbit | 14,16 | 1:300 | D11 XP (R) | Cell Signaling |
| GAPDH (Control) | Mouse (Conj.) | 37 | 1:15000 | GA1R | Thermo Scientific |
| α-tubulin (Control) | Mouse | 55 | 1:1000 | TU-02: sc 8035 | Santa Cruz Biotechnology |

## 3.6 Flow Cytometry

### *3.6.1 Cell Staining for Analysis of Mitochondrial Health*

Cells were plated in triplicates on a 96-well flat bottom plate (Sarsedt, Product of Germany) at 2 x $10^5$ cells/well and then centrifuged at 1200 RPM on a plate spinner for five minutes, allowing for removal of media. Cells were re-suspended in 200 µL of a dye-PBS mixture at a given concentration (see table 3.3) and incubated at 37°C for 20 minutes. Following incubation, the cells were centrifuged at 1200 RPM on a plate spinner for 5 minutes and re-suspended in 200 µL PBS/ well. The plate was then placed in the Guava easyCyte 8HT Bench Top Flow Cytometer (Millipore) using GuavaSoft 3.1.1 (Millipore) flow cytometry software., set to acquire 5000 events per well.

Four fluorescent dyes were chosen to probe for various elements of mitochondrial health: DHE, H2DCFDA, Rho 123, and NAO. The first, dihydroethidium (DHE), is a cell-permeant dye which is oxidized by the ROS superoxide ($O_2^{\cdot -}$) to generate a fluorescent product[106]. The second, dihydrodichlorofluorescein diacetate (H2DCFDA), is a dye which undergoes two-electron oxidation in the presence of peroxides (notably: hydrogen peroxide ($H_2O_2$) produced by a variety of oxidase enzymes) and other ROS such as nitrate and hypochlorous acid to generate the fluorescent product 2', 7' dichlorodihydrofluorescein (DCF)[107]. Importantly, $H_2O_2$-dependent oxidation of H2DCF is dependent on ferrous iron (as found in cytochrome c)[108]. H2DCF is unable to react directly with superoxide[109–111]. The third, NAO binds to cardiolipin, a component of the inner mitochondrial membrane, giving an approximate quantitative measure of mitochondrial mass [112]. Finally, the fourth dye, Rho 123, is a cationic dye readily sequestered by mitochondria in a relationship proportional to the negative (hyperpolarized) mitochondrial membrane potential [113]. In all analyses, a spherical marker was used to exclude debris and dying cells from the forward vs side scatter plots, as apoptosis is associated with increased ROS and altered membrane potentials[114]. Table 3.3 provides pertinent information relating to flow cytometry analysis.

**Table 3.3 Concentrations of Fluorescent Dyes Used as Mitochondrial Health Probes**

| Dye | Concentration Per Well (diluted in PBS) (uM) | Excitation/ Emission | Channel Used for Probe | Manufacturer |
|---|---|---|---|---|
| NAO | 0.35 uM | 518/530[112] | Green | Enzo Life Sciences |
| Rhodamine 123 | 0.6 uM | 507/529[115] | Green | Enzo Life Sciences |
| DHE | 3 uM | 518/605[116] | Yellow | Sigma-Aldrich |
| DCF | .0.15 uM | 490/520[116] | Green | Sigma-Aldrich |

*3.6.2 Dose-Response Analysis and Propidium Iodide Staining for Measuring Cell Viability*

In order to produce dose response curves, cells were plated in triplicate on a 96-well flat-bottom plate at 1.8 x $10^5$ cells/well in 95 µL of new media. To this, 5 µL of drug was added to produce the desired final concentration, after which the remaining wells on the plate (outer edges) were filled to 100 µL with PBS, the plate was wrapped with saran wrap, and incubated in a humidified air atmosphere containing 5% $CO_2$ at 37°C for 72 hours (3 days). Table 3.4 provides information relating to the drugs used in the dose-response.

**Table 3.4 Drugs, Solvents, and Manufacturer Data**

| Drug | Solvent | Manufacturer |
|---|---|---|
| Avocatin B | DMSO | Microsource |
| Cytarabine | $H_2O$ | Tocris Bioscience |
| Daunorubicin | $H_2O$ | Tocris Bioscience |
| Doxorubicin | $H_2O$ | Sigma-Aldrich |
| FCCP ( Carbonyl cyanide 4 (trifluoromethoxy)phenylhydrazone) | DMSO | Sigma-Aldrich |
| Oligomycin | DMSO | EMD Chemicals |
| Rapamycin | DMSO | Tocris Bioscience |
| Rotenone | DMSO | Millipore |
| Tigecycline | DMSO | Sigma-Aldrich |

The mechanisms of these drugs are as follows:

1. Cytarabine is an antimetabolite drug which interferes with DNA synthesis by combining a cytosine base with arabinose instead of deoxyribose[15]

2. Doxorubicin and daunorubicin are anthracyclines which impart their activity by intercalating with DNA and subsequently inhibiting the progression of DNA topoisomerase II[16].
3. Avocatin B is an inhibitor of fatty acid oxidation that accumulates in the mitochondria [117,118].
4. FCCP is a protonionophore and uncoupler of oxidative phosphorylation, which exerts its effects by dissipating the mitochondrial membrane potential, leading to ATP depletion and increased ROS production[119].
5. Oligomycin is an ATP synthase inhibitor which acts by blocking the proton channel necessary for the oxidative phosphorylation of ADP to ATP. As a result, movement of the electron transport chain is greatly reduced, leading to mitochondrial destabilization and ultimately cell death[120,121].
6. Rapamycin is an inhibitor of mTOR complex 1[122].
7. Rotenone is an electron transport chain (ETC) inhibitor which acts by blocking the ETC between NADH dehydrogenase (complex I) and CoQ, thereby blocking the formation of the proton motive force (PMF) required for the oxidative phosphorylation of ADP to ATP. Again, movement of the electron transport chain is halted, leading to mitochondrial destabilization and consequently cell death[123,124].
8. Tigecycline is an inhibitor of mitochondrial translation and inhibitor of mitochondrial function[77].

Propidium iodide is a DNA intercalating agent that is only able to permeate dead cells[125]. As a result, it is commonly used to quantify the dead cells in a population. Following incubation, cells were re-suspended in buffered PI (1% PI (Biovision), 2% BSA in PBS), and read immediately on the Guava easyCyte 8HT Bench Top Flow Cytometer (Millipore) using GuavaSoft 3.1.1 (Millipore) flow cytometry software at 2500 events/ well.

## 3.7 Statistical Analyses

### *3.7.1 One-Way ANOVA and Dunnett Multiple Comparisons Test*

A one-way analysis of variance (ANOVA) is a statistical technique used to identify significant differentces within a set of measurements[126]. This analysis tests the null hypothesis that samples from two or more groups have have the same mean values[126]. The null hypothesis is rejected if the computed p value is smaller than the significance level: α[126]. For our purposes, we used $\alpha = 0.05$. Dunnett's multiple comparisons test is a followup to ANOVA which compares every mean to the control mean – in our case, the transduced control: TRC[127]. This test allows for computation of multiplicity-adjusted p values – i.e the smallest significance level applied to the family of comparisons at which the comparison of interest will be deemed statistically significant[128]. One-way ANOVA and Dunnett's tests were performed using Graphpad Prism 6.0 Software (Graphpad Software Inc.).

### *3.7.2 Unpaired T-Tests*

T-tests are similar to the one-way ANOVA in their goal of identifying significant differences, however they only compare two data sets[126]. T-tests compute p values which are compared to the chosen significance level ($\alpha = 0.05$) to determine if the null hypothesis should be accepted or rejected[126]. T-tests were performed using Graphpad Prism 6.0 Software (Graphpad Software Inc.).

# Chapter 4: Results

## 4.1 Confirmation of knockdown

Western blot analysis of protein expression was performed to assess gene knockdown for the NIX, ATG7, and SQ cell lines. Band intensity of each protein was compared and normalized to the loading control, GAPDH, as shown in figures 4.1 A-C. TRC represents the transduced scramble control cell line.

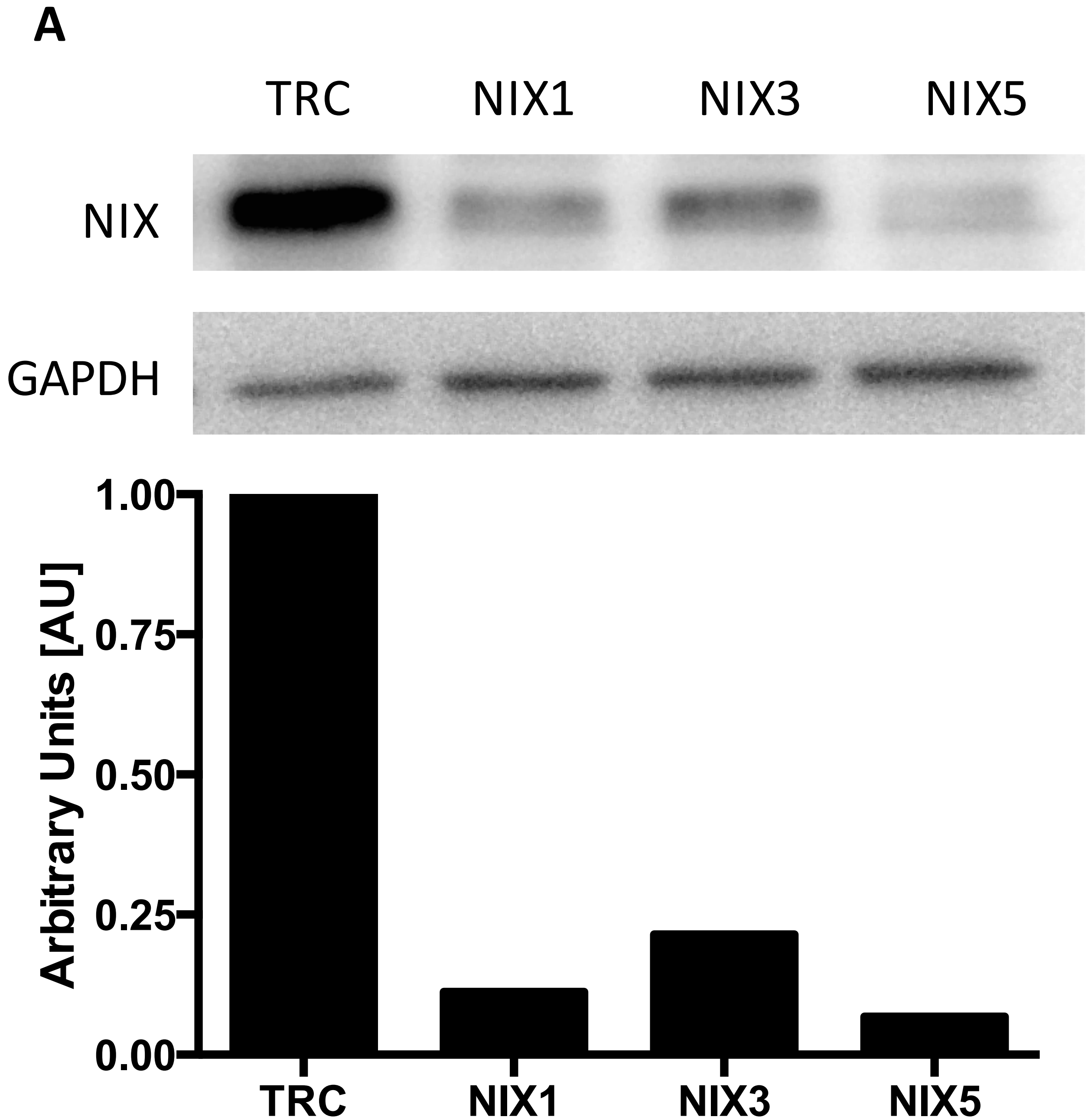


**Figure 4.1A shRNA Knockdown of Autophagy Gene BNIP3L**
Autophagy gene BNIP3L (protein: NIX, cell line IDs: NIX1, NIX3, NIX5) was successfully knocked down by lentiviral mediated shRNA and confirmed by immunoblotting.

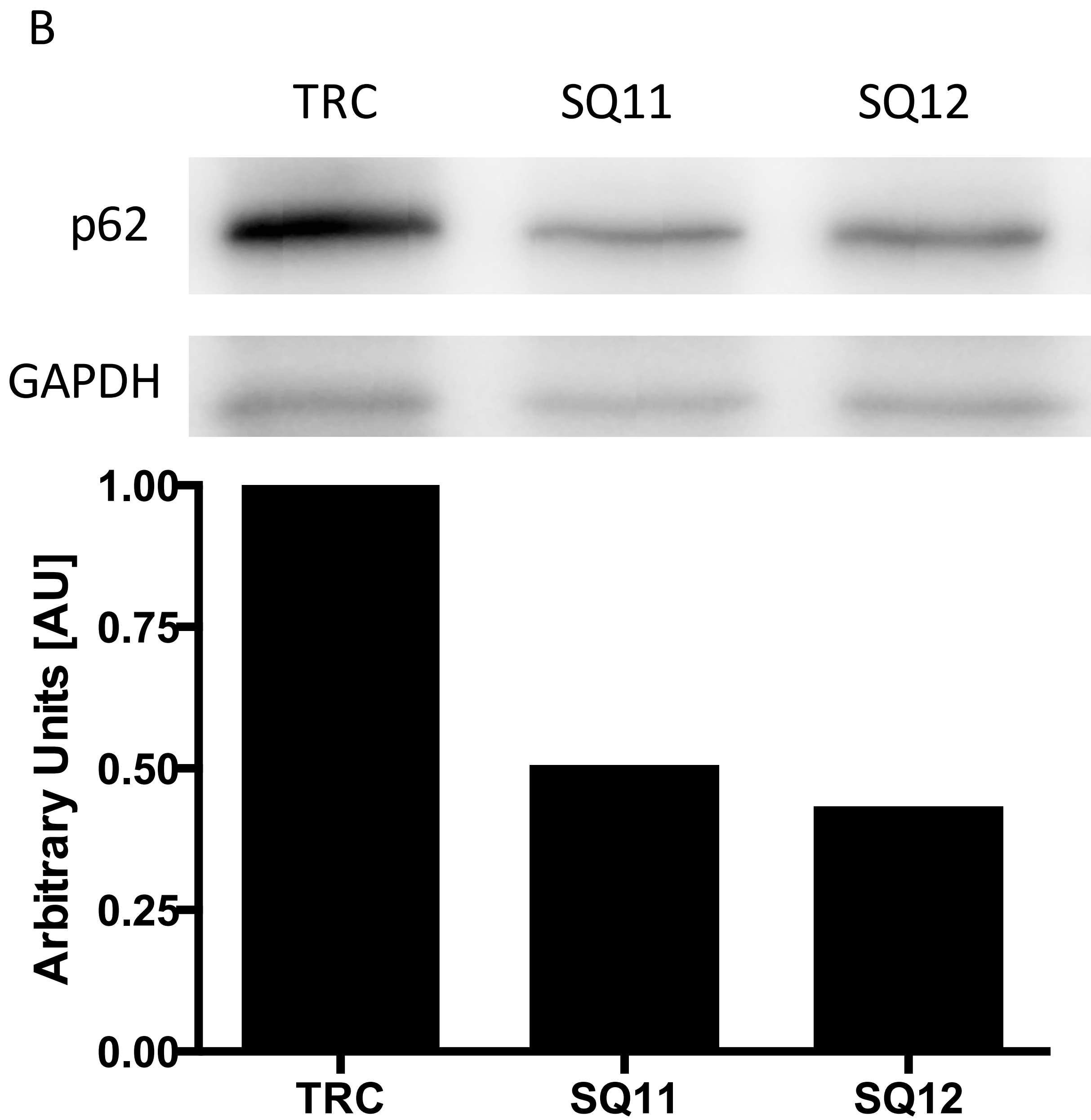


**Figure 4.1B shRNA Knockdown of Autophagy Gene SQSTM1**
Autophagy gene SQSTM1 (protein: p62, cell line IDs: SQ11, SQ12) was successfully knocked down by lentiviral mediated shRNA and confirmed by immunoblotting.

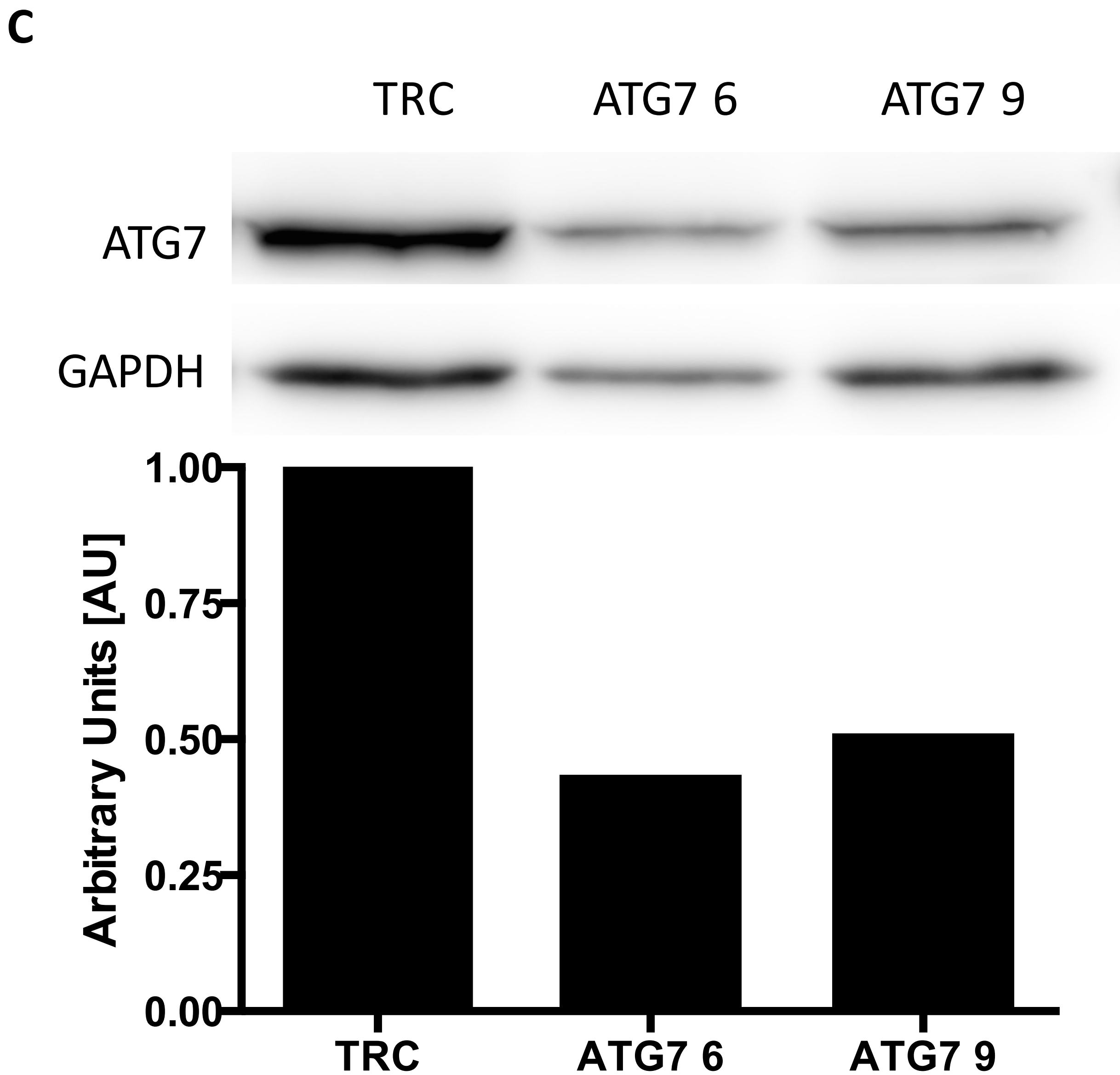


**Figure 4.1C shRNA Knockdown of Autophagy Gene ATG7**
Autophagy gene ATG7 (protein: ATG7, cell line IDs: ATG7 6, ATG7 9) was successfully knocked down by lentiviral mediated shRNA and confirmed by immunoblotting.

As shown in figures 4.1 A-C, all three genes were successfully knocked down. NIX protein expression was reduced to 10-30% of TRC levels, p62 protein expression was reduced to 40-50% of TRC levels and ATG7 protein expression was reduced to 40-50% of TRC levels.

### 4.2 Cell Proliferation Assay

Viable cells were enumerated over the course of 3-4 days to assess the effects of gene knockdown on cell proliferation. Data was normalized to the previous day to give the population doubling (PD) per 24 hour period as shown in the equation below[129].

$$PD = \frac{Count\ on\ Day\ 2}{Count\ on\ Day\ 1}$$

The data was then normalized to the starting population doubling value. Population doubling data is shown in figures 4.2 A- C for the NIX, SQ, and ATG7 cell lines respectively.

A

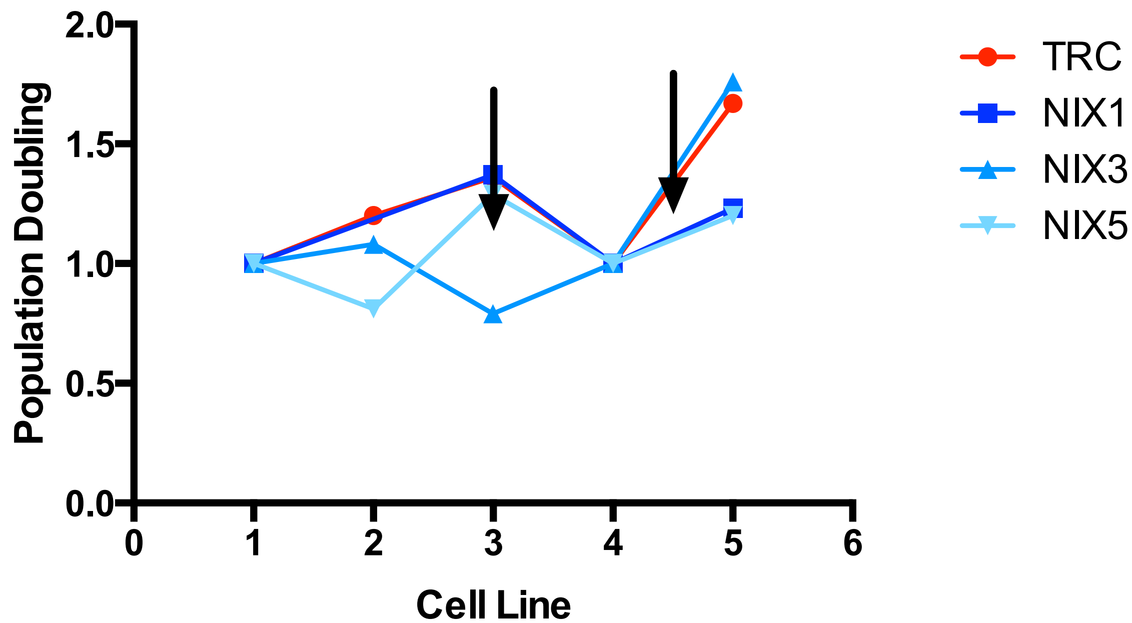


**Figure 4.2A Cell Proliferation for the NIX (BNIP3L KD) Cell Lines Measured by Daily Cell Counts**
Two non-consecutive data sets are displayed. Arrows indicate the starting population doubling value to which subsequent values are normalized.

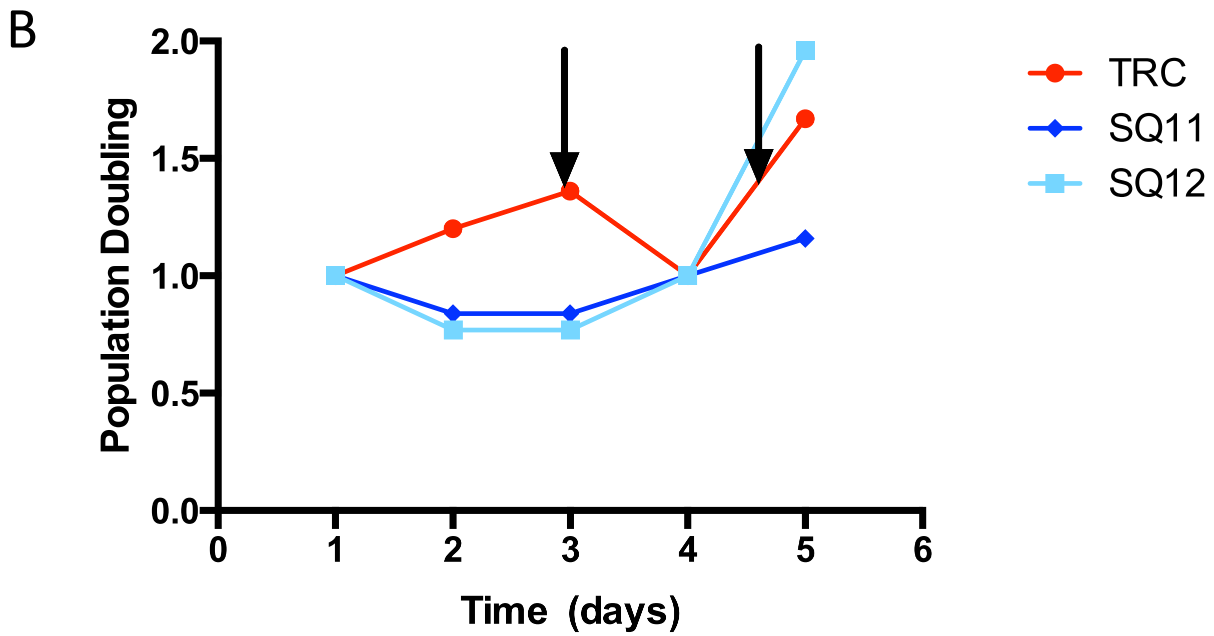


**Figure 4.2B Cell Proliferation for the SQ (SQSTM1 KD) Cell Lines Measured by Daily Cell Counts**
Two non-consecutive data sets are displayed. Arrows indicate the starting population doubling value to which subsequent values are normalized.

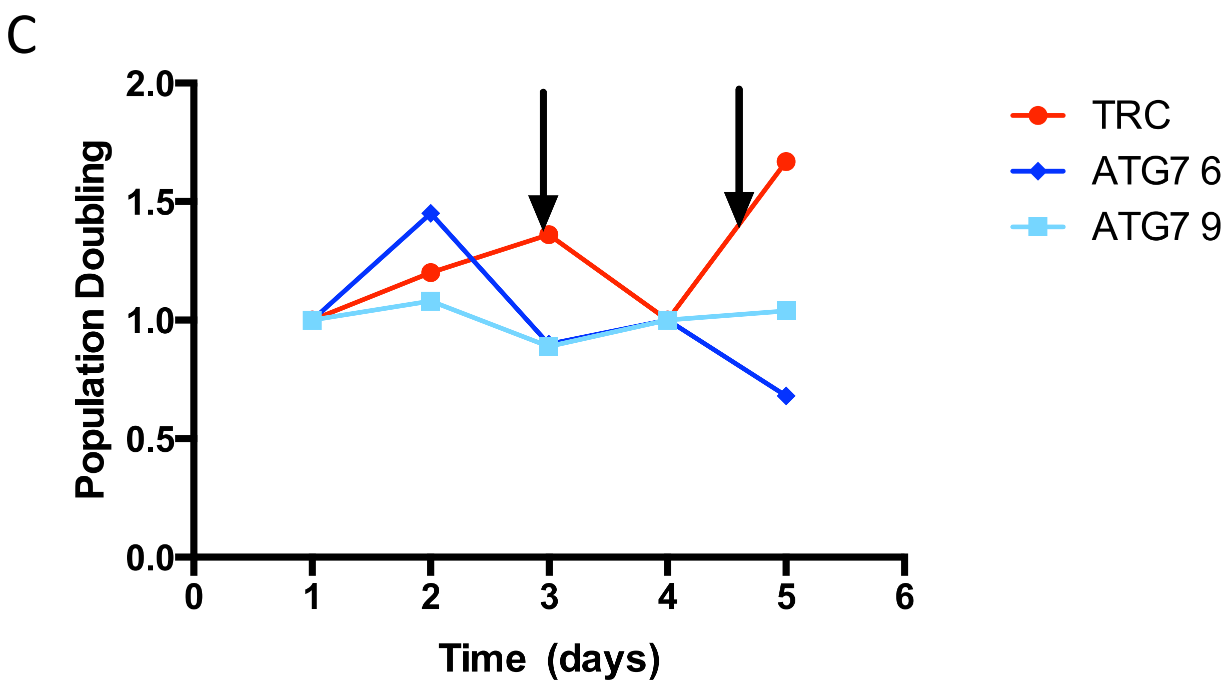


**Figure 4.2C Cell Proliferation for the ATG7 (ATG7 KD) Cell Lines Measured by Daily Cell Counts**
Two non-consecutive data sets are displayed. Arrows indicate the starting population doubling value to which subsequent values are normalized.

As shown in figures 4.2 A-C, cell proliferation was altered as a result of autophagy gene knockdown. Unlike the TRC cell line, for which proliferation increased over the count days in a stepwise manner, most knockdown cell lines either showed decreased proliferation or bi-directional changes in proliferation rate.

**4.3 Cell Size Measurements**

Cell size was measured using the Multisizer 4 Particle Analyzer (Beckman Coulter). Mean cell size values were obtained in triplicate. Averaged triplicate values are shown in figures 4.3 A-C for the NIX, p62, and ATG7 cell lines.

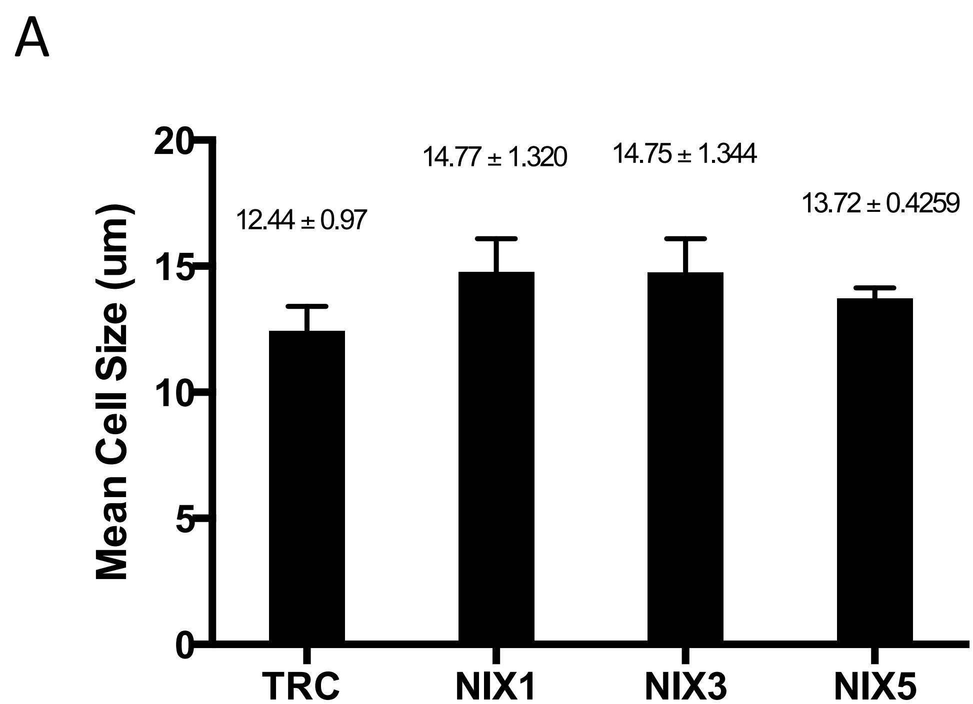


**Figure 4.3A Cell Size Measurements for the NIX (BNIP3L KD) Cell Lines**
Average cell size was measured in triplicate with n=3.

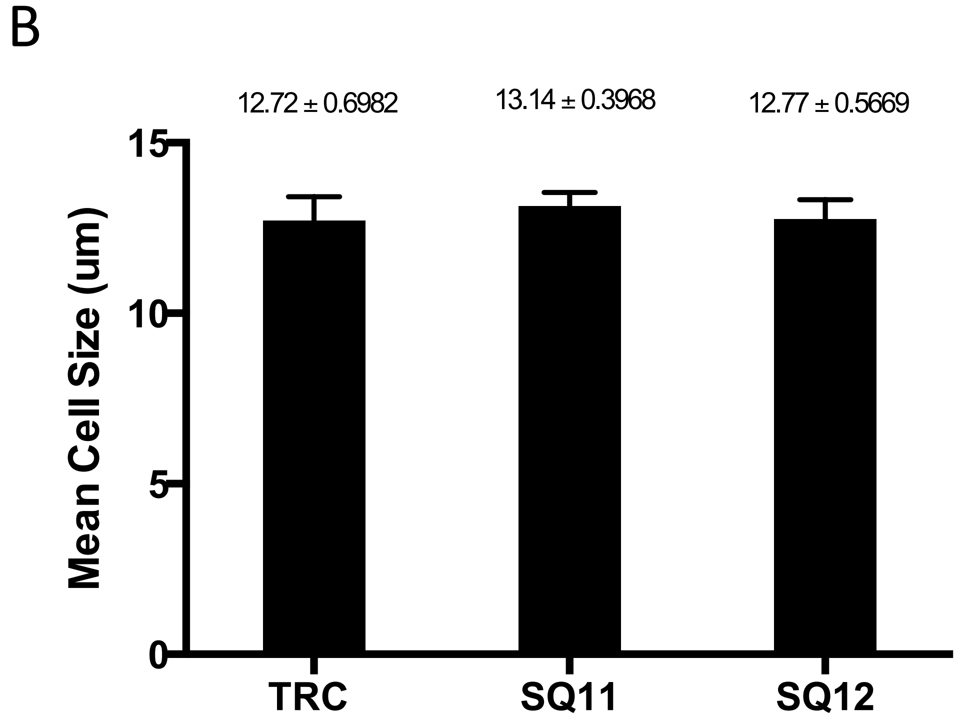


**Figure 4.3B Cell Size Measurements for the SQ (SQSTM1 KD) Cell Lines**
Average cell size was measured in triplicate with n=5.

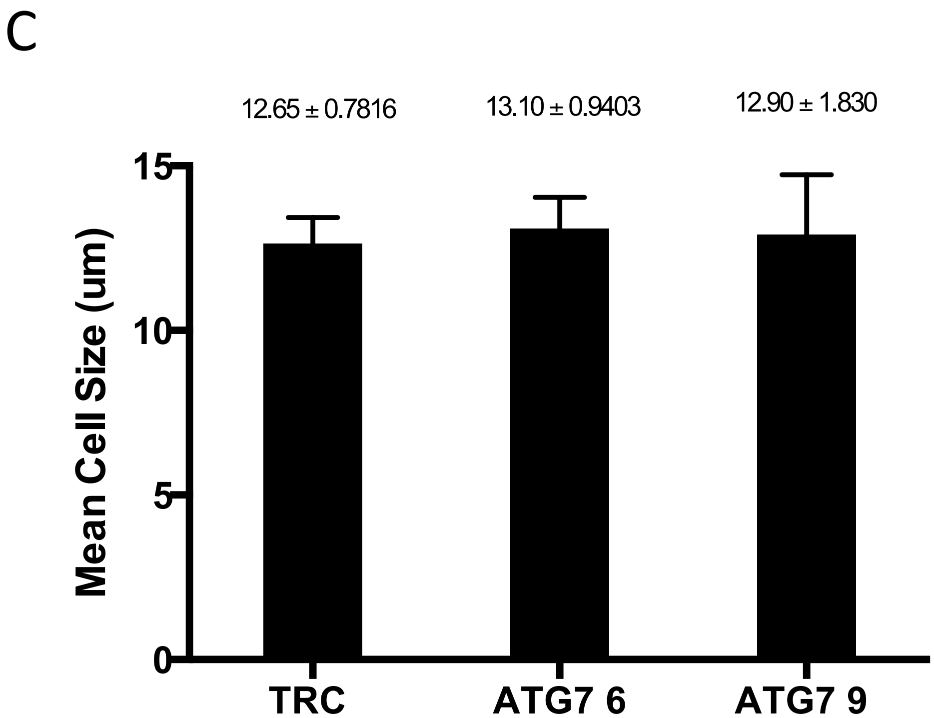


**Figure 4.3C Cell Size Measurements for the ATG7 (ATG7 KD) Cell Lines**
Average cell size was measured in triplicate with n=4.

As shown in figures 4.3 A-C, average cell size did not change with autophagy gene knockdown. A one-way ANOVA with a Dunnett's multiple comparisons test confirmed these changes to be statistically insignificant compared to TRC (ns $p>0.05$). The multiplicity adjusted p values are shown in table 4.1.

**Table 4.1 Multiplicity Adjusted P Values for Cell Size Measurements**

| Cell Line | Multiplicity adjusted p value |
|---|---|
| NIX1 | $F_8=2.644$; $p=0.0709$ |
| NIX3 | $F_8=2.621$; $p=0.0734$ |
| NIX5 | $F_8=1.454$; $p=0.3847$ |
| SQ11 | $F_{12}=1.165$; $p=0.4252$ |
| SQ12 | $F_{12}=0.1170$; $p=0.9900$ |
| ATG7 6 | $F_9=0.5009$; $p=0.8378$ |
| ATG7 9 | $F_9=0.2810$; $p=0.9443$ |

### 4.4 Colony Formation

Colony formation assays were also completed in triplicate for one knockdown cell line for each knockdown group. Colonies were grown in MethoCult GF H4434 medium for a period of 1 week at which time they were enumerated manually using a microscope. The number of colonies per dish set were averaged to get the colony count per dish. Triplicate measures were averaged and are shown in figures 4.4 A-C.

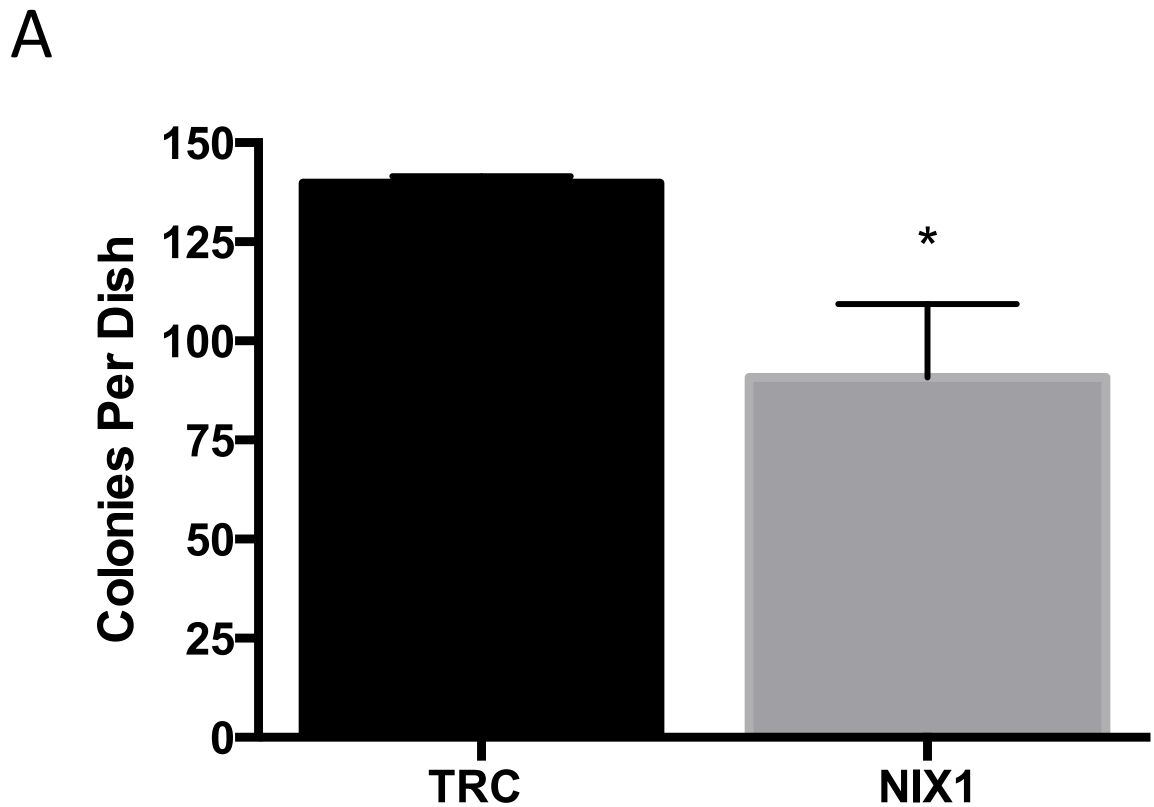


**Figure 4.4A Colony Growth Formation for the NIX1 (BNIP3L KD) Cell Line**
Average number of colonies grown in a one-week period was measured in triplicate. One TRC data point was rejected as an outlier after performing Grubb's test ($p<0.05$).
ns $p>0.05$, *$p\leq0.05$

B

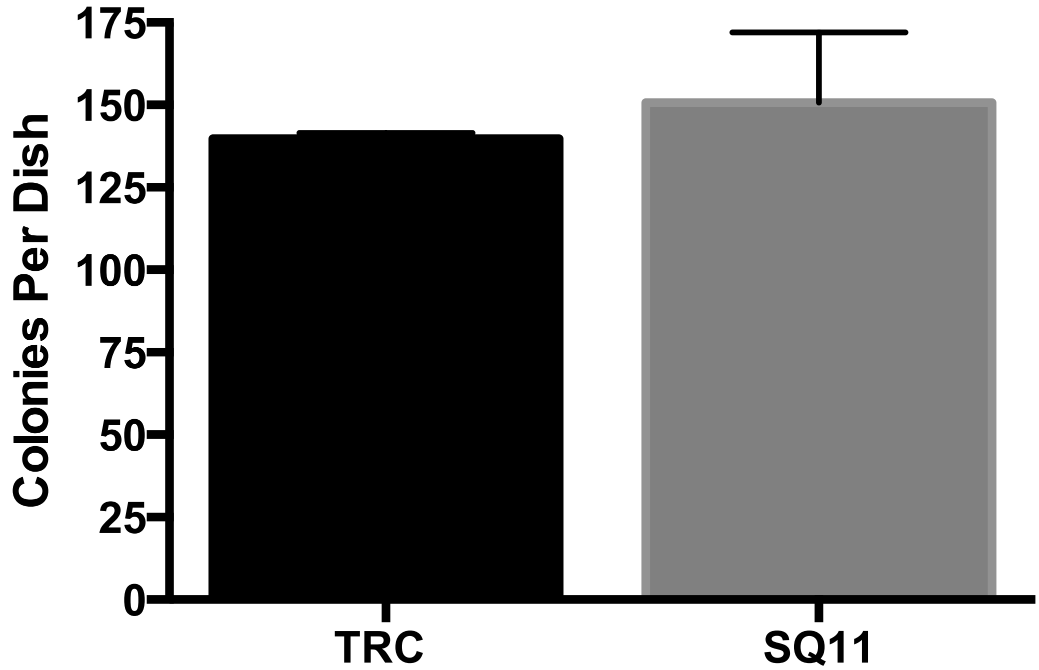


**Figure 4.4B Colony Growth Formation for the SQ11 (SQSTM1 KD) Cell Line**
Average number of colonies grown in a one-week period was measured in triplicate. One TRC data point was rejected as an outlier after performing Grubb's test ($p<0.05$).
ns $p>0.05$

C

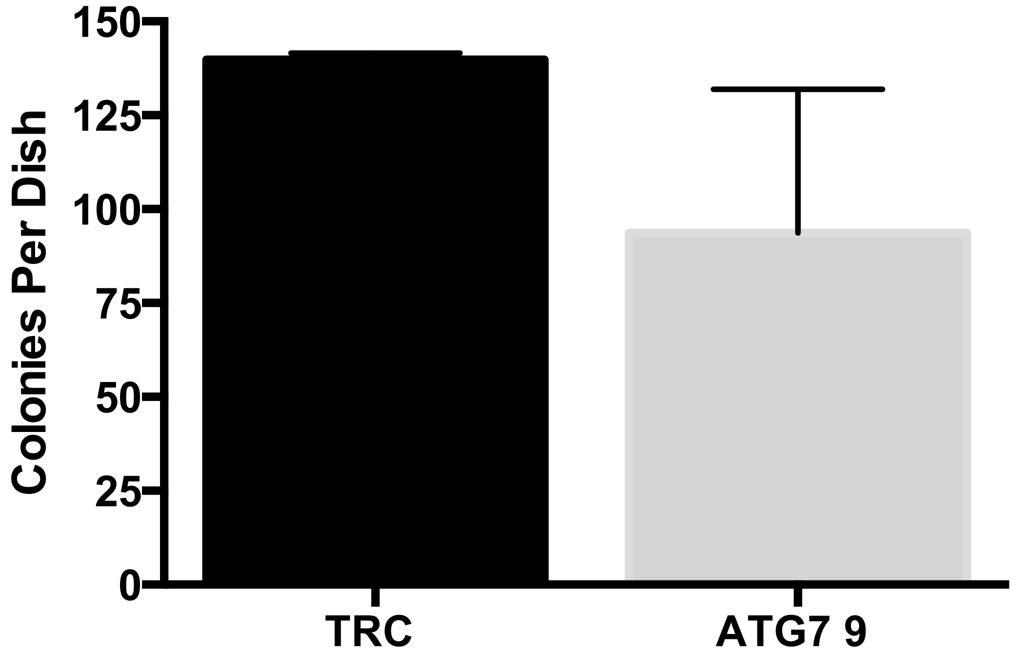


**Figure 4.4C Colony Growth Formation for the ATG7 9 (ATG7 KD) Cell Line**
Average number of colonies grown in a one-week period was measured in triplicate. One TRC data point was rejected as an outlier after performing Grubb's test ($p<0.05$).
ns $p>0.05$

Unpaired T-tests confirmed a statistically significant decrease in colony formation for the NIX1 cell line ($F_3=3.538$; $p=0.0384$), but not the SQ11 ($F_3=0.6854$; $p=5423$) or ATG7 ($F_3=1.614$; $p=0.2049$) cell lines when compared to TRC (ns $p>0.05$, *$p\leq0.05$).

## 4.5 Fluorescent Dyes as Probes for Mitochondrial Health

Fluorescence levels of DHE, DCF, and Rho 123 were measured using a Guavasoft flow cytometer to provide an assessment of superoxide levels. A single-assay representative graph of each triplicate measure is presented in figure 4.5A. Each measurement is normalized to the TRC cell line.

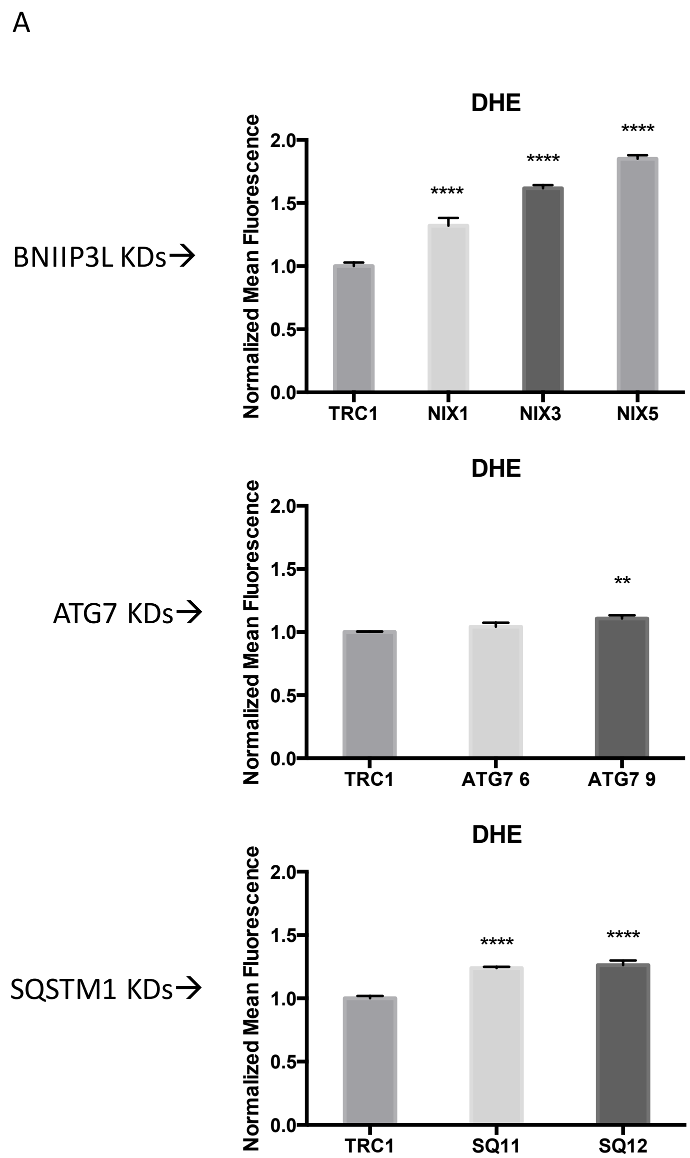


**Figure 4.5A Measuring Markers of Mitochondrial Health: Dihydroethidium (DHE)**
DHE levels are increased in almost all knockdowns indicating increased superoxide. Outliers in each measurement were rejected according to Grubb's test ($p<0.05$).
ns $p>0.05$, $*p\leq0.05$, $**p\leq0.01$, $***p\leq0.001$, $****p\leq0.0001$

Fluorescence levels of DCF were measured using a Guavasoft flow cytometer to provide an assessment of peroxide and other ROS levels. A single-assay representative graph of each triplicate measure is presented in figure 4.5B. Each measurement is normalized to the TRC cell line.

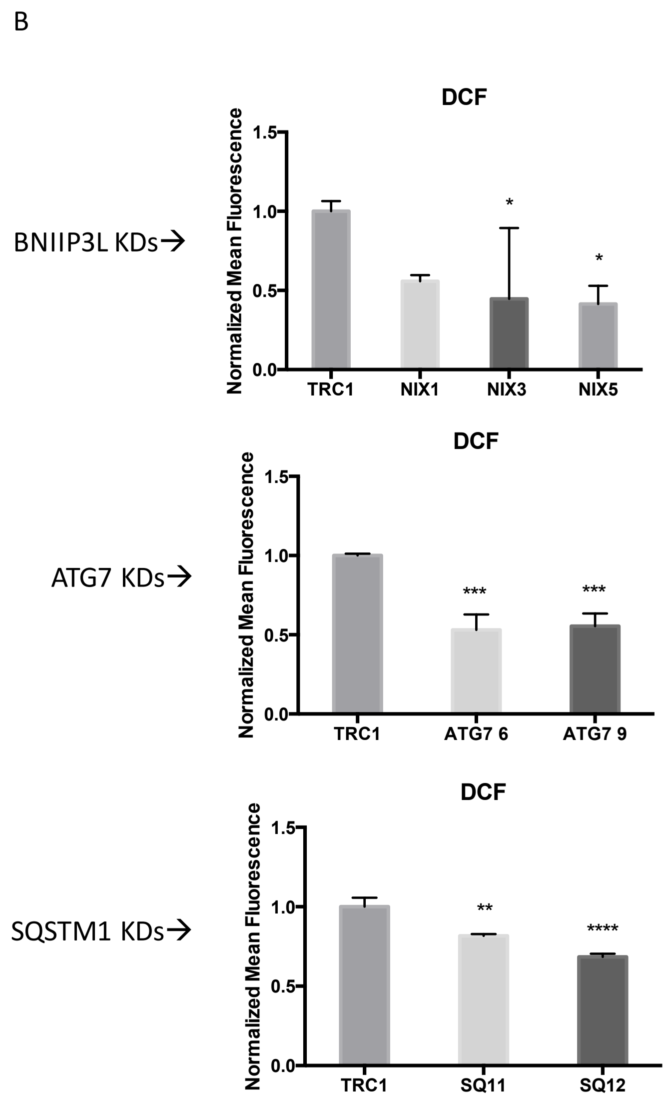


**Figure 4.5B Measuring Markers of Mitochondrial Health: Dichlorofluorescein (DCF)**
DCF levels are decreased in almost all knockdowns indicating decreased levels of peroxide and other ROS. Outliers in each measurement were rejected according to Grubb's test ($p<0.05$).
ns $p>0.05$, *$p\leq0.05$, **$p\leq0.01$, ***$p\leq0.001$, ****$p\leq0.0001$

Fluorescence levels of Rho 123 were measured using a Guavasoft flow cytometer to provide an assessment of the mitochondrial membrane potential. A single-assay representative graph of each triplicate measure is presented in figure 4.5C. Each measurement is normalized to the TRC cell line.

C

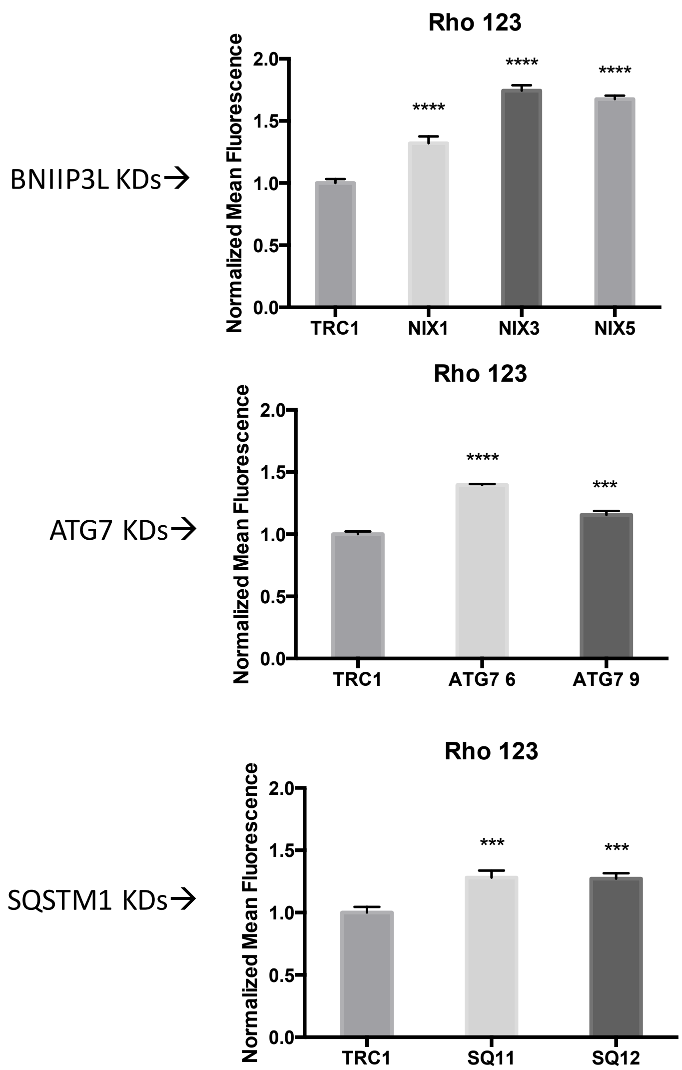


**Figure 4.5C Measuring Markers of Mitochondrial Function: Rhodamine 123 (Rho 123)**
Rho 123 levels are increased in almost all knockdowns indicating a hyperpolarized mitochondrial membrane potential. Outliers in each measurement were rejected according to Grubb's test ($p<0.05$).
ns $p>0.05$, *$p\leq0.05$, **$p\leq0.01$, ***$p\leq0.001$, ****$p\leq0.0001$

As shown in figures 4.5A-D, mean fluorescence of DHE was increased in all KD cell lines, indicating increases in the ROS superoxide[106]. DCF was decreased in all KD cell lines, indicating decreases in the ROS associated with this dye, which is particularly sensitive to hydrogen peroxide[107]. Levels of Rho 123 were increased in all KD lines indicating hyperpolarization of the mitochondrial membrane potential[113]. A one-way ANOVA with a Dunnett's multiple comparisons test was used to compare the mean of each knockdown to the mean of TRC (ns $p>0.05$, $*p\leq0.05$, $**p\leq0.01$, $***p\leq0.001$, $****p\leq0.0001$). Table 4.2 provides the multiplicity adjusted p values associated with each measurement.

**Table 4.2 Multiplicity Adjusted P Values for DHE, DCF, and Rho 123 Measurements**

| Cell Line | DHE | DCF | Rho 123 |
|---|---|---|---|
| NIX1 | $F_8=10.12$; $p<0.0001$ | $F_8=2.313$; $p=0.1159$ | $F_8=9.455$; $p<0.0001$ |
| NIX3 | $F_8=19.46$; $p<0.0001$ | $F_8=2.892$; $p=0.0491$ | $F_8=21.97$; $p<0.0001$ |
| NIX5 | $F_8=26.78$; $p<0.0001$ | $F_8=3.065$; $p=0.0380$ | $F_8=19.96$; $p<0.0001$ |
| SQ11 | $F_6=11.95$; $p<0.0001$ | $F_6=6.410$; $p=0.0012$ | $F_6=7.087$; $p=0.0007$ |
| SQ12 | $F_6=13.09$; $p<0.0001$ | $F_6=11.07$; $p<0.0001$ | $F_6=6.880$; $p=0.0008$ |
| ATG7 6 | $F_6=2.215$; $p=0.1168$ | $F_6=7.879$; $p=0.0004$ | $F_6=21.20$; $p<0.0001$ |
| ATG7 9 | $F_6=5.756$; $p=0.0022$ | $F_6=7.490$; $p=0.0006$ | $F_6=8.291$; $p=0.0003$ |

### 4.6 Measures of Mitochondrial Quantity

Fluorescence levels of NAO were measured using a Guavasoft flow cytometer to provide an assessment of the quantity of mitochondria in the cell population. A single-assay representative graph of each triplicate measure is presented in figure 4.6A. Each measurement is normalized to the TRC cell line.

A

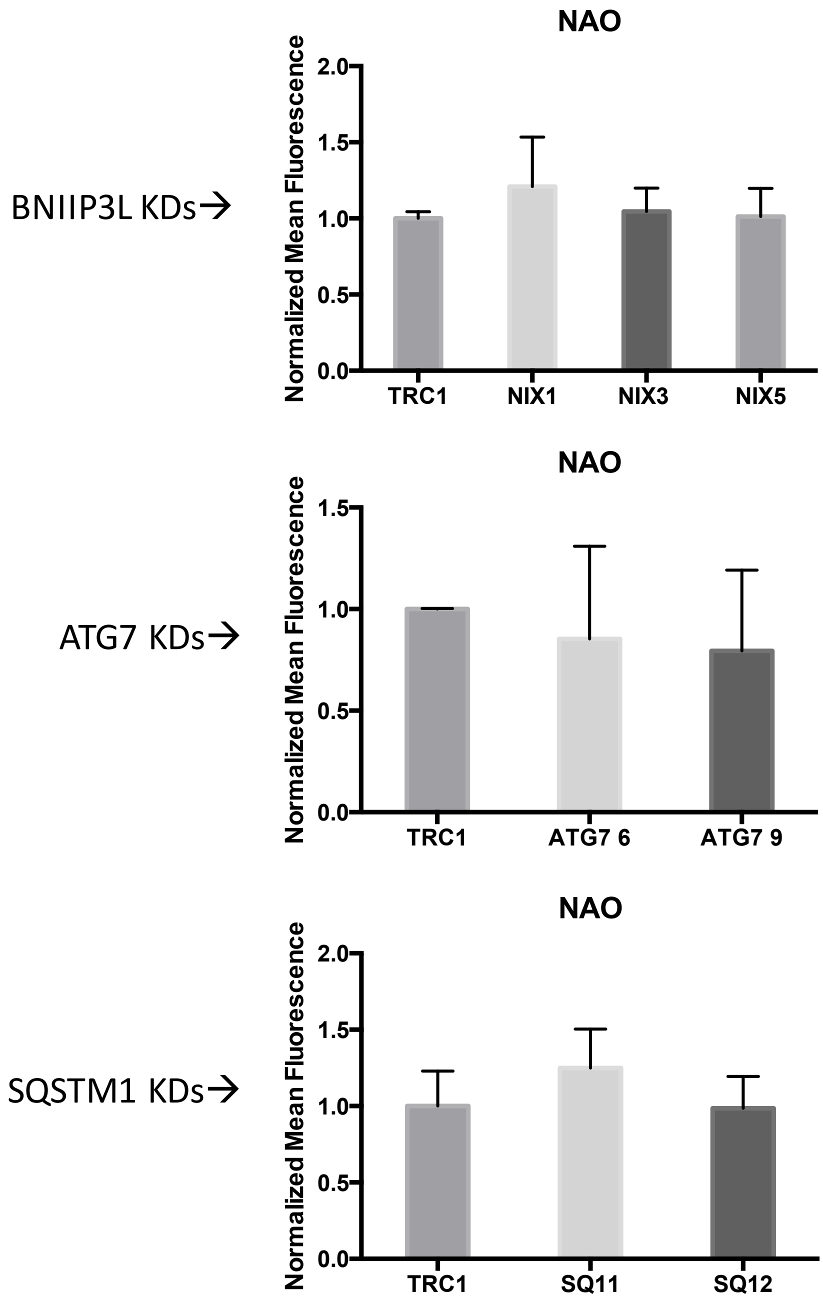


**Figure 4.6A Measuring Markers of Mitochondrial Quantity: Nonyl Acridine Orange (NAO)**
NAO levels were not significantly changed in the knockdowns indicating no overall effect on mitochondrial quantity. Outliers in each measurement were rejected according to Grubb's test ($p<0.05$).
ns $p>0.05$, *$p\leq0.05$, **$p\leq0.01$, ***$p\leq0.001$, ****$p\leq0.0001$

As shown in figures 4.6A, mean fluorescence of NAO was not significantly altered in all KD cell lines, indicating no overall effect on mitochondrial quantity[106]. A one-way ANOVA with a Dunnett's multiple comparisons test was used to compare the mean of each knockdown to the mean of TRC (ns $p>0.05$, *$p\leq0.05$, **$p\leq0.01$, ***$p\leq0.001$, ****$p\leq0.0001$). Table 4.3 provides the multiplicity adjusted p values associated with each measurement.

**Table 4.3 Multiplicity Adjusted P values for NAO Measurements**

| Cell Line | NAO |
|---|---|
| NIX1 | F7=1.224; p=0.5123 |
| NIX3 | F7=0.2387; p=0.9899 |
| NIX5 | F7=0.06940; p=0.9997 |
| SQ11 | F6=1.313; p=0.3762 |
| SQ12 | F6=0.07597; p=0.9958 |
| ATG7 6 | F5=0.4213; p=0.8824 |
| ATG7 9 | F5=0.5856; p=0.7914 |

Quantitative (real-time) PCR was used to assess the relative concentration of mitochondrial gene ND1 in order to estimate the quantity of mitochondria in the cell population. The results were analyzed using LinRegPCR software and the starting quantity of mtDNA was determined using the ΔΔCT method The results, normalized to TRC are shown in figure 4.6B.

B

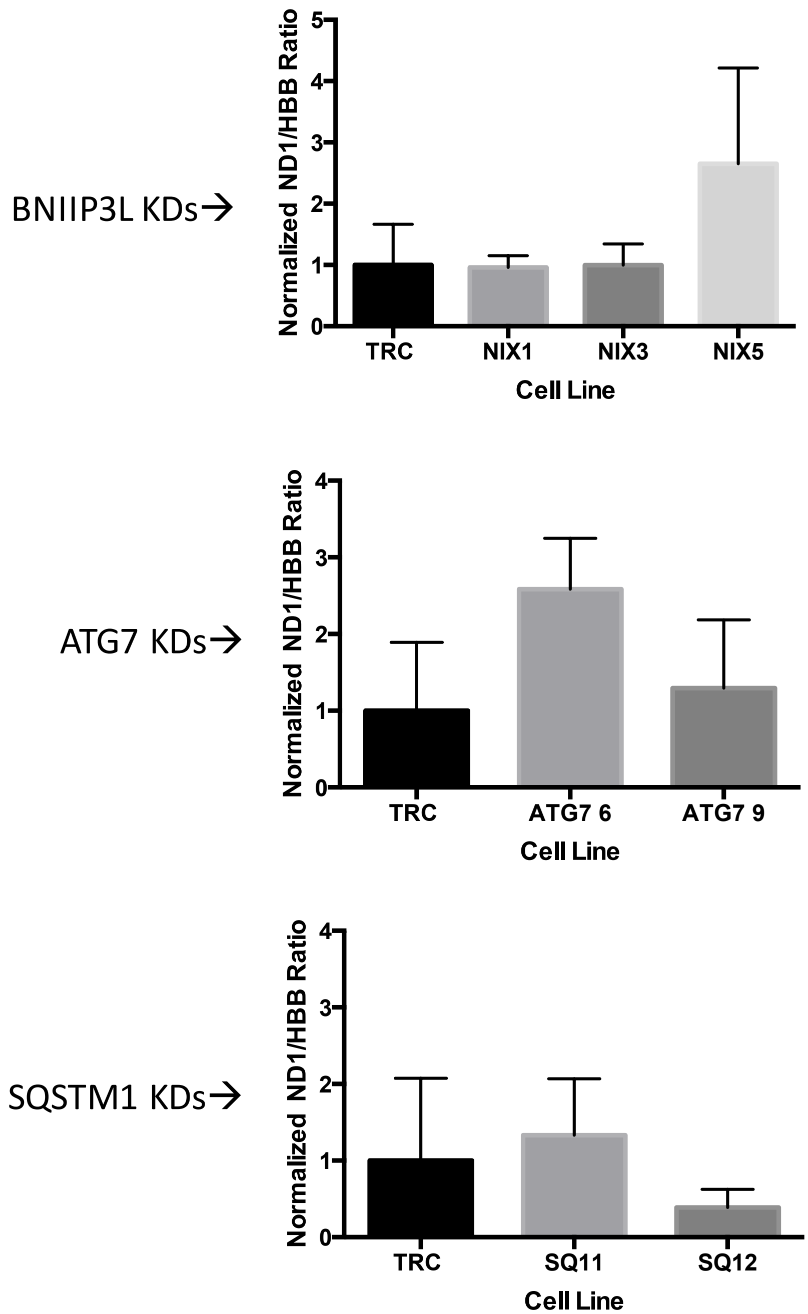


**Figure 4.6B qPCR Estimation of Relative mtDNA Copy Number**
(A) NIX (B) SQ and (C) ATG7 cell lines were probed for the quantity of mitochondrial gene ND1 relative to the nuclear gene HBB. All results are normalized to TRC. For NIX n=4, p62 n=4, and ATG7 n=3. A Grubb's outlier test was performed to identify any outliers in the data.

As shown in figure 4.6B, mtDNA copy number undergoes significant flux over the course of the measurements for both the KDs and control line. A one-way ANOVA with a Dunnett's multiple comparisons test was used to compare the mean of each knockdown to the mean of TRC and showed that these changes were statistically insignificant (ns $p>0.05$). Table 4.4 provides the multiplicity adjusted p values associated with each measurement.

**Table 4.4 Multiplicity Adjusted P Values for mtDNA Measurements**

| Cell Line | Multiplicity adjusted p values |
|---|---|
| NIX1 | F12=0.06205; p=0.9999 |
| NIX3 | F12=0.003193; p=>0.9999 |
| NIX5 | F12=2.677 p=0.0506 |
| SQ11 | F9=0.6128; p=0.7710 |
| SQ12 | F9=1.133; p=0.4506 |
| ATG7 6 | F5=2.045; p=0.1601 |
| ATG7 9 | F5=0.4249; p=0.8806 |

### 4.7 Serum Starvation

Serum starvation was run for one cell line for each knockdown group. These were the NIX5, SQ11, and ATG7 9 cell lines, chosen based on the best knockdown from the most recent Western blot the assay. We selected the proteins Beclin1 and ATG7 for analysis of early autophagy, as both play important roles in initiation[22]. Since conversion of LC3-I to LC3-II results in recruitment to the autophagosomal membrane, and LC3-II is degraded along with the contents of the autophagosome, monitoring LC3-I and LC3-II levels provides an excellent measure of autophagy flux[39]. Finally, to analyze late autophagy at the point of cargo recruitment, we selected the mitochondrial receptors NIX and p62[59]. Levels of autophagy proteins Beclin 1, ATG7, LC3-I, LC3-II, NIX, and p62 were measured by Western blotting, and normalized to the transduced control (TRC) cell line to provide data on key stages of autophagy. The results of the serum starvation assay are shown in figure 4.7 A-E.

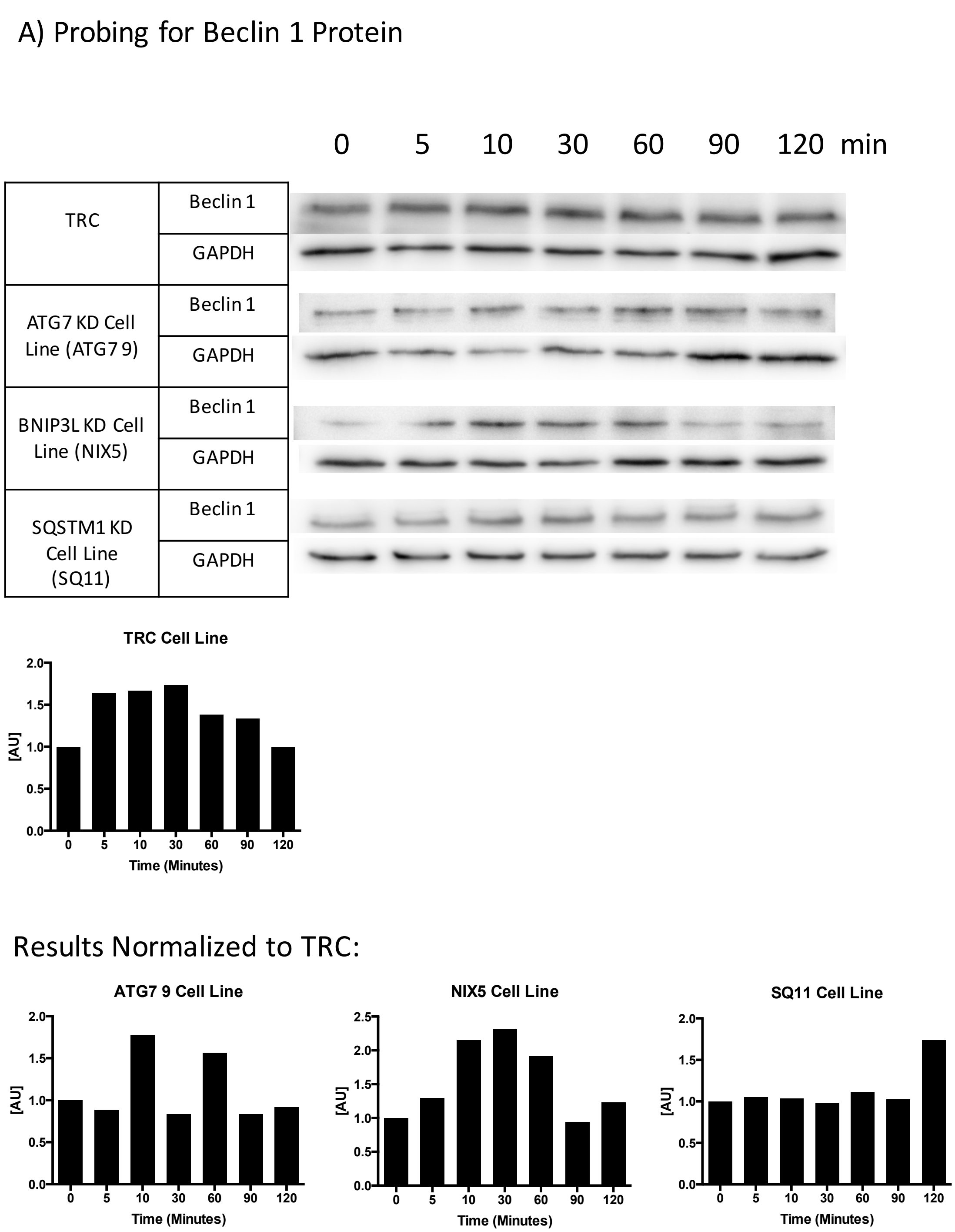


**Figure 4.7A Serum Starvation Results – Probing for Upstream and Downstream Autophagy Proteins**
The TRC, NIX5 (BNIP3L KD), SQ11 (SQSTM1 KD), and ATG7 9 (ATG7 KD) cell lines were probed for the autophagy protein Beclin 1 following serum starvation by Western blotting. Graphed results are normalized to TRC values.

B) Probing for ATG7 Protein

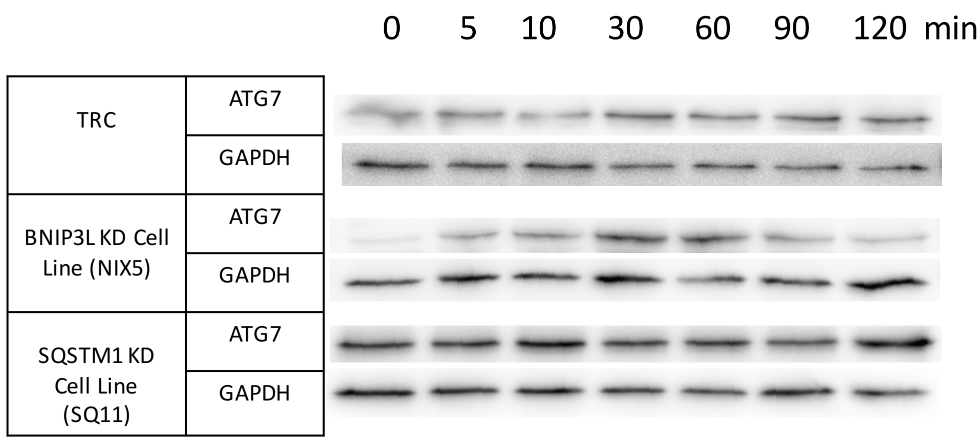


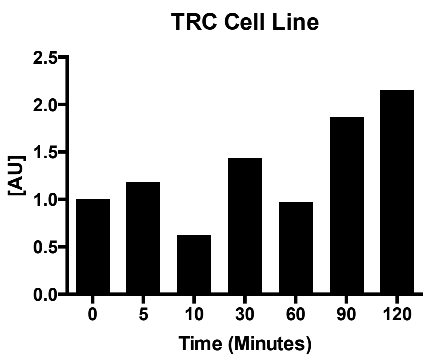


Results Normalized to TRC:

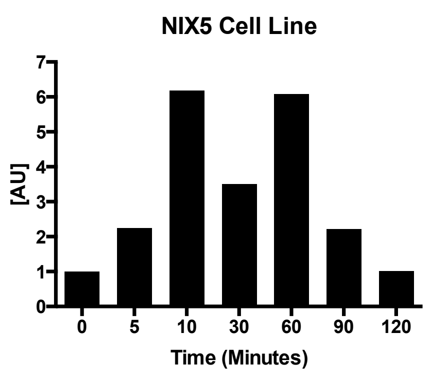


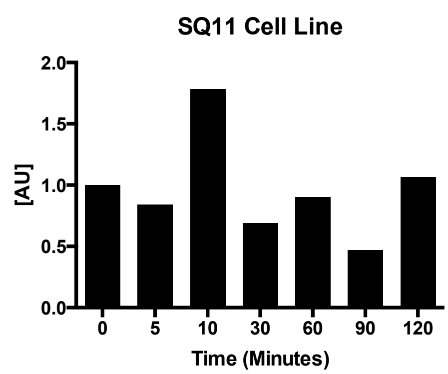


**Figure 4.7B Serum Starvation Results – Probing for Upstream and Downstream Autophagy Proteins**
The TRC, NIX5 (BNIP3L KD), and SQ11 (SQSTM1 KD) cell lines were probed for the autophagy protein ATG7 following serum starvation by Western blotting. Graphed results are normalized to TRC values.

C) Probing for LC3-II Protein and LC3-II/LC3-I Ratio

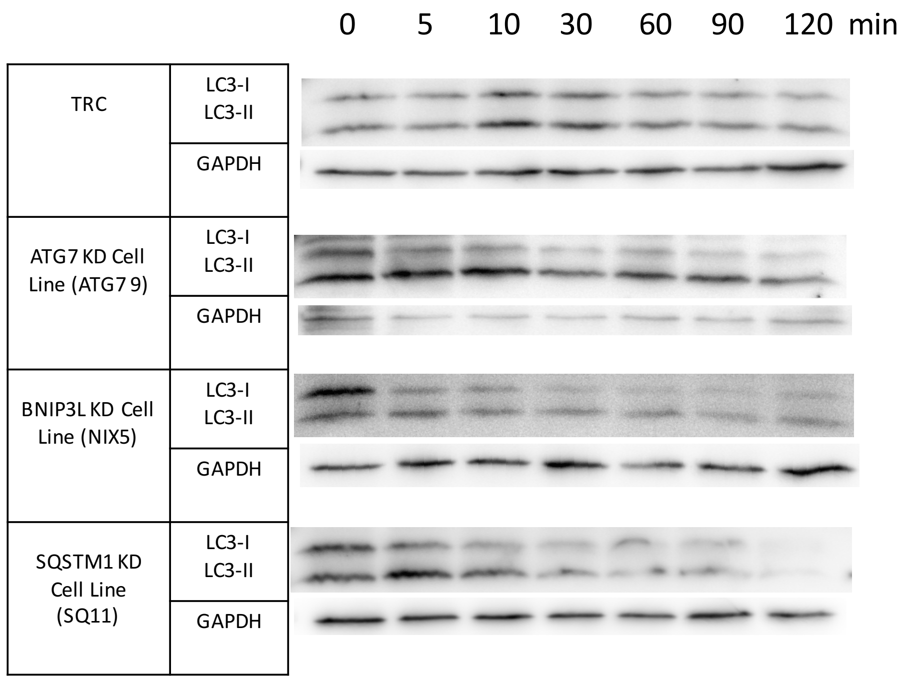


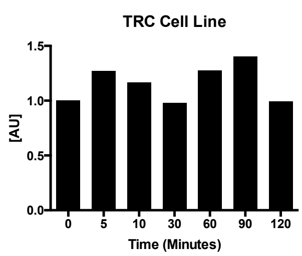


Results Normalized to TRC:

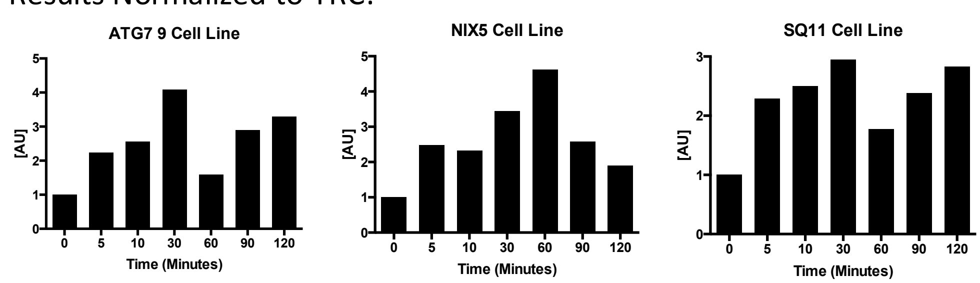


**Figure 4.7C Serum Starvation Results – Probing for Upstream and Downstream Autophagy Proteins**
The TRC, NIX5 (BNIP3L KD), SQ11 (SQSTM1 KD), and ATG7 9 (ATG7 KD) cell lines were probed for the autophagy proteins LC3-I and LC3-II following serum starvation by Western blotting. Graphed results are normalized to TRC values.

D) Probing for NIX Protein

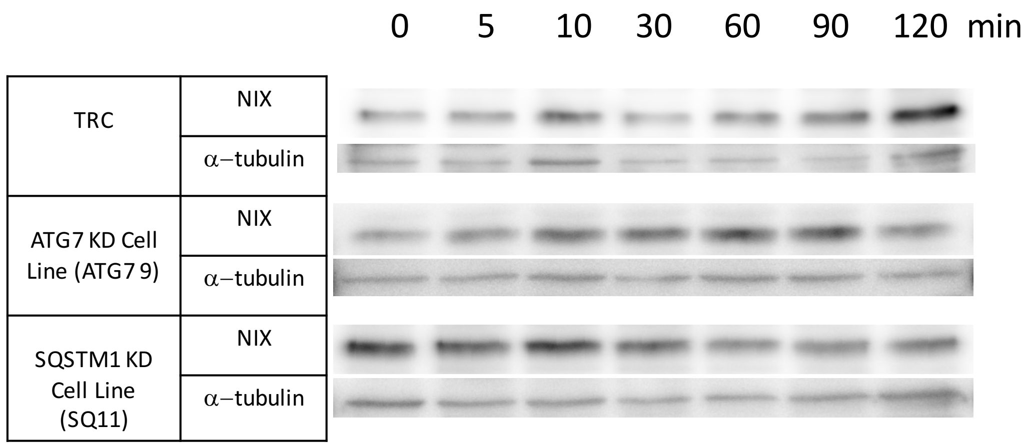


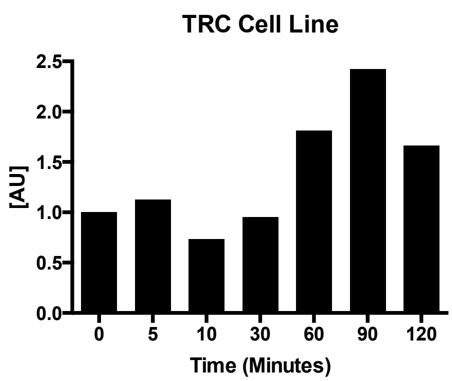


Results Normalized to TRC:

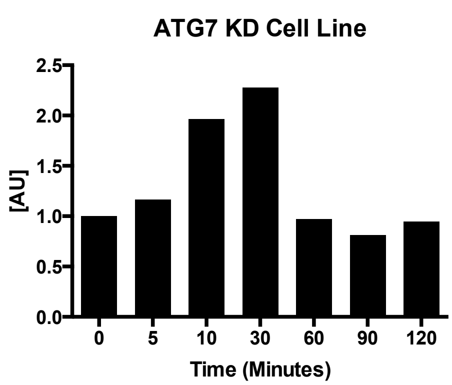


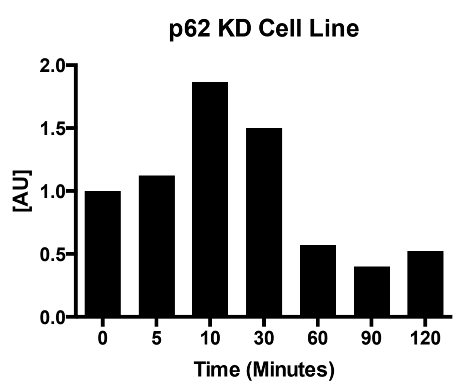


**Figure 4.7D Serum Starvation Results – Probing for Upstream and Downstream Autophagy Proteins**
The TRC, SQ11 (SQSTM1 KD), and ATG7 9 (ATG7 KD) cell lines were probed for the autophagy protein NIX following serum starvation by Western blotting. Graphed results are normalized to TRC values.

E) Probing for p62 Protein

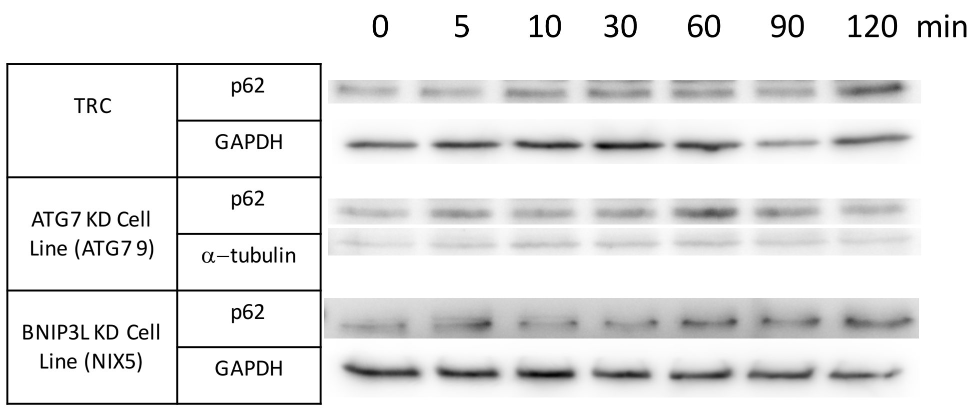


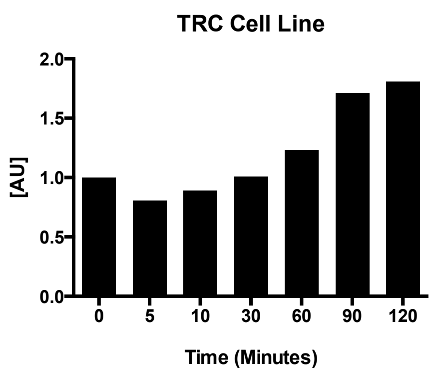


Results Normalized to TRC:

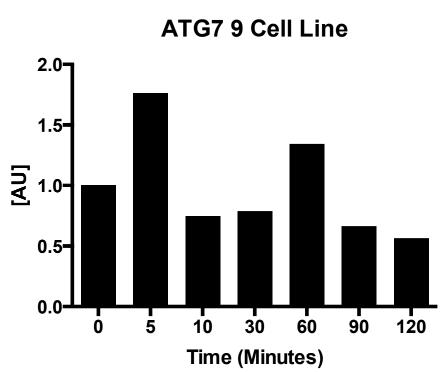


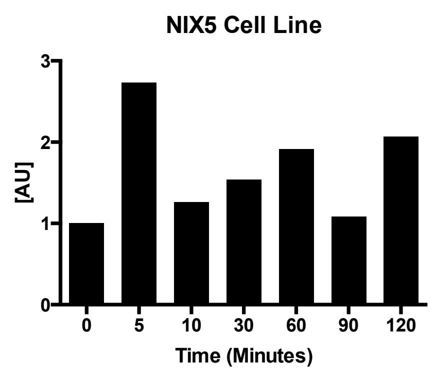


**Figure 4.7E Serum Starvation Results – Probing for Upstream and Downstream Autophagy Proteins**
The TRC, NIX5 (BNIP3L KD), and ATG7 9 (ATG7 KD) cell lines were probed for the autophagy protein p62 following serum starvation by Western blotting. Graphed results are normalized to TRC values.

As shown in figures 4.7 A-E, the early, mid, and late-stage autophagy proteins are all upregulated at various time points in the ATG7 9, NIX5, and SQ11 cell lines compared to the transduced scramble control.

### 4.8 Dose Response Data

Cells were treated with a panel of drugs which were classified as DNA-targeting, mitochondrial-targeting, or an mTOR inhibitor. All dose response data was performed in triplicate. Results of the DNA-targeting panel (class I) are shown in figures 4.8 A-C. LD50 values were calculated using the log (inhibitor) vs. response – variable slope (four parameters) non-linear fit on Graphpad Prism and are shown in table 4.5 a, b and c.

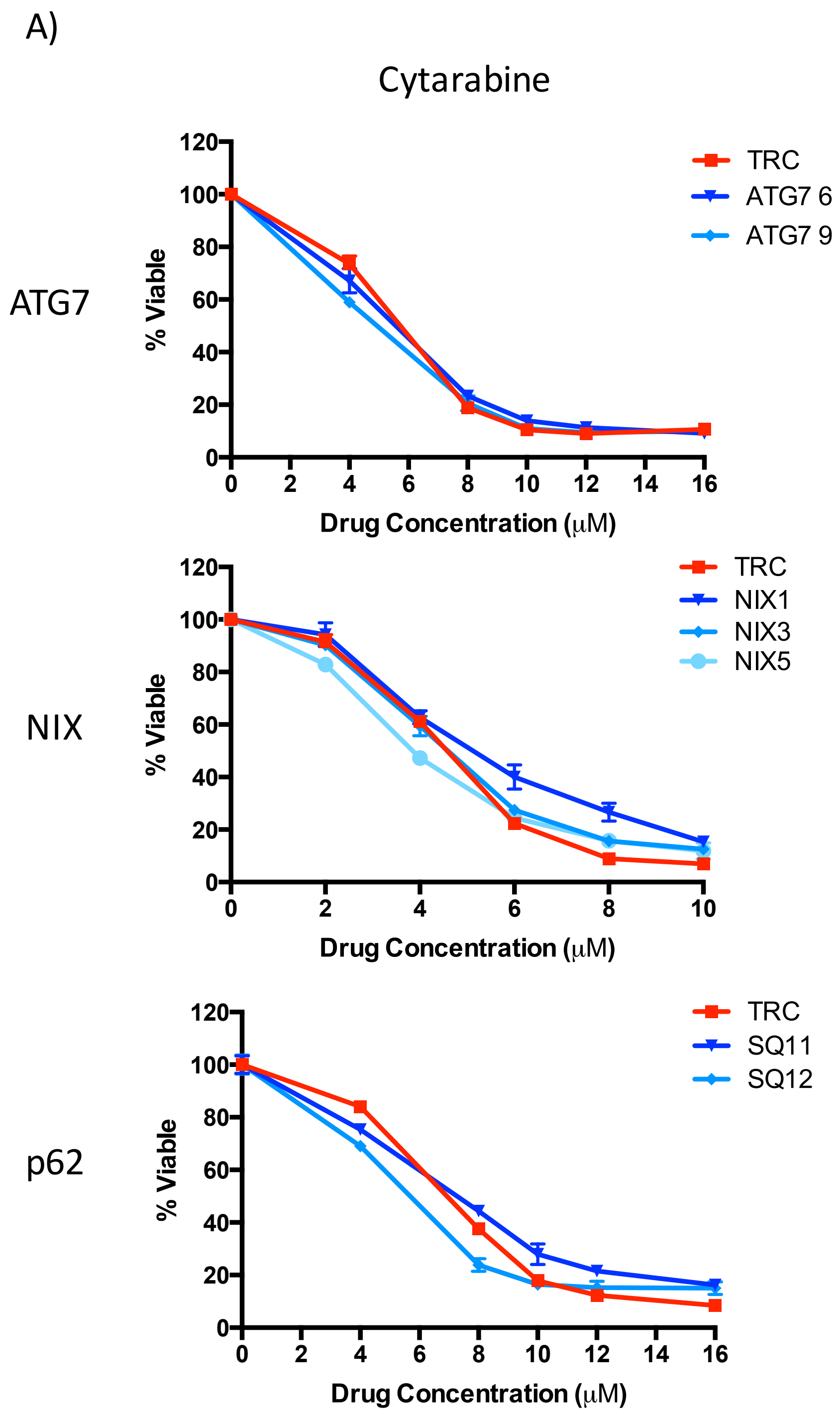


**Figure 4.8A Dose Responses with DNA-Targeting Drugs: Cytarabine**
Cell lines ATG7, NIX, and SQ were run alongside TRC in dose-response studies with the DNA-targeting drug cytarabine.

B)

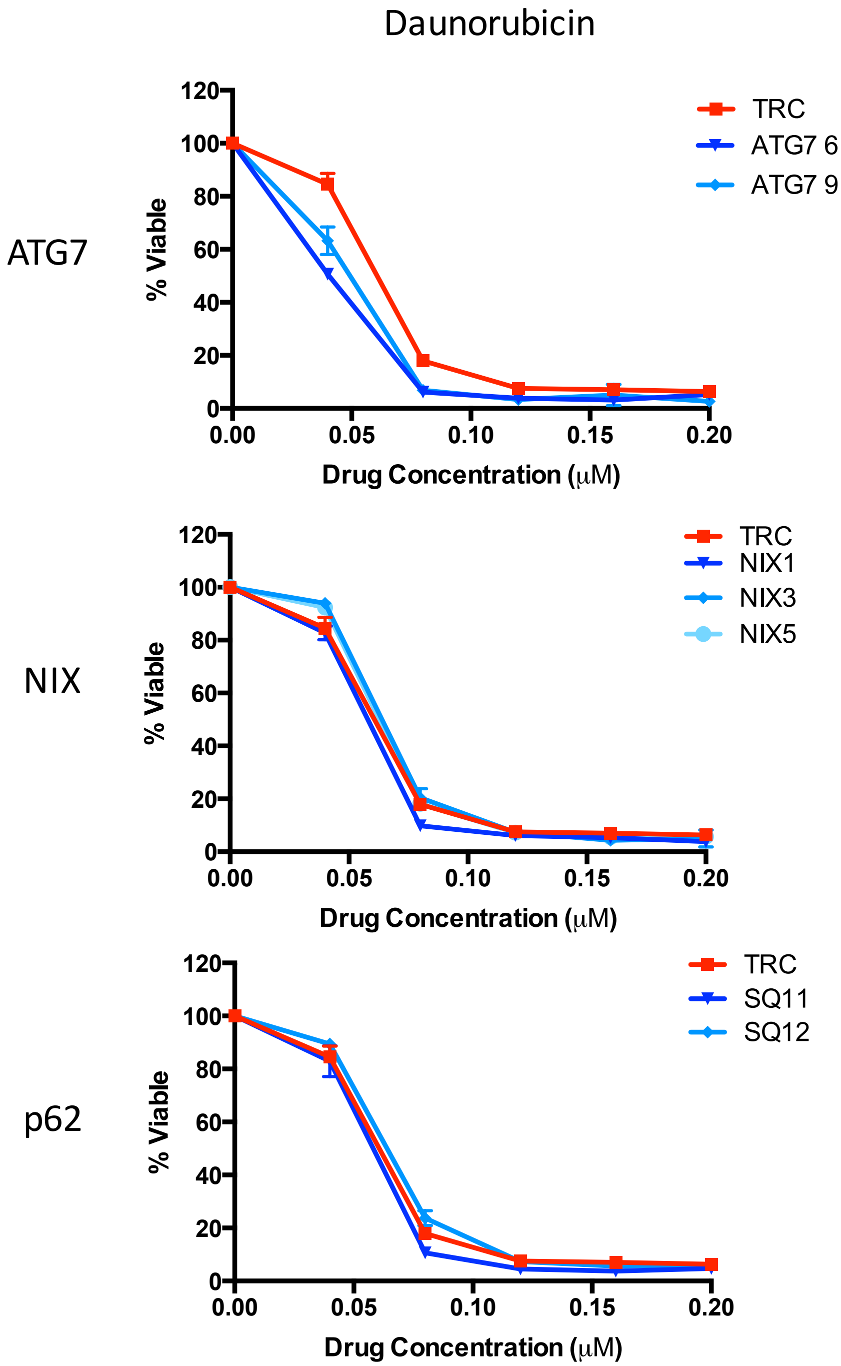


**Figure 4.8B Dose Responses with DNA-Targeting Drugs: Daunorubicin**
Cell lines ATG7, NIX, and SQ were run alongside TRC in dose-response studies with the DNA-targeting drug daunorubicin.

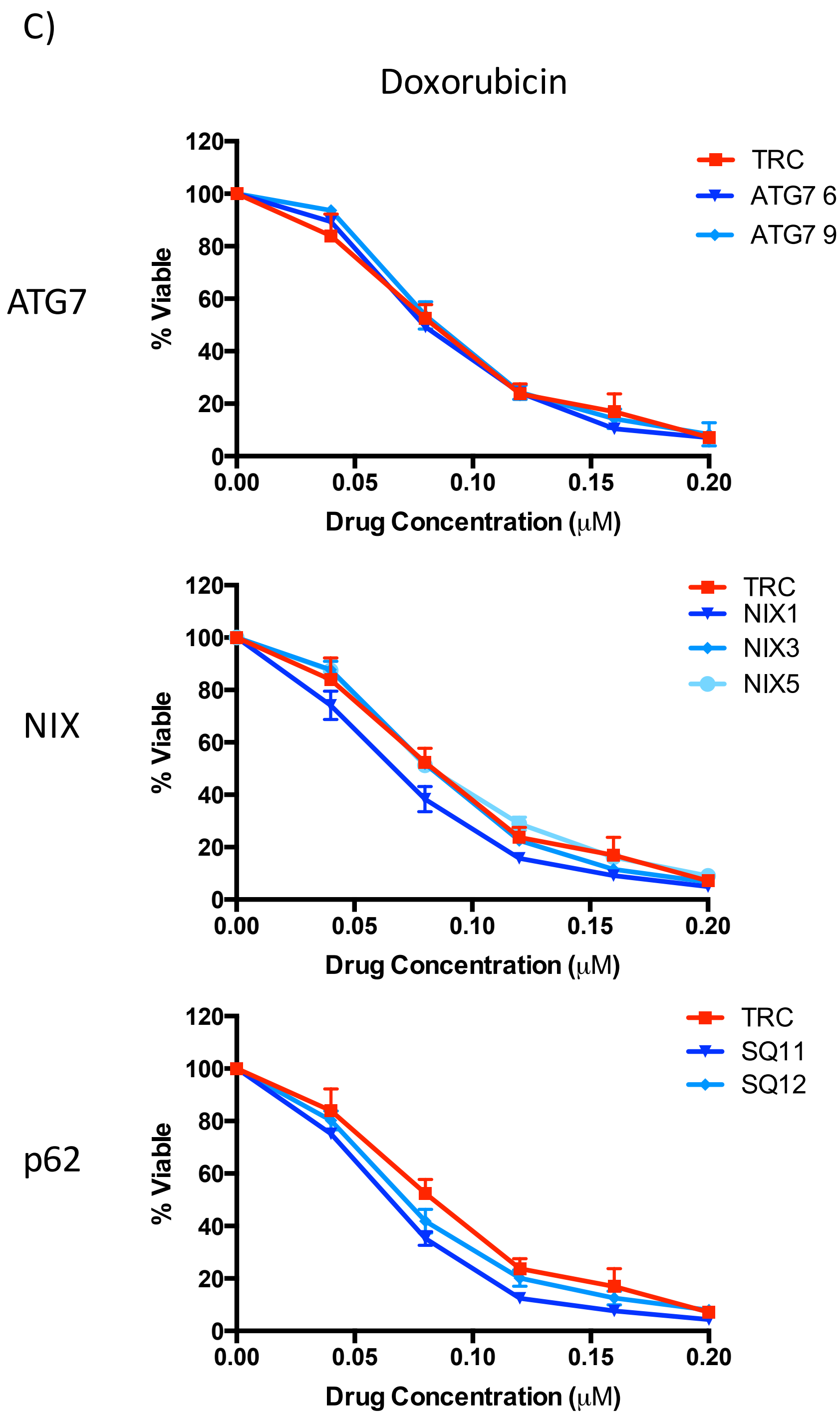


**Figure 4.8C Dose Responses with DNA-Targeting Drugs: Doxorubicin**
Cell lines ATG7, NIX, and SQ were run alongside TRC in dose-response studies with the DNA-targeting drug doxorubicin.

**Table 4.5a LD50 Values for Dose Responses with DNA-Targeting Drugs with the NIX Cell Lines**

| Class I | TRC | TRC 95% Confidence Interval | NIX1 | NIX1 95% Confidence Interval | NIX3 | NIX3 95% Confidence Interval | NIX5 | NIX5 95% Confidence Interval |
|---|---|---|---|---|---|---|---|---|
| Cytarabine | 4.414 | 4.144 to 4.702 | 5.121 | 4.823 to 5.437 | 4.469 | 4.184 to 4.773 | 3.835 | 3.653 to 4.025 |
| Daunorubicin | 0.05825 | 0.05077 to 0.06685 | 0.05382 | 0.04764 to 0.06079 | 0.06338 | 0.05606 to 0.07166 | 0.06164 | 0.05354 to 0.07096 |
| Doxorubicin | 0.08029 | 0.07457 to 0.08644 | 0.06325 | 0.05983 to 0.06687 | 0.0807 | 0.07837 to 0.08310 | 0.08303 | 0.08076 to 0.08537 |

**Table 4.5b LD50 Values for Dose Responses with DNA-Targeting Drugs with the SQ Cell Lines**

| Class I | TRC | TRC 95% Confidence Interval | SQ11 | SQ11 95% Confidence Interval | SQ12 | SQ12 95% Confidence Interval |
|---|---|---|---|---|---|---|
| Cytarabine | 6.68 | 6.226 to 7.167 | 6.825 | 6.294 to 7.401 | 5.381 | 4.480 to 6.463 |
| Daunorubicin | 0.05825 | 0.05077 to 0.06685 | 0.05412 | 0.04893 to 0.05986 | 0.06278 | 0.05612 to 0.07023 |
| Doxorubicin | 0.08029 | 0.07457 to 0.08644 | 0.06168 | 0.05864 to 0.06488 | 0.07014 | 0.06826 to 0.07207 |

**Table 4.5c LD50 Values for Dose Responses with DNA-Targeting Drugs with the ATG7 Cell Lines**

| Class I | TRC | TRC 95% Confidence Interval | ATG7 6 | ATG7 95% Confidence Interval | ATG7 9 | ATG7 9 95% Confidence Interval |
|---|---|---|---|---|---|---|
| Cytarabine | 5.378 | 4.702 to 6.150 | 5.205 | 4.793 to 5.652 | 4.604 | 4.098 to 5.173 |
| Daunorubicin | 0.02368 | 0.01712 to 0.03277 | 0.01013 | 0.008168 to 0.01256 | 0.0133 | 0.01110 to 0.01593 |
| Doxorubicin | 0.04757 | 0.02916 to 0.07761 | 0.04735 | 0.03548 to 0.06321 | 0.05335 | 0.03519 to 0.08089 |

Results of the mitochondrial-targeting panel (class II) are shown in figures 4.9 A-E. LD50 values were calculated using the log (inhibitor) vs. response – variable slope (four parameters) non-linear fit on Graphpad Prism and are shown in table 4.6 a, b and c.

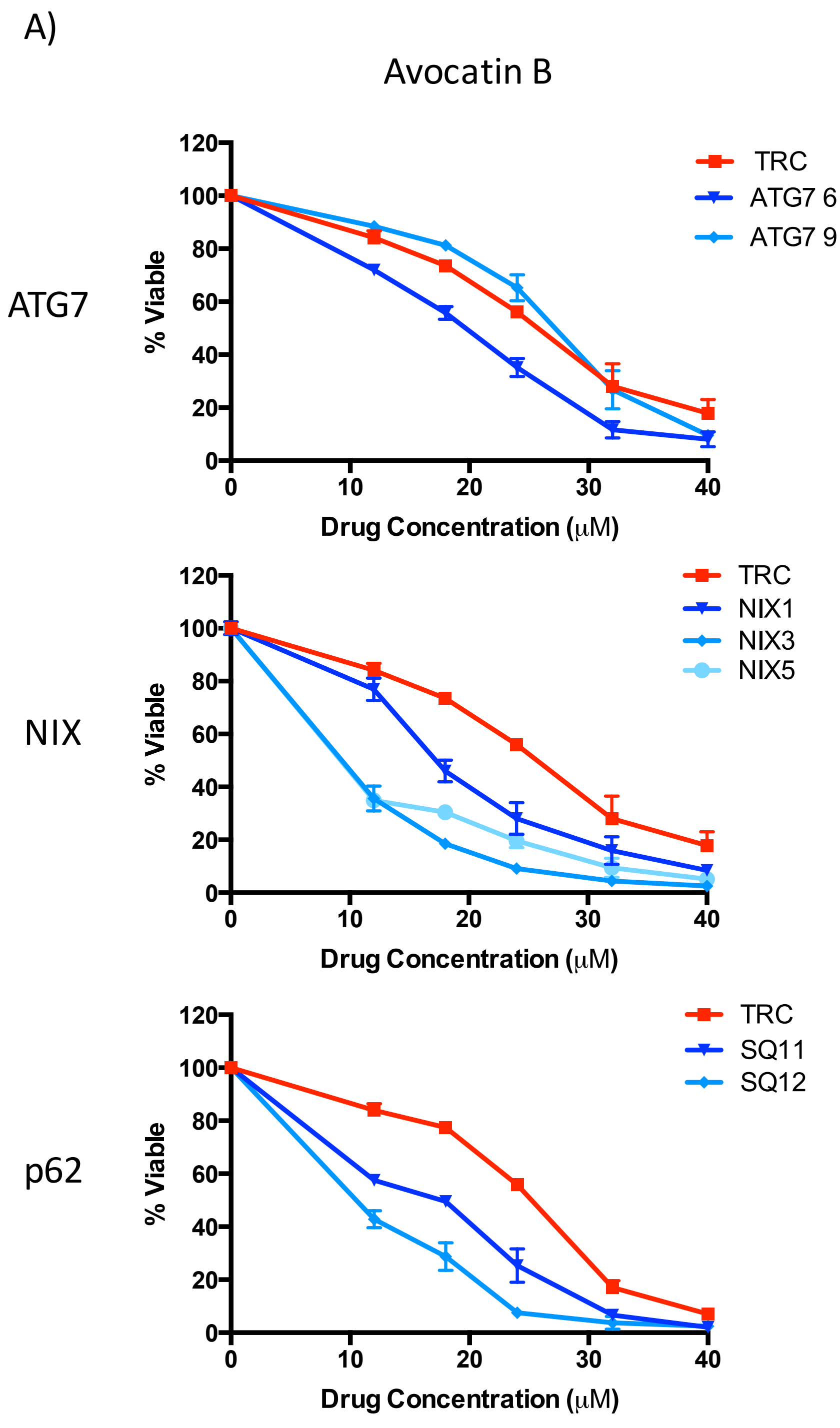


**Figure 4.9A Dose Responses with Mitochondrial-Targeting Drugs: Avocatin B**
ATG7, NIX, and SQ cell lines were run alongside TRC in dose-response studies with the mitochondrial-targeting drug avocatin B.

B)

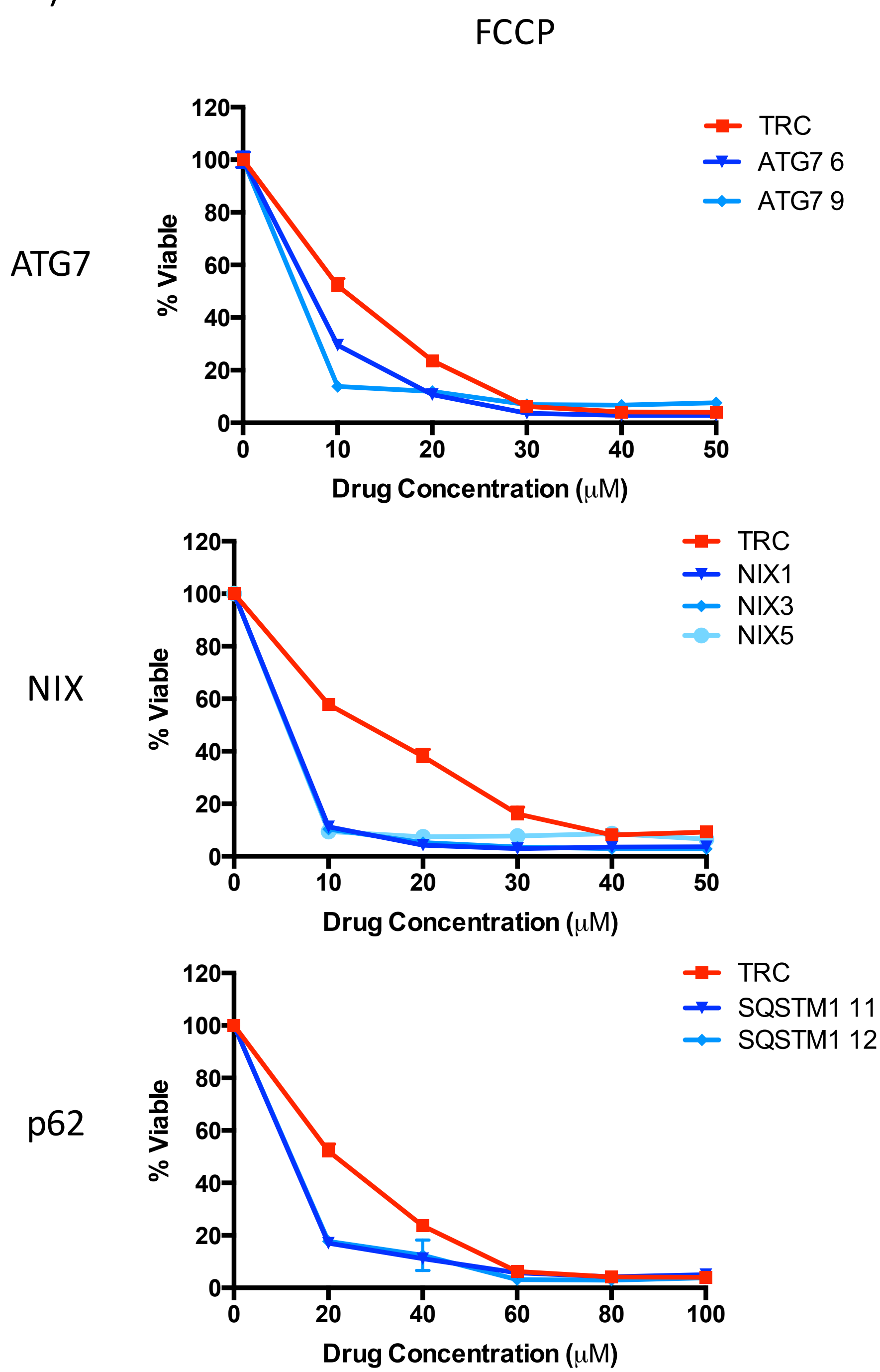


**Figure 4.9B Dose Responses with Mitochondrial-Targeting Drugs: FCCP**
ATG7, NIX, and SQ cell lines were run alongside TRC in dose-response studies with the mitochondrial-targeting drug FCCP.

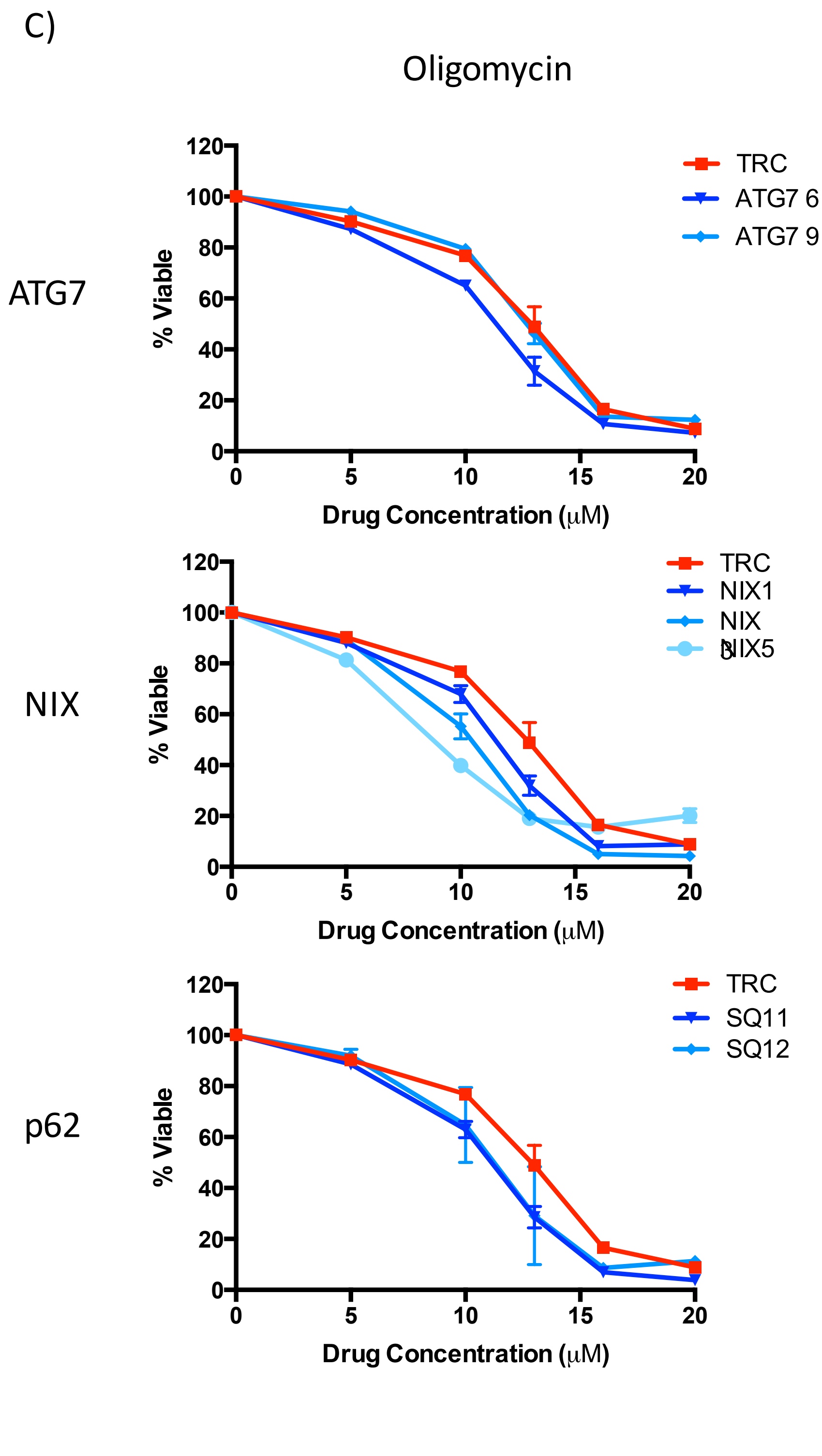


**Figure 4.9C Dose Responses with Mitochondrial-Targeting Drugs: Oligomycin**
ATG7, NIX, and SQ cell lines were run alongside TRC in dose-response studies with the mitochondrial-targeting drug oligomycin.

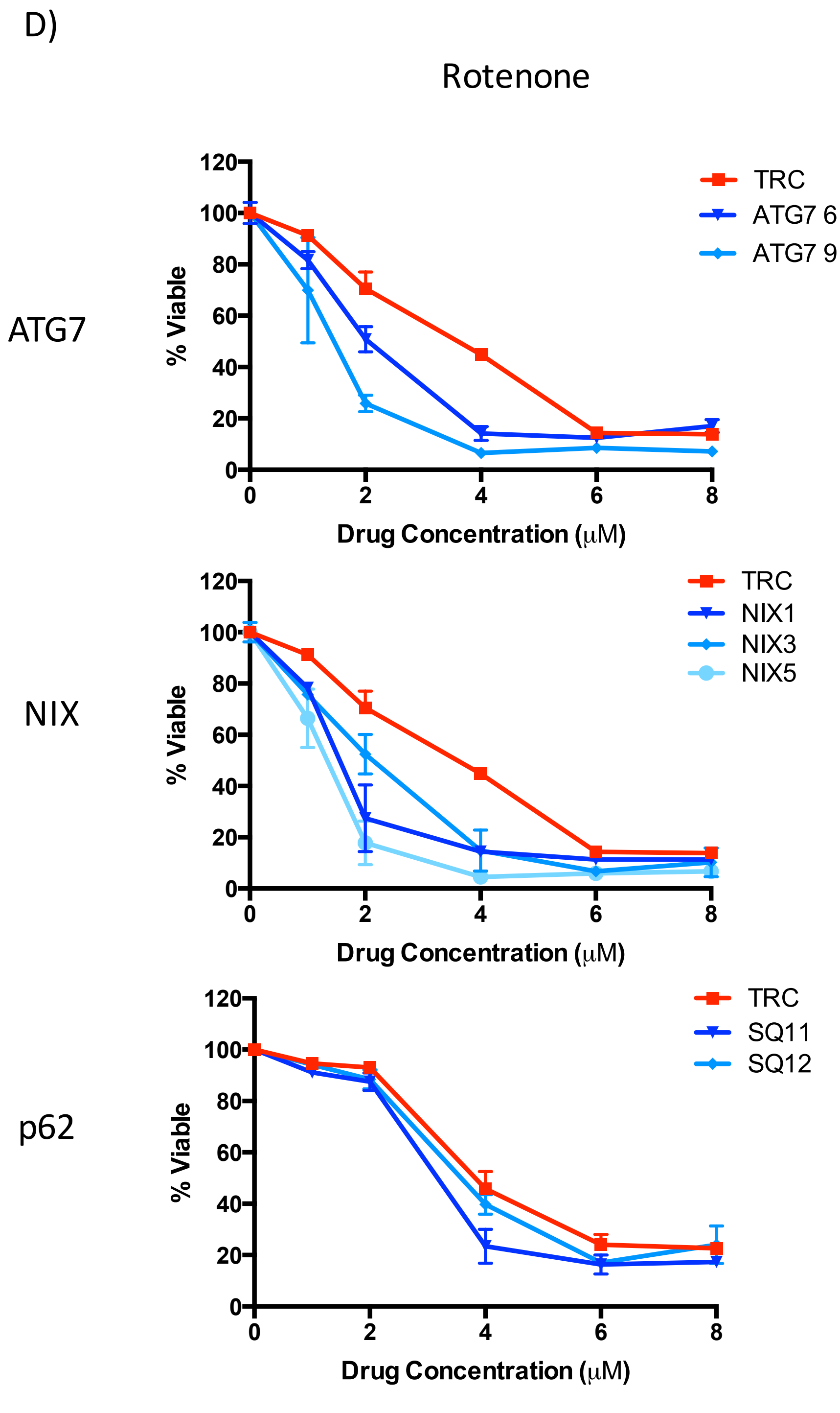


**Figure 4.9D Dose Responses with Mitochondrial-Targeting Drugs: Rotenone**
ATG7, NIX, and SQ cell lines were run alongside TRC in dose-response studies with the mitochondrial-targeting drug rotenone.

E)

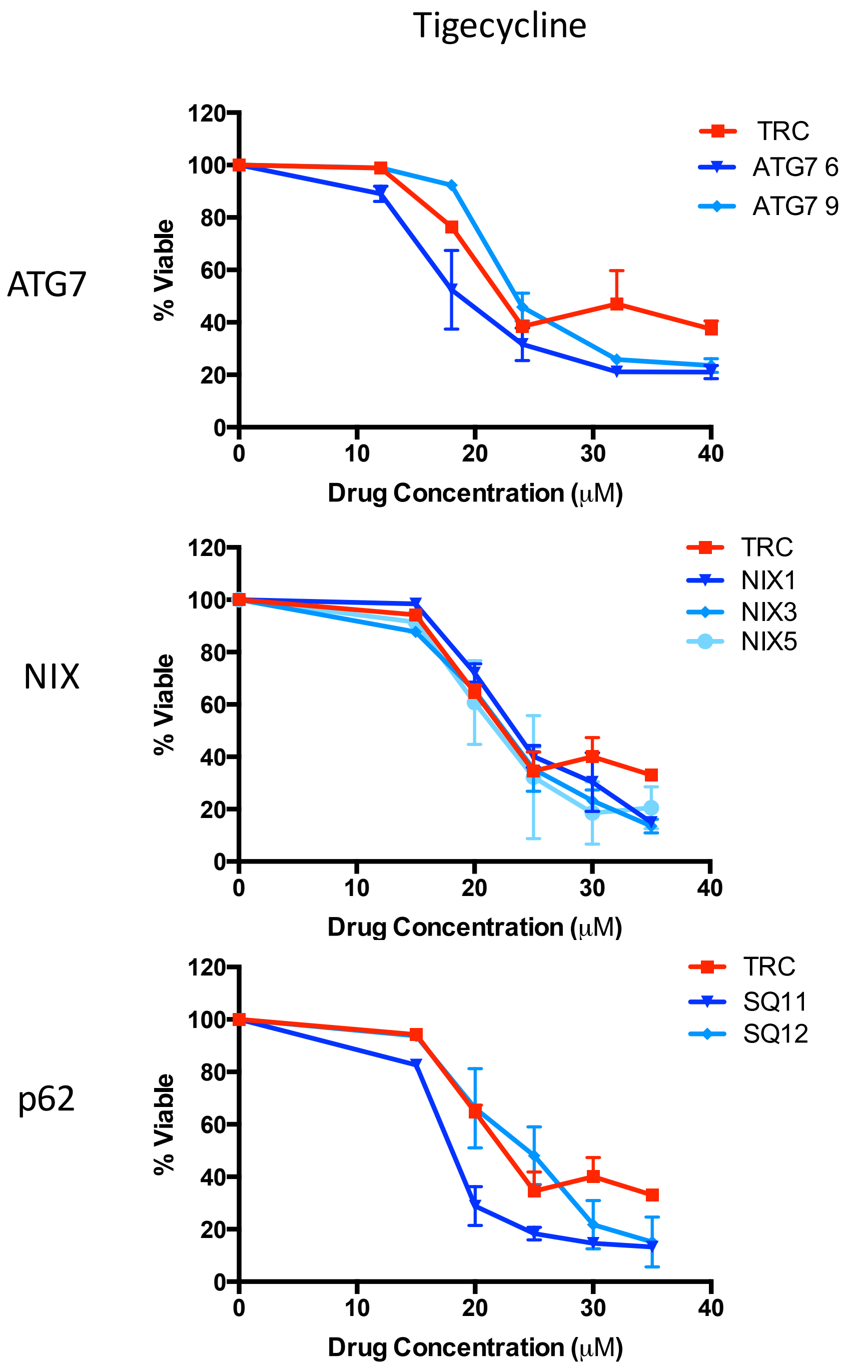


**Figure 4.9E Dose Responses with Mitochondrial-Targeting Drugs: Tigecycline**
ATG7, NIX, and SQ cell lines were run alongside TRC in dose-response studies with the mitochondrial-targeting drug tigecycline.

## Table 4.6a LD50 Values for Dose Responses with Mitochondrial-Targeting Drugs with the NIX Cell Lines

| Class II | TRC | TRC 95% Confidence Interval | NIX1 | NIX1 95% Confidence Interval | NIX3 | NIX3 95% Confidence Interval | NIX5 | NIX5 95% Confidence Interval |
|---|---|---|---|---|---|---|---|---|
| **Avocatin B** | 24.62 | 22.62 to 26.80 | 17.51 | 16.89 to 18.16 | 9.453 | 8.98 to 8.95 | 8.78 | 5.79 to 13.31 |
| **FCCP** | 12.77 | 10.33 to 15.80 | 1.28 | 0.3693 to 4.35 | 1.043 | 0.6954 to 1.57 | 0.004483 | $5.34e^{-005}$ to 0.3757 |
| **Oligomycin** | 12.57 | 11.61 to 13.61 | 11.31 | 10.23 to 12.50 | 10.24 | 9.38 to 11.19 | 8.475 | 7.00 to 10.27 |
| **Rotenone** | 3.197 | 2.69 to 3.81 | 1.549 | 1.14 to 2.11 | 1.925 | 1.62 to 2.29 | 1.245 | 1.08 to 1.44 |
| **Tigecycline** | 24.81 | 20.45 to 30.11 | 24.24 | 22.56 to 26.05 | 22.67 | 21.90 to 23.46 | 22.24 | 20.27 to 24.39 |

## Table 4.6b LD50 Values for Dose Responses with Mitochondrial-Targeting Drugs with the SQ Cell Lines

| Class II | TRC | TRC 95% Confidence Interval | SQ11 | SQ11 95% Confidence Interval | SQ12 | SQ12 95% Confidence Interval |
|---|---|---|---|---|---|---|
| **Avocatin B** | 23.90 | 21.11 to 27.05 | 15.19 | 12.06 to 19.12 | 11.13 | 9.13 to 13.56 |
| **FCCP** | 21.13 | 18.73 to 23.83 | 3.955 | 2.07 to 7.57 | 5.727 | 2.18 to 15.05 |
| **Oligomycin** | 12.57 | 11.61 to 13.61 | 10.91 | 10.00 to 11.92 | 11.05 | 10.11 to 12.08 |
| **Rotenone** | 4.054 | 3.36 to 4.89 | 3.161 | 2.38 to 4.21 | 3.666 | 2.87 to 4.69 |
| **Tigecycline** | 24.81 | 20.45 to 30.11 | 18.44 | 15.95 to 21.30 | 23.85 | 22.63 to 25.13 |

## Table 4.6c LD50 Values for Dose Responses with Mitochondrial-Targeting Drugs with the ATG7 Cell Lines

| Class II | TRC | TRC 95% Confidence Interval | ATG7 6 | ATG7 6 95% Confidence Interval | ATG7 9 | ATG7 9 95% Confidence Interval |
|---|---|---|---|---|---|---|
| **Avocatin B** | 24.62 | 22.62 to 26.80 | 18.35 | 16.35 to 20.60 | 26.14 | 23.70 to 28.83 |
| **FCCP** | 10.56 | 9.364 to 11.92 | 6.349 | 5.698 to 7.074 | 0.3168 | 0.02734 to 3.671 |
| **Oligomycin** | 12.57 | 11.61 to 13.61 | 11.11 | 10.02 to 12.31 | 12.53 | 11.67 to 13.45 |
| **Rotenone** | 3.197 | 2.686 to 3.805 | 2.027 | 1.558 to 2.637 | 1.372 | 1.160 to 1.622 |
| **Tigecycline** | 27.76 | 19.91 to 38.69 | 19.89 | 16.85 to 23.48 | 25.49 | 21.61 to 30.08 |

Results of the mTOR inhibitor, rapamycin (class III) are shown in figures 4.10 A.  LD50 values were calculated using the log (inhibitor) vs. response – variable slope (four parameters) non-linear fit on Graphpad Prism and are shown in table 4.7 a, b and c.

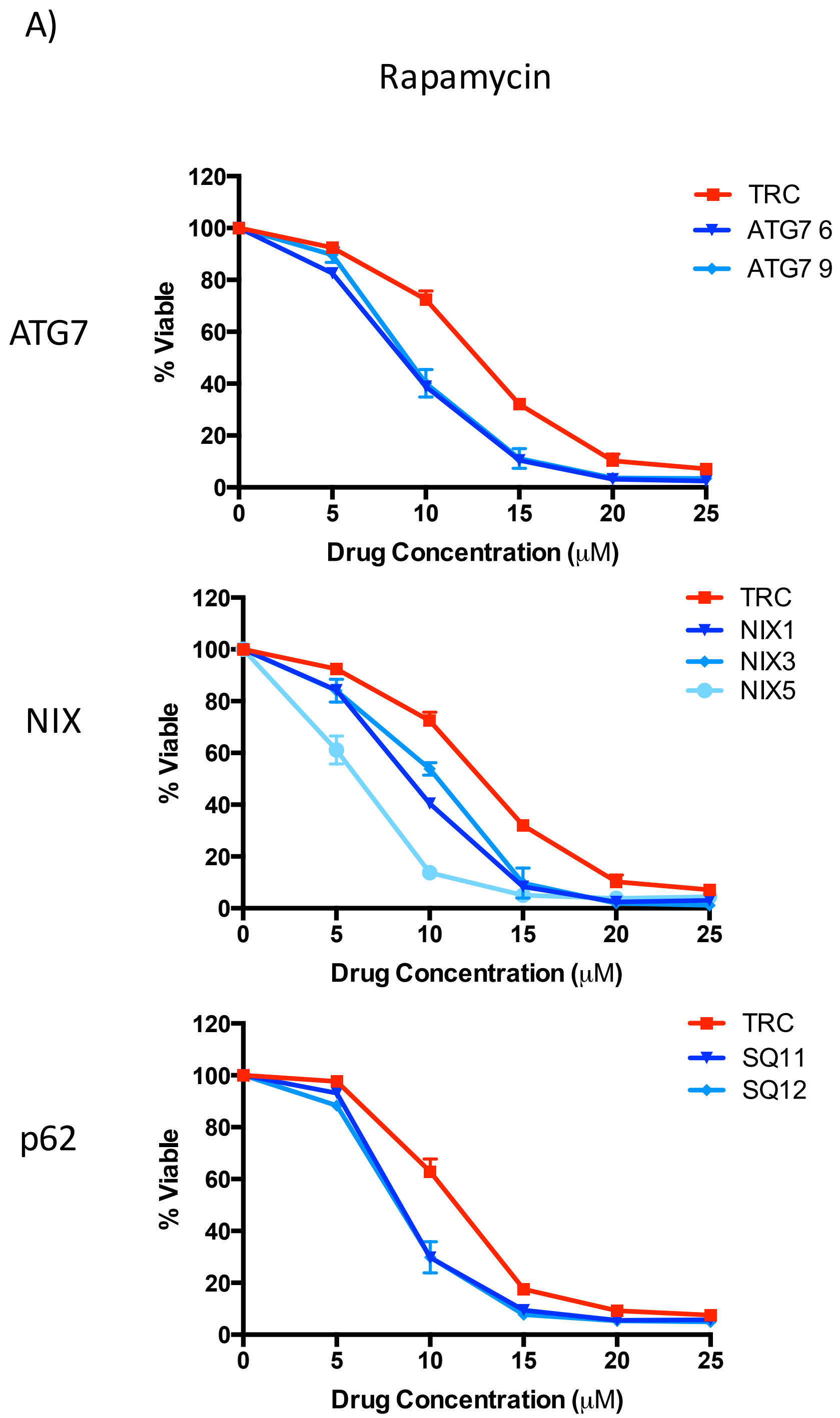


**Figure 4.10 A Dose Responses with the mTOR Inhibitor: Rapamycin**
ATG7, NIX, and SQ cell lines were run alongside TRC in dose-response studies with the mTOR inhibitor rapamycin.

**Table 4.7a LD50 Values for Dose Responses with an mTOR Inhibitor with the NIX Cell Lines**

| Class III | TRC | TRC 95% Confidence Interval | NIX1 | NIX1 95% Confidence Interval | NIX3 | NIX3 95% Confidence Interval | NIX5 | NIX5 95% Confidence Interval |
|---|---|---|---|---|---|---|---|---|
| **Rapamycin** | 12.48 | 11.68 to 13.33 | 8.597 | 7.82 to 9.46 | 9.852 | 9.38 to 11.58 | 5.75 | 5.38 to 6.15 |

**Table 4.7b LD50 Values for Dose Responses with an mTOR Inhibitor with the SQ Cell Lines**

| Class III | TRC | TRC 95% Confidence Interval | SQ11 | SQ11 95% Confidence Interval | SQ12 | SQ12 95% Confidence Interval |
|---|---|---|---|---|---|---|
| **Rapamycin** | 11.13 | 10.38 to 11.94 | 8.412 | 7.59 to 9.32 | 8.144 | 7.59 to 8.74 |

**Table 4.7c LD50 Values for Dose Responses with an mTOR Inhibitor with the ATG7 Cell Lines**

| Class III | TRC | TRC 95% Confidence Interval | ATG7 6 | ATG7 6 95% Confidence Interval | ATG7 9 | ATG7 9 95% Confidence Interval |
|---|---|---|---|---|---|---|
| **Rapamycin** | 12.48 | 11.68 to 13.33 | 8.4 | 7.801 to 9.045 | 8.941 | 8.675 to 9.214 |

As shown in figures 4.8-4.9 and tables 4.4- 4.5, all KD cell lines were increasingly sensitive to the majority of the mitochondrial-target panel and the mTOR inhibitor drug, however insensitive to the panel of DNA-targeting drugs.

# Chapter 5: Discussion

## 5.1 Analysis of Mitochondrial Function

Using fluorescent dyes as probes, we sought to understand the mitochondrial transformations in our knockdown cell lines. ROS was measured to provide key data on mitochondrial health[114]. We utilized two fluorescent probes for ROS: DHE, which primarily reacts with superoxide, and H2DCFDA (fluorescent product: DCF), which is primarily used as a probe for hydrogen peroxide, but is known to additionally react with other ROS such as nitrate and hypochlorous acid [106,107,130,131,]. Interestingly, our results indicate an increase in superoxide in all knockdown lines, however a decrease in the ROS associated with DCF fluorescence. Importantly, superoxide is the main mitochondria-derived ROS, produced from the electron transport chain (ETC) when the final electron acceptor, oxygen, is partially reduced[46,132]. Mitochondrial-derived ROS can escape the mitochondria and propagate oxidative chain reactions as well as damage proteins, lipids, and DNA[46]. Hydrogen peroxide can be produced by various oxidases as well as through the dismutation of superoxide, as shown in the reaction below[133].

$$O_2^{\cdot -} + e^- + 2H^+ \xrightarrow{\text{Mn-SOD}} H_2O_2$$

Decreased activity of mitochondrial superoxide dismutase (Mn-SOD), the enzyme which carries out this reaction, has been shown to produce a ROS profile similar to our findings[134,135]. In concordance with our results, cells treated with the late-stage autophagy inhibitor bafilomycin A1 (BafA) showed decreases in DCF fluorescence and increases in DHE fluorescence with these results attributed to decreased SOD activity and expression[136]. The SOD alterations were postulated to be caused by increased degradation or stability changes brought on by protein modifications[136]. DCF fluorescence could be further reduced by factors affecting the oxidation reaction with this dye. Oxidation of H2DCF by hydrogen peroxide to produce the fluorescent product DCF is dependent on enzymatic oxidation by a source of ferrous iron such as cytochrome c, which is released from mitochondria in a two-step process requiring membrane permeabilization[137]. Membrane permeabilization is facilitated by Bax, which is translocated to the membrane in a manner dependent on the loss of mitochondrial membrane potential[138]. Interestingly, we have shown that our knockdown lines have hyperpolarized mitochondrial membrane potentials, which may explain the decrease in fluorescence of the hydrogen peroxide indicator. Overall, the increase in superoxide in the absence of increases in other ROS suggests that this superoxide was mitochondria-derived and lends support to the hypothesis that deficiency of NIX, p62, and ATG7 causes accumulation of dysfunctional mitochondria that results in increases in mitochondrial ROS[65,139].

As the electron transport chain of mitochondria is associated with high levels of ROS production, we next sought to investigate whether increased ROS was related to alterations in the mitochondrial membrane potential (ΔΨM) – thus indicating altered mitochondrial function. The constant pumping of protons across their concentration gradient by the ETC creates a highly negative ΔΨM typically close to -180 mV[140]. The fluorescent dye Rhodamine 123, which is a lipophilic cationic dye, selectively accumulates in mitochondria in proportion to negative charge, allowing for analysis of ΔΨM [113]. More negative (hyperpolarized) mitochondria accumulate more dye, resulting in increased fluorescence[113]. Our results indicate that knockdown of autophagy genes results in hyperpolarization of ΔΨM, a condition indicating dysfunction in the ETC[141,142]. Consistent with our results showing increased ETC-derived ROS, studies have shown that hyperpolarization of ΔΨM triggers uncoupling of the respiratory chain complexes, resulting in increased ROS production[143,144]. Specifically, hyperpolarization has been shown to increase the $NADH/NAD^+$ ratio causing decreases in the rate of electron flow, which subsequently prolongs the lifespan of reactive intermediates in the ETC that promote the formation of the superoxide anion[102,143,132,145]. Furthermore, ROS-induced damage can contribute to defects in the electron transport chain complexes, thereby mediating further changes to the mitochondrial membrane potential.[146,147,148]. Given that the strict coupling and maintenance of ΔΨM are necessary for efficient energy production through oxidative phosphorylation, and that mitochondrial hyperpolarization and ROS generation are common features in apoptosis induction in various cell types, accumulation of mitochondrial dysfunction as seen in autophagy-deficient cells would be expected to increase susceptibility to apoptosis[149–151].

**5.2 Estimates of Mitochondrial Content**

Given that knockdown of autophagy genes increased ROS and altered the mitochondrial membrane potential, we next sought to determine whether these knockdowns had any effect on the quantity of mitochondrial content in the cells. Mitochondrial content was estimated using two methods: 1) cell staining using the fluorescent dye NAO and 2) quantification of mtDNA using qPCR. NAO is a dye which binds cardiolipin, a phospholipid which is almost exclusively found on the inner mitochondrial membrane where it is synthesized[152]. Due to its association with mitochondria-localized cardiolipin, NAO is commonly used as a measure of mitochondrial content[153]. Results of both the NAO and qPCR analysis showed flux over the course of the triplicate measures, with mitochondrial content values flipping above and below the TRC value over the course of the measurement cycle. Previous published data with $ATG7^{-/-}$ mice and various ATG7 knockout cell types showed increases in mitochondrial content as demonstrated by increased fluorescence of MitoTracker agents[62,64,154,155]. As adaptor/receptor proteins of mitophagy, knockdown of BNIP3L (cell line: NIX) and SQSTM1 (cell line: SQ) is expected to increase mitochondrial content[84,156]. This discrepancy could be due to the use of knockdown instead of knockout in our study, as knockdown allows for mitochondrial clearance to still occur, albeit at a lower level. Dispersed measurements of mtDNA and NAO fluorescence may also have contributed to the increased flux seen in our data, as measurements with conditional ATG7 knockouts would be run in quick succession due to impending lethality within 8-14 weeks[64]. The impact of ATG7 (cell line: ATG7), BNIP3L (cell line: NIX), and SQSTM1 (cell line: SQ) knockdowns on mitochondrial clearance could be further diminished by the presence of protective pathways in the cell. Indeed, as the small circular DNA of mitochondria is proximal to the ETC and has limited mechanisms for DNA-repair, ROS-induced damage to mtDNA may impair mitochondrial fission (replication) abilities leading to a decrease in mitochondrial content compared to a control undergoing regular mitochondrial fission [157]. Furthermore, due to the compactness of the mitochondrial genome, it follows that mutations run a higher chance of affecting a gene product, which provides a new means for further production of dysfunctional elements of the ETC[158,159,160].

### 5.3 Cell Homeostasis Measurements

Cell size, counts, and colony formation studies were run as a method of identifying substantial changes in cellular homeostasis. Mean cell size was not significantly altered in any of the knockdown cell lines. Increased cell size has been previously reported in ATG7 and ATG5 knockout mice, whereby autophagy was established to be a negative regulator of cell size[161–163]. Recently published data suggests that regulation of cell size occurs at least in part through the mevalonate pathway, which involves RAB11, a signaling molecule essential to basal autophagic flux[161]. The lack of significant changes in cell size may reflect the use of knockdown instead of knockout in our study. Next, we measured cell proliferation via cell counts. Cell Proliferation is known to be controlled by cell size-dependent and independent mechanisms[164]. While proliferation in the TRC cell line increased in a stepwise manner, most knockdown cell lines demonstrated decreased proliferation or bi-directional changes in proliferation rate over the course of the measurements. Previous studies have shown that autophagy inhibition increases proliferation in various cancer cells via altered mTOR signaling and other factors (ex. Twist1 stabilization for SQSTM1 knockdowns)[76,165,166]. The dysregulation seen in our cell lines could be caused by using knockdown instead of knockout. Our final measurement of cell homeostasis was colony formation. Colony forming abilities were diminished in the NIX cell line and unchanged in the ATG7 and SQ cell lines. These results were in accordance with most previously published knockdown and knockout data [167–172]. It is worth noting that some conflicting reports have shown colony formation to be reduced in SQSTM1 knockdowns and increased in some ATG7 knockdowns[168,173,174]. This disparity could be caused by differing levels of knockdown which would thus alter colony forming abilities to differing degrees (or not at all).

### 5.4 Analysis of Upstream & Downstream Autophagy Response to Cellular Stress

As both cellular and mitochondrial dysfunction was demonstrated in the autophagy-deficient cell lines, we next sought to understand the effects of these knockdowns on the dynamics of upstream and downstream autophagy proteins to give an indicator of the burden of these knockdowns on the process of autophagy. Autophagy is known to be upregulated in response to cellular stress signals such as nutrient deprivation[175,176]. Previous reports have indicated that serum starvation elicits an acute autophagic response within minutes of nutrient deprivation which is mediated by de-phosphorylation of the autophagy initiation factor ULK1[177]. In line with this, we ran our study along a similar 2-hour time course in buffered saline solution[177]. Beclin 1 and ATG7 represent early autophagy factors as they contribute to formation of the isolation membrane and vesicle elongation respectively, as shown in figure 1.4 of the introduction[178]. The conversion of LC3-I to LC3-II is a commonly used measure of autophagic flux as LC3-I conjugated to PE to create LC3-II during autophagy initiation, and LC3-II is then recruited to the autophagosome, where it acts as a cargo adaptor until it is degraded with the cargo[179]. NIX and p62 represent factors of late autophagy at the level of cargo recruitment as both can specifically act as adaptors/receptors of mitophagy[47]. Importantly, upregulation of all of these genes are part of the early response to nutrient deprivation[180,181,182]. The typical autophagic response demonstrated in the TRC cell line shows stepwise increases, and in some cases, subsequent decreases in autophagy proteins within the 2-hour assay. In response to serum starvation, AML cells deficient in ATG7, p62, and NIX demonstrated upregulation of all proteins of interest at various time points. Furthermore, all knockdowns show early upregulation of both mitochondrial cargo adaptors: NIX and p62, which suggests the presence of damaged mitochondria at the onset or soon after starvation initiation.

Upregulation of autophagy factors during nutrient deprivation has been shown to be mediated by several mechanisms involving the production of ROS[183]. Indeed, superoxide and peroxide are produced by mitochondria during nutrient deprivation and positively regulate autophagy through activation of AMPK (which activates the ULK1 complex), inactivation of ATG4's de-lipidating activity on LC3-II (leading to the accumulation of pro-autophagic LC3-II), and alterations to the thiol reduction state leading to an increase in ubiquitination of substrates[183].

The increased production of ROS shown previously for all knockdown cell lines may contribute to the increases in autophagy flux compared to the transduced control. Furthermore, the presence of damaged and dysfunctional mitochondria could contribute to the upregulation of autophagy, as selective mitochondrial clearance is activated as part of starvation-induced autophagy[184,185]. The more substantial changes in the ATG7 and NIX cell lines compared to the SQ cell line may reflect the essential vs dispensable nature of these proteins in the process of autophagy[163,85]. Indeed, redundancy has been shown to exist in this system whereby various adaptor proteins and receptors may function to link mitochondria to the autophagosome[59]. Deficiencies in adaptor proteins such as p62 may therefore not significantly affect the regulation of upstream autophagy proteins[186]. Levels of knockdown could further affect the response seen in this assay, as increased levels of the knockdown protein may allow autophagy to proceed in a manner more similar to TRC[187].

Having shown increased stress-induced autophagy as demonstrated by upregulation of early and late stage autophagy proteins in response to starvation, we next sought to understand the dose-dependent response of our knockdown cells to an autophagy activating drug. When treated with Rapamycin, which exerts its effect by inhibiting mTOR (a main autophagy signaling center), all knockdown cell lines were increasingly sensitive to cell death compared to the TRC contro[188,189]. This sensitivity could be due to the cumulative effects of blocking autophagy at both the control center and autophagosome initiation/ cargo recruitment phases, resulting in the inability to perform stress-induced protective autophagy[190].

### 5.5 Dose Response Data

We next assessed the impact of autophagy gene knockdown on two classes of drugs organized as being class I: DNA-targeting, and class II: mitochondrial-targeting. The DNA-targeting class was selected to represent standard AML therapeutics. Cytarabine is an antimetabolite drug which interferes with DNA synthesis whereas doxorubicin and daunorubicin are anthracyclines which impart their activity by intercalating with DNA and subsequently inhibit the progression of DNA topoisomerase II[15,16]. As expected, cytotoxicity of these DNA-damaging agents was not affected by autophagy gene knockdown.

Given that knockdown had no impact on cytotoxicity of DNA-targeting drugs, we next investigated a class of drugs which impart their activity by targeting mitochondria. The mechanisms of these agents affect mitochondrial function in various ways: blockage of the ETC, inhibition of ATP synthase, inhibition of fatty acid oxidation, etc. With exception of tigecycline, cytotoxicity of the mitochondrial-targeting drug class was increased by autophagy gene knockdown. Consistent with our previous indications of mitochondrial dysfunction imparted by increased ROS and altered mitochondrial membrane potential, our results suggest that autophagy-deficient cells are particularly sensitive to mitochondrial injury. The lack of sensitivity in KD lines treated with tigecycline may be explained by instability of this drug after reconstitution, as has been previously reported[191].

**Summary of Findings**

This study aimed to explore the relationship between autophagy and AML using genetic silencing of autophagy genes ATG7, SQSTM1, and BNIP3L. In particular, we were interested in the response of these cells to a panel of drugs with hopes of defining the value of using targeted chemotherapy in autophagy deficient cells. Our results have shown that knockdown of autophagy genes produces cells with various mitochondrial dysfunctions which we attributed to decreased clearance of damaged or dysfunctional mitochondria resulting from regular metabolism and further exacerbated by the accumulation ROS. These cell lines were increasingly sensitive to a panel of mitochondrial-targeting drugs with a broad range of mechanisms, which we similarly attributed to decreased clearance of damaged or dysfunctional mitochondria and increased mitochondrial ROS. The knockdown cell lines were also sensitive to an mTOR inhibitor, which may be linked to rapid depletion of autophagy proteins, preventing the protective autophagy effect. The results of this project are summarized in figure 5.0.

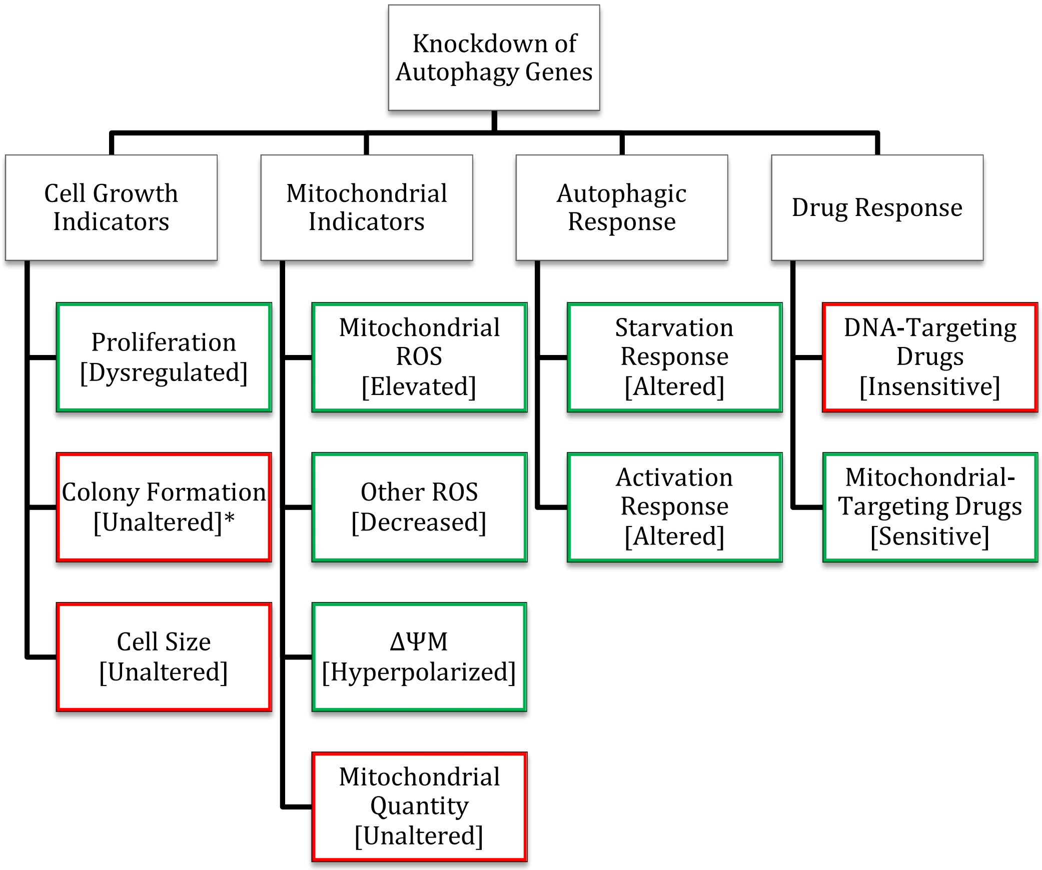


**Figure 5.0 Study Summary**
Knockdown of autophagy genes led to dysregulation of cell proliferation, increased mitochondrial ROS, decreased levels of other ROS, hyperpolarized ΔΨM, altered autophagy activation responses when stimulated by starvation and chemical means, and finally increased sensitivity to mitochondrial-targeting drugs.
*Exception: NIX1

Overall, our results suggest that deficiencies in the gene products of ATG7, SQSTM1 and BNIP3L may be used as prognostic markers to determine sensitivity to mitochondrial target drugs. Tailored therapies yield promise in the new age of chemotherapy as they provide a means to exploit specific dysfunctions known to be present in a cell population.

**Limitations**

This research explored the topic of single autophagy gene defects on mitochondrial sensitivity, however in a real-life scenario, it is possible (and most likely) that a variety of genetic dysfunctions exist in the patient[192]. AML is known to be a highly heterogeneous disease between patients, within a patient, and over the course of disease progression[192,193,194]. Further studies using the commonly grouped genetic defects seen in patients would provide more translatable data which could be applied to specific patient populations. As loss of genetic material in particular chromosomal regions is common in AML, inclusion of autophagy genes which reside in these regions would provide a good starting point for these studies[66].

Since an all-encompassing study of autophagy proteins was not feasible, we focused our study instead on three autophagy proteins which would serve to exemplify autophagic deficiency at two key stages: autophagosome formation (ATG7), and cargo recruitment (p62 and NIX). Further studies with other autophagy proteins and mitochondrial adaptors/receptors should be undertaken to create database of defects which confer sensitivity to mitochondria and m-TOR-targeting drugs.

The measures of mitochondrial characteristics used in this project provided a means to quantify ROS, mitochondrial content, and the $\Delta\Psi M$. Various other dyes and assays could be used to further detect dysfunction in the mitochondria. MitoSOX Red provides a means to detect superoxide within the mitochondria[195]. MitoTracker Green provides another means to measure mitochondrial mass in a manner which is independent of $\Delta\Psi M$[196]. Other mitochondrial genes could be probed for to validate the ND1 measurements[197].

We selected three classes of drugs for the purpose of this study: DNA-targeting, mitochondrial-targeting, and an mTOR inhibitor. The DNA-targeting class was selected to represent standard AML therapeutics, the mitochondrial-targeting class was selected as we were expecting an accumulation of mitochondrial dysfunction in our cells, and the mTOR inhibitor was selected as inhibition of mTOR activates autophagy. At present, mitochondrial-targeting drugs are not commonly used to treat AML[198]. Further study could uncover other drug classes for which the KD lines are sensitive, such as drugs which effect ROS levels or regulators of cell homeostasis.

The ultimate utility of this study relies on detection of autophagic dysfunction in AML patients. Karyotyping provides information on chromosomal loss of autophagy genes and provides a starting point for detecting dysfunction[66]. Proteomics, the study of an organism's entire set of proteins, yields the most hope for providing personalized cancer care, as it can detect differences brought on by transcriptional regulation[199]. Although the use of proteomics in cancer care currently resides in the research domain, this emerging field, when employed, could provide the foundation for application of this research[199].

**Conclusions**

In this study, we sought to better understand the mitochondria-specific changes in AML2 cells with deficits of autophagy proteins ATG7, NIX, or p62 by measuring a variety of mitochondrial health and function markers. Our results indicate that knockdown of our proteins of interest cause an abnormal mitochondrial phenotype that results in increased sensitivity to mitochondrial target drugs. Our research is particularly significant as some AML patient populations have been shown to be deficient in autophagy proteins[165]. Furthermore, an altered mitochondrial phenotype is a feature of AML[77,78,79]. Given the low survival rate of adult AML, our results suggest that pharmacological approaches which target mitochondria should be explored, as AML patients with autophagic deficiencies would be particularly sensitive to these drugs. Furthermore, once mitochondrial drugs for AML are approved, autophagy deficiencies may provide a useful prognostic indictaor for patients receiveing these therapies.

# References


1. NCBI. NCBI Gene. *Gene Catalog* (2016). at <http://www.ncbi.nlm.nih.gov/gene/>
2. Hanahan, D. & Weinberg, R. A. Hallmarks of cancer: The next generation. *Cell* **144,** 646–674 (2011).
3. Kumar, C. C. Genetic abnormalities and challenges in the treatment of acute myeloid leukemia. *Genes Cancer* **2,** 95–107 (2011).
4. Vardiman, J. W., Harris, N. L. & Brunning, R. D. The World Health Organization (WHO) classification of the myeloid neoplasms. *Blood* **100,** 2292–2302 (2002).
5. Passegué, E., Jamieson, C. H. M., Ailles, L. E. & Weissman, I. L. Normal and leukemic hematopoiesis: are leukemias a stem cell disorder or a reacquisition of stem cell characteristics? *Proc. Natl. Acad. Sci. U. S. A.* **100 Suppl,** 11842–9 (2003).
6. Grossmann, V. *et al.* A novel hierarchical prognostic model of AML solely based on molecular mutations. *Blood* **120,** 2963–2972 (2012).
7. Snyder, R. Leukemia and benzene. *International journal of environmental research and public health* **9,** 2875–2893 (2012).
8. Hahn, C. N. *et al.* Heritable GATA2 mutations associated with familial myelodysplastic syndrome and acute myeloid leukemia. *Nat. Genet.* **43,** 1012–7 (2011).
9. Czuczman, M. S. *et al.* Treatment-related myelodysplastic syndrome and acute myelogenous leukemia in patients treated with ibritumomab tiuxetan radioimmunotherapy. *J. Clin. Oncol.* **25,** 4285–4292 (2007).
10. Facts and Statistics. *Leukemia & Lymphoma Society* (2016). at <http://www.lls.org/http%3A/llsorg.prod.acquia-sites.com/facts-and-statistics/facts-and-statistics-overview/facts-and-statistics>

11. Acute Myelogenous Leukemia Statistics. *Canadian Cancer Society* (2016). at <http://www.cancer.ca/en/cancer-information/cancer-type/leukemia-acute-myelogenous-aml/statistics/?region=on>

12. Facts and Statistics. *Leukemia & Lymphoma Society of Canada* (2016). at <http://www.llscanada.org/disease-information/facts-and-statistics>

13. Döhner, H. *et al.* Diagnosis and management of acute myeloid leukemia in adults: Recommendations from an international expert panel, on behalf of the European LeukemiaNet. *Blood* **115,** 453–474 (2010).

14. Lichtman, M. A. A historical perspective on the development of the cytarabine (7 days) and daunorubicin (3 days) treatment regimen for acute myelogenous leukemia: 2013 the 40th anniversary of 7 + 3. *Blood Cells, Mol. Dis.* **50,** 119–130 (2013).

15. Sreenivasan, Y., Sarkar, A. & Manna, S. K. Mechanism of cytosine arabinoside-mediated apoptosis: role of Rel A (p65) dephosphorylation. *Oncogene* **22,** 4356–4369 (2003).

16. Nitiss, J. L. Targeting DNA topoisomerase II in cancer chemotherapy. *Nat. Rev. Cancer* **9,** 338–350 (2009).

17. Schuh, A. C., Fletcher, G. G., Leber, B. & Sabloff, M. *A Quality Initiative of the Program in Evidence-Based Care ( PEBC ), Cancer Care Ontario ( CCO ) Systemic Treatment of Acute Myeloid Leukemia ( AML ) Section 1 : Recommendations The complete guideline is available on the CCO website : Cancer Care Ontario* (2016). at <https://www.cancercare.on.ca/common/pages/UserFile.aspx?fileId=352602>

18. Puigvert, J. C., Sanjiv, K. & Helleday, T. Targeting DNA repair, DNA metabolism and replication stress as anti-cancer strategies. *FEBS Journal* **283,** 232–245 (2016).

19. Darzynkiewicz, Z. Novel strategies of protecting non-cancer cells during chemotherapy:

are they ready for clinical testing? *Oncotarget* **2,** 107–8 (2011).

20. Azarova, A. M. *et al.* Roles of DNA topoisomerase II isozymes in chemotherapy and secondary malignancies. *Proc. Natl. Acad. Sci. U. S. A.* **104,** 11014–11019 (2007).

21. Lilienbaum, A. Relationship between the proteasomal system and autophagy. *International Journal of Biochemistry and Molecular Biology* **4,** 1–26 (2013).

22. Parzych, K. R. & Klionsky, D. J. An overview of autophagy: morphology, mechanism, and regulation. *Antioxid. Redox Signal.* **20,** 460–73 (2014).

23. Ohsumi, Y. Historical landmarks of autophagy research. *Cell Res.* **24,** 9–23 (2014).

24. Mochida, K. *et al.* Receptor-mediated selective autophagy degrades the endoplasmic reticulum and the nucleus. *Nature* **522,** 359–62 (2015).

25. Klionsky, D. J. The molecular machinery of autophagy: unanswered questions. *J. Cell Sci.* **118,** 7–18 (2005).

26. Santambrogio, L. & Cuervo, A. M. Chasing the elusive mammalian microautophagy. *Autophagy* **7,** 652–654 (2011).

27. Li, W. W., Li, J. & Bao, J. K. Microautophagy: Lesser-known self-eating. *Cellular and Molecular Life Sciences* **69,** 1125–1136 (2012).

28. Majeski, A. E. & Fred Dice, J. Mechanisms of chaperone-mediated autophagy. *International Journal of Biochemistry and Cell Biology* **36,** 2435–2444 (2004).

29. Zaffagnini, G. & Martens, S. Mechanisms of Selective Autophagy. *Journal of Molecular Biology* **428,** 1714–1724 (2016).

30. Johansen, T. & Lamark, T. Selective autophagy mediated by autophagic adapter proteins. *Autophagy* **7,** 279–296 (2011).

31. Tooze, S. A. & Yoshimori, T. The origin of the autophagosomal membrane. *Nat. Cell*

*Biol.* **12,** 831–835 (2010).

32. Yang, Z. & Klionsky, D. J. Eaten alive: a history of macroautophagy. *Nat. Cell Biol.* **12,** 814–22 (2010).

33. Kim, J., Kundu, M., Viollet, B. & Guan, K.-L. AMPK and mTOR regulate autophagy through direct phosphorylation of Ulk1. *Nat. Cell Biol.* **13,** 132–41 (2011).

34. Sarkar, S. Regulation of autophagy by mTOR-dependent and mTOR-independent pathways: autophagy dysfunction in neurodegenerative diseases and therapeutic application of autophagy enhancers. *Biochem. Soc. Trans.* **41,** 1103–30 (2013).

35. Hosokawa, N. *et al.* Atg101, a novel mammalian autophagy protein interacting with Atg13. *Autophagy* **5,** 973–979 (2009).

36. Nakatogawa, H. Two ubiquitin-like conjugation systems that mediate membrane formation during autophagy. *Essays Biochem.* **55,** 39–50 (2013).

37. Mizushima, N. Autophagy: Process and function. *Genes and Development* **21,** 2861–2873 (2007).

38. Mizushima, N. *et al.* A protein conjugation system essential for autophagy. *Nature* **395,** 395–398 (1998).

39. Tanida, I., Ueno, T. & Kominami, E. LC3 and autophagy. *Methods Mol. Biol.* **445,** 77–88 (2008).

40. Ugland, H., Naderi, S., Brech, A., Collas, P. & Blomhoff, H. K. cAMP induces autophagy via a novel pathway involving ERK, cyclin E and Beclin 1. *Autophagy* **7,** 1199–1211 (2011).

41. Ravikumar, B. *et al.* Mammalian macroautophagy at a glance. *J. Cell Sci.* **122,** 1707–1711 (2009).

42. Sarkar, S. *et al.* Lithium induces autophagy by inhibiting inositol monophosphatase. *J. Cell Biol.* **170,** 1101–1111 (2005).

43. Williams, A. *et al.* Novel targets for Huntington's disease in an mTOR-independent autophagy pathway. *Nat. Chem. Biol.* **4,** 295–305 (2008).

44. Youle, R. J. & Narendra, D. P. Mechanisms of mitophagy. *Nat. Rev. Mol. Cell Biol.* **12,** 9–14 (2011).

45. Perry, S. W., Norman, J. P., Barbieri, J., Brown, E. B. & Gelbard, H. A. Mitochondrial membrane potential probes and the proton gradient: A practical usage guide. *BioTechniques* **50,** 98–115 (2011).

46. Shirihai, O. S., Song, M. & Dorn, G. W. How mitochondrial dynamism orchestrates mitophagy. *Circulation Research* **116,** 1835–1849 (2015).

47. Ding, W. X. & Yin, X. M. Mitophagy: Mechanisms, pathophysiological roles, and analysis. *Biological Chemistry* **393,** 547–564 (2012).

48. Sandoval, H. *et al.* Essential role for Nix in autophagic maturation of erythroid cells. *Nature* **454,** 232–235 (2008).

49. Zhang, J. & Ney, P. A. NIX induces mitochondrial autophagy in reticulocytes. *Autophagy* **4,** 354–356 (2008).

50. Narendra, D. P. *et al.* PINK1 is selectively stabilized on impaired mitochondria to activate Parkin. *PLoS Biol.* **8,** (2010).

51. Shiba-Fukushima, K. *et al.* Phosphorylation of Mitochondrial Polyubiquitin by PINK1 Promotes Parkin Mitochondrial Tethering. *PLoS Genet.* **10,** (2014).

52. Okatsu, K. *et al.* Phosphorylated ubiquitin chain is the genuine Parkin receptor. *J. Cell Biol.* **209,** 111–128 (2015).

53. Koyano, F. *et al.* Ubiquitin is phosphorylated by PINK1 to activate parkin. *Nature* **510,** 162–6 (2014).

54. Kane, L. A. *et al.* PINK1 phosphorylates ubiquitin to activate parkin E3 ubiquitin ligase activity. *J. Cell Biol.* **205,** 143–153 (2014).

55. Lazarou, M. *et al.* The ubiquitin kinase PINK1 recruits autophagy receptors to induce mitophagy. *Nature* **524,** 309–14 (2015).

56. Sandebring, A. & Cedazo-Mínguez, A. Parkin- An E3 Ubiquitin Ligase with Multiple Substrates. *J Alzheimers Dis Park.* **S10,** 1–6 (2012).

57. Moore, Andrew S Holzbaur, E. L. F. Dynamic recruitment and activation of ALS-associated TBK1 with its target optineurin are required for efficient mitophagy. *Proc. Natl. Acad. Sci. U. S. A.* **113,** E3349–E3358 (2016).

58. Richter, B. *et al.* Phosphorylation of OPTN by TBK1 enhances its binding to Ub chains and promotes selective autophagy of damaged mitochondria. *Proc. Natl. Acad. Sci. U. S. A.* 1–6 (2016). doi:10.1073/pnas.1523926113

59. Birgisdottir, Å. B., Lamark, T. & Johansen, T. The LIR motif - crucial for selective autophagy. *J. Cell Sci.* **126,** 3237–47 (2013).

60. Strappazzon, F. *et al.* AMBRA1 is able to induce mitophagy via LC3 binding, regardless of PARKIN and p62/SQSTM1. *Cell Death Differ.* **22,** 419–32 (2015).

61. Hoshii, T. *et al.* mTORC1 is essential for leukemia propagation but not stem cell self-renewal. *J. Clin. Invest.* **122,** 2114–2129 (2012).

62. Mortensen, M. *et al.* The autophagy protein Atg7 is essential for hematopoietic stem cell maintenance. *J. Exp. Med.* **208,** 455–467 (2011).

63. Liu, F. *et al.* FIP200 is required for the cell-autonomous maintenance of fetal

hematopoietic stem cells. *Blood* **116,** 4806–4814 (2010).

64. Mortensen, M. *et al.* Loss of autophagy in erythroid cells leads to defective removal of mitochondria and severe anemia in vivo. *Proc. Natl. Acad. Sci. U. S. A.* **107,** 832–837 (2010).

65. Mortensen, M. *et al.* The autophagy protein Atg7 is essential for hematopoietic stem cell maintenance. *J. Exp. Med.* **208,** 455–467 (2011).

66. Watson, A. S., Mortensen, M. & Simon, A. K. Autophagy in the pathogenesis of myelodysplastic syndrome and acute myeloid leukemia. *Cell Cycle* **10,** 1719–1725 (2011).

67. Sung Mi Park, Jianhong Ou, Lynn Chamberlain, Tessa M. Simone, Huan Yang, Ching-Man Virbasius, Abdullah M. Ali, Lihua Julie Zhu, Siddhartha Mukherjee, Azra Raza, M. R. G. U2AF35(S34F) Promotes Transformation by Directing Aberrant ATG7 Pre-mRNA 3′ End Formation. *Mol. Cell* **62,** 479–490 (2016).

68. Lazarini, M. *et al.* Nix (BNIP3L) Is Downregulated in High-Risk Myelodysplastic Syndromes and Acute Myeloid Leukemia and Its Silencing Enhances Decitabine-Mediated Apoptosis. *Blood* **124,** 3239 (2014).

69. Watson, A. *et al.* Autophagy limits proliferation and glycolytic metabolism in acute myeloid leukemia. *Cell Death Discov.* **1,** 15008 (2015).

70. Subramani, S. & Malhotra, V. Non-autophagic roles of autophagy-related proteins. *EMBO Rep* **14,** 143–151 (2013).

71. Lee, I. H. *et al.* Atg7 Modulates p53 Activity to Regulate Cell Cycle and Survival During Metabolic Stress. *Science* **336,** 225–228 (2012).

72. Chen, G. *et al.* Nix and Nip3 form a subfamily of pro-apoptotic mitochondrial proteins. *J. Biol. Chem.* **274,** 7–10 (1999).

73. Zhang, J. & Ney, P. a. Role of BNIP3 and NIX in cell death, autophagy, and mitophagy. *Cell Death Differ.* **16,** 939–946 (2009).

74. Mathew, R. *et al.* Autophagy Suppresses Tumorigenesis through Elimination of p62. *Cell* **137,** 1062–1075 (2009).

75. Moscat, J. & Diaz-Meco, M. T. p62 at the Crossroads of Autophagy, Apoptosis, and Cancer. *Cell* **137,** 1001–1004 (2009).

76. Qiang, L. *et al.* Regulation of cell proliferation and migration by p62 through stabilization of Twist1. *Proc. Natl. Acad. Sci. U. S. A.* **111,** 9241–6 (2014).

77. Skrtić, M. *et al.* Inhibition of mitochondrial translation as a therapeutic strategy for human acute myeloid leukemia. *Cancer Cell* **20,** 674–88 (2011).

78. Sriskanthadevan, S. *et al.* AML cells have low spare reserve capacity in their respiratory chain that renders them susceptible to oxidative metabolic stress. *Blood* **125,** 2120–2130 (2015).

79. Samudio, I. *et al.* Pharmacologic inhibition of fatty acid oxidation sensitizes human leukemia cells to apoptosis induction. *J. Clin. Invest.* **120,** 142–56 (2010).

80. Schwarten, M. *et al.* Nix directly binds to GABARAP: A possible crosstalk between apoptosis and autophagy. *Autophagy* **5,** 690–698 (2009).

81. Novak, I. *et al.* Nix is a selective autophagy receptor for mitochondrial clearance. *EMBO Rep.* **11,** 45–51 (2010).

82. Komatsu, M. *et al.* The selective autophagy substrate p62 activates the stress responsive transcription factor Nrf2 through inactivation of Keap1. *Nat. Cell Biol.* **12,** 213–223 (2010).

83. Geisler, S. *et al.* PINK1/Parkin-mediated mitophagy is dependent on VDAC1 and

p62/SQSTM1. *Nat. Cell Biol.* **12,** 119–131 (2010).

84. Ding, W. X. *et al.* Nix is critical to two distinct phases of mitophagy, reactive oxygen species-mediated autophagy induction and Parkin-ubiquitin-p62-mediated mitochondrial priming. *J. Biol. Chem.* **285,** 27879–27890 (2010).

85. Narendra, D. P., Kane, L. A., Hauser, D. N., Fearnley, I. M. & Youle, R. J. p62/SQSTM1 is required for Parkin-induced mitochondrial clustering but not mitophagy; VDAC1 is dispensable for both. *Autophagy* **6,** 1090–1106 (2010).

86. Li, X. *et al.* Autophagy modulation as a target for anticancer drug discovery. *Acta Pharmacol. Sin.* **34,** 612–24 (2013).

87. Chresta, C. M. *et al.* AZD8055 is a potent, selective, and orally bioavailable ATP-competitive mammalian target of rapamycin kinase inhibitor with in vitro and in vivo antitumor activity. *Cancer Res.* **70,** 288–298 (2010).

88. Cao, C. *et al.* Inhibition of mammalian target of rapamycin or apoptotic pathway induces autophagy and radiosensitizes PTEN null prostate cancer cells. *Cancer Res.* **66,** 10040–10047 (2006).

89. Crazzolara, R., Bradstock, K. F. & Bendall, L. J. RAD001 (everolimus) induces autophagy in acute lymphoblastic leukemia. *Autophagy* **5,** 727–728 (2009).

90. Fu, L. *et al.* Perifosine inhibits mammalian target of rapamycin signaling through facilitating degradation of major components in the mTOR axis and induces autophagy. *Cancer Res.* **69,** 8967–8976 (2009).

91. Cirstea, D. *et al.* Dual inhibition of akt/mammalian target of rapamycin pathway by nanoparticle albumin-bound-rapamycin and perifosine induces antitumor activity in multiple myeloma. *Mol. Cancer Ther.* **9,** 963–975 (2010).

92. Tomic, T. *et al.* Metformin inhibits melanoma development through autophagy and apoptosis mechanisms. *Cell Death Dis.* **2,** e199 (2011).

93. Cao, B. *et al.* Clioquinol induces pro-death autophagy in leukemia and myeloma cells by disrupting the mTOR signaling pathway. *Sci. Rep.* **4,** 5749 (2014).

94. Sen, S. *et al.* Novel mTOR inhibitory activity of ciclopirox enhances parthenolide antileukemia activity. *Exp. Hematol.* **41,** 799–807 (2013).

95. Torgersen, M. L., Engedal, N., Bøe, S. O., Hokland, P. & Simonsen, A. Targeting autophagy potentiates the apoptotic effect of histone deacetylase inhibitors in t(8;21) AML cells. *Blood* **122,** 2467–2476 (2013).

96. Qian, W., Liu, J., Jin, J., Ni, W. & Xu, W. Arsenic trioxide induces not only apoptosis but also autophagic cell death in leukemia cell lines via up-regulation of Beclin-1. *Leuk. Res.* **31,** 329–339 (2007).

97. Yang, Y., Liang, Z., Gao, B., Jia, Y. & Qin, Z. Dynamic effects of autophagy on arsenic trioxide-induced death of human leukemia cell line HL60 cells. *Acta Pharmacol. Sin.* **29,** 123–34 (2008).

98. Ito, S., Koshikawa, N., Mochizuki, S. & Takenaga, K. 3-Methyladenine suppresses cell migration and invasion of HT1080 fibrosarcoma cells through inhibiting phosphoinositide 3-kinases independently of autophagy inhibition. *Int. J. Oncol.* **31,** 261–268 (2007).

99. Li, J. *et al.* Inhibition of autophagy by 3-MA enhances the effect of 5-FU-induced apoptosis in colon cancer cells. *Ann. Surg. Oncol.* **16,** 761–771 (2009).

100. Tseng, H. C. *et al.* Sensitizing effect of 3-methyladenine on radiation-induced cytotoxicity in radio-resistant HepG2 cells in vitro and in tumor xenografts. *Chem. Biol. Interact.* **192,** 201–208 (2011).

101. Wu, Y. C. *et al.* Inhibition of macroautophagy by bafilomycin A1 lowers proliferation and induces apoptosis in colon cancer cells. *Biochem. Biophys. Res. Commun.* **382,** 451–456 (2009).

102. Kanematsu, S. *et al.* Autophagy inhibition enhances sulforaphane-induced apoptosis in human breast cancer cells. *Anticancer Res.* **30,** 3381–3390 (2010).

103. Amaravadi, R. K. *et al.* Autophagy inhibition enhances therapy-induced apoptosis in a Myc-induced model of lymphoma. *J. Clin. Invest.* **117,** 326–336 (2007).

104. Franken, N. a P., Rodermond, H. M., Stap, J., Haveman, J. & van Bree, C. Clonogenic assay of cells in vitro. *Nat. Protoc.* **1,** 2315–9 (2006).

105. Livak, K. J. & Schmittgen, T. D. Analysis of relative gene expression data using real-time quantitative PCR and the 2(-Delta Delta C(T)) Method. *Methods* **25,** 402–8 (2001).

106. Wang, X. *et al.* Imaging ROS signaling in cells and animals. *Journal of Molecular Medicine* **91,** 917–927 (2013).

107. Kalyanaraman, B. *et al.* Measuring reactive oxygen and nitrogen species with fluorescent probes: Challenges and limitations. *Free Radical Biology and Medicine* **52,** 1–6 (2012).

108. Rothe, G. & Valet, G. Flow cytometric analysis of respiratory burst activity in phagocytes with hydroethidine and 2',7'-dichlorofluorescin. *J. Leukoc. Biol.* **47,** 440–448 (1990).

109. Bilski, P., Belanger, A. G. & Chignell, C. F. Photosensitized oxidation of 2,7-dichlorofluorescin: Singlet oxygen does not contribute to the formation of fluorescent oxidation product 2,7-dichlorofluorescein. *Free Radic. Biol. Med.* **33,** 938–946 (2002).

110. Tang, C. *et al.* Evidence for a role of superoxide generation in glucose-induced beta-cell dysfunction in vivo. *Diabetes* **56,** 2722–2731 (2007).

111. Mahfouz, R., Sharma, R., Lackner, J., Aziz, N. & Agarwal, A. Evaluation of

chemiluminescence and flow cytometry as tools in assessing production of hydrogen peroxide and superoxide anion in human spermatozoa. *Fertil. Steril.* **92,** 819–827 (2009).

112. Kaewsuya, P., Danielson, N. D. & Ekhterae, D. Fluorescent determination of cardiolipin using 10-N-nonyl acridine orange. *Anal. Bioanal. Chem.* **387,** 2775–2782 (2007).

113. Baracca, A., Sgarbi, G., Solaini, G. & Lenaz, G. Rhodamine 123 as a probe of mitochondrial membrane potential: Evaluation of proton flux through F0 during ATP synthesis. *Biochim. Biophys. Acta - Bioenerg.* **1606,** 137–146 (2003).

114. Circu, M. L. & Aw, T. Y. Reactive oxygen species, cellular redox systems, and apoptosis. *Free Radical Biology and Medicine* **48,** 749–762 (2010).

115. Sakamuru, S. *et al.* Application of a homogenous membrane potential assay to assess mitochondrial function. *Physiol Genomics* **44,** 495–503 (2012).

116. Kessel, D., Price, M. & Reiners, J. J. The Bcl-2 antagonist HA14-1 forms a fluorescent albumin complex that can be mistaken for several oxidized ROS probes. *Photochem. Photobiol.* **84,** 1272–1276 (2008).

117. Lee, E. A. *et al.* Targeting mitochondria with avocatin B induces selective leukemia cell death. *Cancer Res.* **75,** 2478–2488 (2015).

118. Lee, E. A. *et al.* Inhibition of Fatty Acid Oxidation with Avocatin B Selectively Targets AML Cells and Leukemia Stem Cells. *Blood* **124,** 268 (2014).

119. Benz, R. & McLaughlin, S. The molecular mechanism of action of the proton ionophore FCCP (carbonylcyanide p-trifluoromethoxyphenylhydrazone). *Biophys. J.* **41,** 381–98 (1983).

120. Shchepina, L. A. *et al.* Oligomycin, inhibitor of the F0 part of H+-ATP-synthase, suppresses the TNF-induced apoptosis. *Oncogene* **21,** 8149–57 (2002).

121. Palorini, R., Simonetto, T., Cirulli, C. & Chiaradonna, F. Mitochondrial complex i inhibitors and forced oxidative phosphorylation synergize in inducing cancer cell death. *Int. J. Cell Biol.* (2013). doi:10.1155/2013/243876

122. Weichhart, T., Hengstschläger, M. & Linke, M. Regulation of innate immune cell function by mTOR. *Nat. Rev. Immunol.* **15,** 599–614 (2015).

123. Matsunaga, T. *et al.* Rotenone, a mitochondrial NADH dehydrogenase inhibitor, induces cell surface expression of CD13 and CD38 and apoptosis in HL-60 cells. *Leuk. Lymphoma* **20,** 487–494 (1996).

124. Li, N. *et al.* Mitochondrial complex I inhibitor rotenone induces apoptosis through enhancing mitochondrial reactive oxygen species production. *J Biol Chem* **278,** 8516–8525 (2003).

125. Dengler, W. a, Schulte, J., Berger, D. P., Mertelsmann, R. & Fiebig, H. H. Development of a propidium iodide fluorescence assay for proliferation and cytotoxicity assays. *Anti-cancer drugs* **6,** 522–532 (1995).

126. Anderson, M. & Whitcomb, P. Design of Experiments: Statistical Principles of Research Design and Analysis. *Technometrics* **43,** 236–237 (2001).

127. Maxwell, S. & Delaney, H. *Designing experiments and analyzing data: A model comparison perspective*. *Briefings in functional genomics proteomics* **4,** (2004).

128. Pett, M. . *Nonparametric Statistics for Health Care Research: Statistics for Small Samples and Unusual Distributions*. (SAGE Publications, 2015).

129. Gunther, C., Hauser, A. & Huss, R. *Advances in Pharmaceutical Cell Therapy: Principles of Cell-Based Biopharmaceuticals - Biology, Quality, Manufacturing, Clinical Implementation and Economics*. (World Scientific Publishing Co. Pte. Ltd., 2016).

130. Owusu-Ansah, E., Yavari, A. & Banerjee, U. A protocol for in vivo detection of reactive oxygen species. *Nat. Protoc.* **doi:10.103,** 1–10 (2008).

131. Gomes, A., Fernandes, E. & Lima, J. L. F. C. Fluorescence probes used for detection of reactive oxygen species. *Journal of Biochemical and Biophysical Methods* **65,** 45–80 (2005).

132. Murphy, M. P. How mitochondria produce reactive oxygen species. *Biochem. J.* **417,** 1–13 (2009).

133. Turrens, J. F. Mitochondrial formation of reactive oxygen species. *J. Physiol.* **552,** 335–44 (2003).

134. Zaheer, A., Yang, B., Cao, X. & Lim, R. Decreased Copper--Zinc Superoxide Dismutase Activity and Increased Resistance to Oxidative Stress in Glia Maturation Factor--Null Astrocytes. *Neurochem. Res.* **29,** 1473–1480 (2004).

135. Wang, Y. & Walsh, S. W. Increased superoxide generation is associated with decreased superoxide dismutase activity and mRNA expression in placental trophoblast cells in pre-eclampsia. *Placenta* **22,** 206–212 (2001).

136. In, S., Hong, C. W., Choi, B., Jang, B. G. & Kim, M. J. Inhibition of Mitochondrial Clearance and Cu/Zn-SOD Activity Enhance 6-Hydroxydopamine-Induced Neuronal Apoptosis. *Mol. Neurobiol.* **53,** 777–791 (2016).

137. Ott, M., Robertson, J. D., Gogvadze, V., Zhivotovsky, B. & Orrenius, S. Cytochrome c release from mitochondria proceeds by a two-step process. *Proc. Natl. Acad. Sci. U. S. A.* **99,** 1259–63 (2002).

138. Smaili, S. S., Hsu, Y. T., Sanders, K. M., Russell, J. T. & Youle, R. J. Bax translocation to mitochondria subsequent to a rapid loss of mitochondrial membrane potential. *Cell Death*

*Differ.* **8,** 909–920 (2001).

139. Tal, M. C. *et al.* Absence of autophagy results in reactive oxygen species-dependent amplification of RLR signaling. *Proc. Natl. Acad. Sci. U. S. A.* **106,** 2770–5 (2009).

140. Griffiths, E. J. Mitochondria--potential role in cell life and death. *Cardiovasc Res* **46,** 24–27 (2000).

141. Bose, T., Cieślar-Pobuda, A. & Wiechec, E. Role of ion channels in regulating $Ca^{2+}$ homeostasis during the interplay between immune and cancer cells. *Cell Death Dis.* **6,** e1648 (2015).

142. Yang, M. & Brackenbury, W. J. Membrane potential and cancer progression. *Frontiers in Physiology* **4 JUL,** (2013).

143. Kluge, M. A., Fetterman, J. L. & Vita, J. A. Mitochondria and endothelial function. *Circulation Research* **112,** 1171–1188 (2013).

144. Leanza, L. *et al.* Targeting a mitochondrial potassium channel to fight cancer. *Cell Calcium* **58,** (2015).

145. Widlansky, M. E. & Gutterman, D. D. Regulation of endothelial function by mitochondrial reactive oxygen species. *Antioxid. Redox Signal.* **15,** 1517–30 (2011).

146. Musatov, A. & Robinson, N. C. Susceptibility of mitochondrial electron-transport complexes to oxidative damage. Focus on cytochrome c oxidase. *Free Radic. Res.* **46,** 1313–1326 (2012).

147. Ehlers, R. a *et al.* Mitochondrial DNA damage and altered membrane potential (delta psi) in pancreatic acinar cells induced by reactive oxygen species. *Surgery* **126,** 148–155 (1999).

148. Machida, K. & Tanaka, T. Farnesol-induced generation of reactive oxygen species

dependent on mitochondrial transmembrane potential hyperpolarization mediated by F0F1- ATPase in yeast. *FEBS Lett.* **462,** 108–112 (1999).

149. Galloway, C. a & Yoon, Y. Perspectives on: SGP symposium on mitochondrial physiology and medicine: what comes first, misshape or dysfunction? The view from metabolic excess. *J. Gen. Physiol.* **139,** 455–63 (2012).

150. Gergely, P. *et al.* Mitochondrial hyperpolarization and ATP depletion in patients with systemic lupus erythematosus. *Arthritis Rheum.* **46,** 175–190 (2002).

151. Giovannini, C. *et al.* Mitochondria hyperpolarization is an early event in oxidized low-density lipoprotein-induced apoptosis in Caco-2 intestinal cells. *FEBS Lett.* **523,** 200–206 (2002).

152. Paradies, G., Paradies, V., De Benedictis, V., Ruggiero, F. M. & Petrosillo, G. Functional role of cardiolipin in mitochondrial bioenergetics. *Biochimica et Biophysica Acta - Bioenergetics* **1837,** 408–417 (2014).

153. Lizard, G., Chardonnet, Y., Chignol, M. C. & Thivolet, J. Evaluation of mitochondrial content and activity with nonyl-acridine orange and rhodamine 123: flow cytometric analysis and comparison with quantitative morphometry. *Cytotechnology* **3,** 179–188 (1990).

154. García-Prat, L. *et al.* Autophagy maintains stemness by preventing senescence. *Nature* **529,** 37–42 (2016).

155. Kamino, H. *et al.* Mieap-regulated mitochondrial quality control is frequently inactivated in human colorectal cancer. *Oncogenesis* **5,** e181 (2016).

156. Ashrafi, G. & Schwarz, T. L. The pathways of mitophagy for quality control and clearance of mitochondria. *Cell Death Differ* **20,** 31–42 (2013).

157. Cline, S. D. Mitochondrial DNA damage and its consequences for mitochondrial gene expression. *Biochim. Biophys. Acta* **1819,** 979–91 (2012).

158. Wei, Y.-H. & Lee, H.-C. Oxidative stress, mitochondrial DNA mutation, and impairment of antioxidant enzymes in aging. *Exp. Biol. Med. (Maywood).* **227,** 671–82 (2002).

159. Linnane, A., Ozawa, T., Marzuki, S. & Tanaka, M. Mitochondrial DNA mutations as an important contributor to ageing and degenerative diseases. *Lancet* **333,** 642–645 (1989).

160. Dutta, D., Calvani, R., Bernabei, R., Leeuwenburgh, C. & Marzetti, E. Contribution of impaired mitochondrial autophagy to cardiac aging: Mechanisms and therapeutic opportunities. *Circulation Research* **110,** 1125–1138 (2012).

161. Miettinen, T. P. & Bj??rklund, M. Mevalonate Pathway Regulates Cell Size Homeostasis and Proteostasis through Autophagy. *Cell Rep.* **13,** 2610–2620 (2015).

162. Hosokawa, N., Hara, Y. & Mizushima, N. Generation of cell lines with tetracycline-regulated autophagy and a role for autophagy in controlling cell size. *FEBS Lett.* **580,** 2623–2629 (2006).

163. Komatsu, M. *et al.* Impairment of starvation-induced and constitutive autophagy in Atg7-deficient mice. *J. Cell Biol.* **169,** 425–434 (2005).

164. Rouzaire-Dubois, B., O'Regan, S. & Dubois, J. M. Cell size-dependent and independent proliferation of rodent neuroblastoma x glioma cells. *J. Cell. Physiol.* **203,** 243–250 (2005).

165. Watson, A. *et al.* Autophagy limits proliferation and glycolytic metabolism in acute myeloid leukemia. *Cell Death Discov.* **1,** 15008 (2015).

166. Cianfanelli, V. *et al.* AMBRA1 links autophagy to cell proliferation and tumorigenesis by promoting c-Myc dephosphorylation and degradation. *Nat. Cell Biol.* **17,** 20–30 (2014).

167. Lazarini, M. *et al.* Nix (BNIP3L) Is Downregulated in High-Risk Myelodysplastic Syndromes and Acute Myeloid Leukemia and Its Silencing Enhances Decitabine-Mediated Apoptosis. *Blood* **124,** 3239 (2014).

168. Goussetis, D. J. *et al.* Autophagic degradation of the BCR-ABL oncoprotein and generation of antileukemic responses by arsenic trioxide. *Blood* **120,** 3555–3562 (2012).

169. Hiruma, Y. *et al.* Increased signaling through p62 in the marrow microenvironment increases myeloma cell growth and osteoclast formation. *Blood* **113,** 4894–4902 (2009).

170. Karvela, M. *et al.* ATG7 regulates energy metabolism, differentiation and survival of Philadelphia-chromosome-positive cells. *Autophagy* **12,** 936–948 (2016).

171. Lin, W. *et al.* Autophagy confers DNA damage repair pathways to protect the hematopoietic system from nuclear radiation injury. *Sci. Rep.* **5,** 12362 (2015).

172. Wang, C. *et al.* Elevated p62/SQSTM1 determines the fate of autophagy-deficient neural stem cells by increasing superoxide. *J. Cell Biol.* **212,** 545–560 (2016).

173. Fang, J. *et al.* Myeloid Malignancies with Chromosome 5q Deletions Acquire a Dependency on an Intrachromosomal NF-??B Gene Network. *Cell Rep.* **8,** 1328–1338 (2014).

174. Chen, K. *et al.* Regulation of glucose metabolism by p62/SQSTM1 through HIF1α. *J. Cell Sci.* **129,** 817–830 (2016).

175. He, C. & Klionsky, D. J. Regulation mechanisms and signaling pathways of autophagy. *Annu. Rev. Genet.* **43,** 67–93 (2009).

176. Russell, R. C., Yuan, H.-X. & Guan, K.-L. Autophagy regulation by nutrient signaling. *Cell Res.* **24,** 42–57 (2014).

177. Shang, L. *et al.* Nutrient starvation elicits an acute autophagic response mediated by Ulk1

dephosphorylation and its subsequent dissociation from AMPK. *Proc. Natl. Acad. Sci. U. S. A.* **108,** 4788–93 (2011).

178. Kang, R., Zeh, H. J., Lotze, M. T. & Tang, D. The Beclin 1 network regulates autophagy and apoptosis. *Cell Death Differ.* **18,** 571–80 (2011).

179. Kadowaki, M. & Karim, M. R. Chapter 13 Cytosolic LC3 Ratio as a Quantitative Index of Macroautophagy. *Methods in Enzymology* **451,** 199–213 (2009).

180. Xu, H. D. *et al.* The Pro-Survival Role of Autophagy Depends on Bcl-2 Under Nutrition Stress Conditions. *PLoS One* **8,** (2013).

181. B'Chir, W. *et al.* The eIF2α/ATF4 pathway is essential for stress-induced autophagy gene expression. *Nucleic Acids Res.* **41,** 7683–7699 (2013).

182. Mammucari, C. *et al.* FoxO3 Controls Autophagy in Skeletal Muscle In Vivo. *Cell Metab.* **6,** 458–471 (2007).

183. Filomeni, G., Zio, D. De, Cecconi, F., De Zio, D. & Cecconi, F. Oxidative stress and autophagy: the clash between damage and metabolic needs. *Cell Death Differ.* **22,** 377–388 (2015).

184. Frank, M. *et al.* Mitophagy is triggered by mild oxidative stress in a mitochondrial fission dependent manner. *Biochim. Biophys. Acta - Mol. Cell Res.* **1823,** 2297–2310 (2012).

185. Eiyama, A., Kondo-Okamoto, N. & Okamoto, K. Mitochondrial degradation during starvation is selective and temporally distinct from bulk autophagy in yeast. *FEBS Lett.* **587,** 1787–1792 (2013).

186. Matsumoto, G., Shimogori, T., Hattori, N. & Nukina, N. TBK1 controls autophagosomal engulfment of polyubiquitinated mitochondria through p62/SQSTM1 phosphorylation. *Hum. Mol. Genet.* **24,** 4429–4442 (2015).

187. Zhang, J. *et al.* Mitochondrial clearance is regulated by Atg7-dependent and -independent mechanisms during reticulocyte maturation. *Blood* **114,** 157–164 (2009).

188. Benjamin, D., Colombi, M., Moroni, C. & Hall, M. N. Rapamycin passes the torch: a new generation of mTOR inhibitors. *Nat. Rev. Drug Discov.* **10,** 868–880 (2011).

189. Li, J., Kim, S. G. & Blenis, J. Rapamycin: One drug, many effects. *Cell Metabolism* **19,** 373–379 (2014).

190. Kapuy, O., Vinod, P. K. & B??nhegyi, G. MTOR inhibition increases cell viability via autophagy induction during endoplasmic reticulum stress - An experimental and modeling study. *FEBS Open Bio* **4,** 704–713 (2014).

191. Jitkova, Y. *et al.* A novel formulation of tigecycline has enhanced stability and sustained antibacterial and antileukemic activity. *PLoS One* **9,** (2014).

192. Marcucci, G., Haferlach, T. & Döhner, H. Molecular genetics of adult acute myeloid leukemia: prognostic and therapeutic implications. *J. Clin. Oncol. Off. J. Am. Soc. Clin. Oncol.* **29,** 475–486 (2011).

193. Hays, L. E. Heterogeneity in the AML stem cell pool. *Blood* **114,** 3976–3977 (2009).

194. Li, S. *et al.* Distinct evolution and dynamics of epigenetic and genetic heterogeneity in acute myeloid leukemia. *Nat Med* **22,** 792–799 (2016).

195. Mukhopadhyay, P., Rajesh, M., Yoshihiro, K., Hask??, G. & Pacher, P. Simple quantitative detection of mitochondrial superoxide production in live cells. *Biochem. Biophys. Res. Commun.* **358,** 203–208 (2007).

196. Agnello, M., Morici, G. & Rinaldi, A. M. A method for measuring mitochondrial mass and activity. *Cytotechnology* **56,** 145–149 (2008).

197. Phillips, N. R., Sprouse, M. L. & Roby, R. K. Simultaneous quantification of

mitochondrial DNA copy number and deletion ratio: a multiplex real-time PCR assay. *Sci. Rep.* **4,** 3887 (2014).

198. Services, U. D. of H. and H. Drugs Approved for Leukemia. *National Cancer Institute* (2016). at <https://www.cancer.gov/about-cancer/treatment/drugs/leukemia>

199. Koomen, J. M. *et al.* Proteomic contributions to personalized cancer care. *Mol. Cell. Proteomics* **7,** 1780–1794 (2008).

200. Kaushik, S. & Cuervo, A. M. Chaperone-mediated autophagy: A unique way to enter the lysosome world. *Trends in Cell Biology* **22,** 407–417 (2012).

201. Boya, P., Reggiori, F. & Codogno, P. Emerging regulation and functions of autophagy. *Nat. Cell Biol.* **15,** 713–20 (2013).

202. Geisler, S. *et al.* PINK1/Parkin-mediated mitophagy is dependent on VDAC1 and p62/SQSTM1. *Nat. Cell Biol.* **12,** 119–131 (2010).